UNIVERSITÀ DEGLI STUDI DI PARMA

Dottorato di Ricerca in Matematica Pura e Applicata

Ciclo XXVII

High order semi-Lagrangian methods for BGK-type models in the kinetic theory of rarefied gases

Coordinatore:
Chiar.ma Prof.ssa Alessandra Lunardi
Tutor:
Chiar.ma Prof.ssa Maria Groppi
Co-Tutor:
Chiar.mo Prof. Giovanni Russo

Dottorando: Giuseppe Stracquadanio

GENNAIO 2015

Contents

Introduction

In hydrodynamic regimes, fluid flows can be described by standard models such as Navier-Stokes or compressible Euler equations. However, some regimes cannot be qualified as hydrodynamic and the continuum equations are not able to correctly describe the dynamics of the flow. The parameter that dictates whether or not a flow is hydrodynamic is the Knudsen number Kn. It is defined as the ratio between the mean free path λ between the particles and the characteristic length of the physical problem L. When this number goes to zero, the hydrodynamic regime is reached. For large Knudsen number (usually higher than 10^{-2}), the regime is qualified as rarefied and it is well described by the kinetic theory and in particular by the Boltzmann equation, an integro-differential equation governing the evolution of the so called distribution function in the phase space [13].
Traditionally, an important field of application of kinetic theory has been the motion of objects in the rarefied layers of the atmosphere, such as re-entry problems in aerospace engineering. Indeed, in these cases, the Knudsen number is large, because the mean free path is of orders of magnitude larger than the characteristic length of the space vehicle. Recently, however, a huge new field of applications of kinetic theory has begun to develop in the modeling of fluid flows in nanotechnology, for example to build Micro-Electro-Mechanical-Systems (MEMS) [14], which are present in accelerometers, micro pumps or micro engines: in this case, the Knudsen number is large because the scale of interest L is so small that the ratio λ/L is of order one and microscopic effects cannot be neglected.
Approximate methods of solution for the Boltzmann equation have a long history tracing back to Hilbert, Chapman and Enskog [13] at the beginning of the last century. The mathematical difficulties related to the Boltzmann equation make it extremely difficult to treat; in particular, analytical solutions in most relevant situations are hard (and sometimes impossible) to find. Most of the difficulties are due to the multidimensional structure of the collision integral. In addition, the numerical integration requires great care since the collision integral is at the basis of the macroscopic properties of the equation. Further

difficulties rely on the presence of stiffness, like in the case of small mean free path or of large velocities.
For such reasons many realistic numerical simulations are based on Monte-Carlo techniques. The most famous examples are Direct Simulation Monte Carlo [6], which is a particle solver especially efficient in the rarefied regime. However, the computational time requirement increases very rapidly as the hydrodynamic regime is reached. The number of collisions increases and a strong restriction appears on the time step. For this reason, attempts have been made to derive numerical solvers for the Boltzmann equation which are not based on particles.
Among deterministic approximation, one of the most popular methods is represented by the so called Discrete Velocity Models (DVM) of the Boltzmann equation [10, 46]. These methods are based on a Cartesian grid in velocity and on a discrete collision mechanism on the points of the grid that preserves the main physical properties. Unfortunately DVM are not competitive with Monte Carlo methods in terms of computational cost.
A reduction of computation time is possible by considering simplified models of the Boltzmann equation. A particularly successful model is the BGK model [8], in which the collision term of the Boltzmann equation is replaced by a relaxation term, simpler to treat. The BGK model by construction reproduces several physical properties of the Boltzmann equation and is consistent with the hydrodynamic limit at the continuous level, i.e., for very small Knudsen numbers the Euler limit is recovered. The numerical schemes used to solve the BGK model that fulfill this property are called asymptotic preserving (AP), after the pioneering work by Jin [31]. For small relaxation time, a strong restriction on the time step exists also for the BGK model, but it can be easily treated by using implicit schemes. Among these implicit schemes, we have to mention Implicit-Explicit Runge-Kutta methods (IMEX)[40, 42]. We focus here our attention on implicit semi-Lagrangian schemes for the BGK equation [49, 50, 51].

This thesis presents high order shock capturing semi-Lagrangian methods for the numerical solutions of BGK-type equations. The starting point is the work of Santagati and Russo [49, 51]. They have developed implicit semi-Lagrangian schemes for the one-dimensional BGK model. The key idea of the semi-Lagrangian formulation is to integrate partial differential equations along the characteristics and then its main advantage is that PDEs become ODEs along such curves. Moreover, semi-Lagrangian schemes allow us to use large time steps, avoiding the classical Courant stability condition. Contrary, the main drawback is that some interpolation is required in order to reconstruct the solution on the feet of the characteristics. The need for a spatial reconstruction could become a

drawback when we are looking for high order methods. Indeed, the computational cost can increase considerably. In detail, in [49, 51] these problems are dealt with L-stable diagonally implicit Runge-Kutta (DIRK) coupled with a WENO-type spatial reconstruction. The choice of DIRK methods allows to avoid strong restrictions on the time step, and the use of a WENO reconstruction allows to preserve accuracy also in stiff regime and in presence of discontinuities.

In the present thesis some substantial improvements of these semi-Lagrangian schemes for the BGK equation are proposed, together with some new applications.
First of all, we tried to reduce the computational cost, due mainly to the interpolation technique. We investigated two directions [24]: the use of multi-step methods instead of DIRK methods and the development of particular semi-Lagrangian schemes that avoid completely spatial interpolation. In the development of high order methods, we observed that the number of spatial interpolations required at each step increases as the order of the method. In particular a DIRK method required 1, 3 or 6 interpolations at each time step to obtain respectively a first, second or third order method. Instead, using multi-step methods, such as backward differentiation formula (BDF) methods, the number of interpolations is 1, 2 and 3, respectively. Thus the use of BDF methods reduces considerably the computational cost, in particular for high order.
The study of methods that avoid interpolation also deserves attention [24]. Interpolation techniques in semi-Lagrangian schemes are required because in general the feet of the characteristic lines are not grid points. Thus if we want to avoid interpolation, we have to find a trick in such a way the feet of characteristics coincide with the grid points. This can be obtained imposing some restriction on the choice of the time step. Numerical experiments show that schemes without interpolation can be cost-effective, especially for problems that do not require a fine mesh in velocity.
Then we investigated some applications and extensions to more physical interesting problems of the numerical schemes proposed for the one dimensional BGK equation. By means of the Chu reduction [15], we extended the schemes to more realistic physical domains, 3D in velocity. Moreover, we considered boundary-value problems and we studied the treatment of reflective and diffusive boundary conditions. Finally, the methods have been extended to different BGK models for inert and reactive gas mixtures.

The thesis is organized as follows. We start by recalling the Boltzmann equation, its main physical properties and the BGK model in Chapter 1. In Chapter 2 we introduce the basics of the Runge-Kutta methods , multi-step methods, WENO reconstruction. Next in

Chapter 3, we present the high order semi-Lagrangian schemes for the BGK equation and their properties. The extension of the methods to treat boundary conditions is presented in Chapter 4. Finally, applications of the numerical schemes to BGK-type equations for gas mixtures both inert and reactive, are described in Chapter 5.

Chapter 1

The Boltzmann equation and the BGK model

Historically, kinetic theory arises for the mathematical modeling of rarefied gas dynamics. What is a rarefied gas?
A gas can be thought as a collection of a huge number of molecules moving freely in space, tending to occupy all the available volume. In the trajectory of a molecule one can distinguish two phases: a phase of free motion, in which the molecule is not affected by the presence of other molecules, and a phase of collision, strongly localized in space and time, in which the molecule collides with another molecule, significantly deviating from the path that would be followed in free flight. The size of the region of space in which the collision takes place is of the order of magnitude of the radius of action of the internal forces, which in turn is of the order of the molecular dimensions. Denote by d this typical size and by λ the mean free path of the molecules, that is the average distance between two subsequent collisions. When

$$\frac{d}{\lambda} << 1,$$

the molecule is spending most of its time in the phase of free flight with collision practically localized and instantaneous, we are in presence of a rarefied gas.
Kinetic theory represents a mesoscopic approach which lies between the macroscopic and the microscopic one, looking at both aspects. Kinetic theory takes into account collisions between particles, but describes their motion without following the individual trajectories and using instead probabilistic considerations and methods of statistical mechanics, which quantify the collective effects in an appropriate balance equation, the Boltzmann equation.

1.1 Boltzmann equation

The Boltzmann equation is named after the Austrian physicist and mathematician Ludwig Boltzmann, who proposed it in 1872 for the first time [13]. The unknown is the distribution function $f(t,x,v)$, defined in the phase space, $(t,x,v) \in \mathbb{R}^+ \times \mathbb{R}^D \times \mathbb{R}^N$ where D and N denote the dimension of the physical and velocity spaces respectively. The Boltzmann equation reads as

$$\frac{\partial f}{\partial t} + v \cdot \nabla_x f = Q(f,f) \tag{1.1}$$

with initial data

$$f(t,x,v) = f_0(x,v),$$

and describes the time evolution of a monoatomic rarefied gas of particles which move with velocity $v \in \mathbb{R}^N$ in the position $x \in \mathbb{R}^D$ at time $t > 0$. The term $v \cdot \nabla_x f$ is the so-called streaming term, which describes the free flight of the particles.
The bilinear collision (integral) operator $Q(f,f)$, which describes the binary collisions of the particles, acts over the velocity variable only

$$Q(f,f)(v) = \int_{\mathbb{R}^N} \int_{\mathbb{S}^2} B(v,w,\Omega)[f(v')f(w') - f(v)f(w)]\, d\Omega\, dw. \tag{1.2}$$

In the above expression, Ω is a unit vector of the sphere $\mathbb{S}^2$ and (v',w') represents the post-collisional velocities associated with the pre-collisional velocities (v,w). The collisional velocities satisfy microscopic momentum and energy conservations

$$v' + w' = v + w, \quad |v'|^2 + |w'|^2 = |v|^2 + |w|^2. \tag{1.3}$$

Moreover, each collision satisfies of course microscopic mass conservation. The above system of algebraic equations has the following parametrized solution

$$v' = \frac{1}{2}(v + w + |v-w|\Omega), \quad w' = \frac{1}{2}(v + w - |v-w|\Omega), \tag{1.4}$$

where $|v-w|$ is the relative speed and Ω is the unit vector of the post-collision relative velocity $v' - w' = g'$.
The collision kernel $B(v,w,\Omega)$ is a non negative function which characterizes the details of the binary interactions and depends only on $|v-w|$ and on the scattering angle χ between pre- and post collision relative velocities $v-w$ and $v'-w' = |v-w|\Omega$, with

$$cos\chi = \frac{(v-w)\cdot\Omega}{|v-w|}.$$

The collision kernel has the form

$$B(v,w,\Omega) = |v-w|\sigma(|v-w|, cos\chi),$$

where the function σ is the scattering cross-section. In the case of inverse $k-th$ power forces between particles, the collision kernel has the form

$$\sigma(|v-w|, cos\chi) = b_\alpha(cos\chi)|v-w|^{\alpha-1}, \;\; B(v,w,\Omega) = b_\alpha(cos\chi)|v-w|^\alpha,$$

with $\alpha = (k-5)/(k-1)$. For $k > 5$ we have hard potentials, for $k < 5$ we have soft potentials. The special situation $k = 5$ gives the Maxwellian model with

$$B(v,w,\Omega) = b_0(cos\chi).$$

1.2 Physical properties

1.2.1 Macroscopic moments

The Boltzmann equation, thanks to the mesoscopic nature of the kinetic approach, takes into account the microscopic collisions between the particles, giving us macroscopic information about the time evolution of the process involving the gas. Indeed, once the distribution function f is known, one is able to recover the macroscopic fields such as macroscopic density $\rho(t,x)$, macroscopic velocity $u(t,x)$ and macroscopic temperature $T(t,x)$.

The distribution function, from a physical point of view, tells us how the molecules of the gas are distributed in the phase space. Therefore, to obtain the numerical density $n(t,x)$ in the physical space, since $f(t,x,v)$ is the number of molecules in x at time t and with velocity v, the total number of molecules in x at time t is given by

$$n(t,x) = \int_{\mathbb{R}^N} f(t,x,v)\, dv.$$

Then the mass density, or macroscopic density, is given by $\rho(t,x) = m\, n(t,x)$, where m is the particle mass. This gives us another key interpretation about the distribution function. Indeed

$$\int_{\mathbb{R}^N} \frac{1}{n(t,x)} f(t,x,v)\, dv = 1,$$

so f/n can be seen as a probability density with respect to the kinetic variable v, that is, $\frac{1}{n} f\, dv$ is the probability to find out a particle in dv, at time t, in the position x.

Now, following the same argument, the mean velocity of the gas is given by

$$u(t,x) = \frac{1}{n(t,x)} \int_{\mathbb{R}^N} v\, f(t,x,v)\, dv.$$

Therefore, the momentum density is

$$\rho u = \int_{\mathbb{R}^N} mv\, f(t,x,v)\, dv.$$

The kinetic energy density is

$$E(t,x) = \int_{\mathbb{R}^N} \frac{1}{2} m v^2 \, f(t,x,v)\, dv.$$

The kinetic energy $E(t,x)$ is related to the temperature $T(t,x)$ by the underlying relation

$$E = \frac{1}{2}\rho u^2 + \frac{N}{2}\rho R T,$$

where R is the gas constant, that is related to the Boltzmann constant K_B by the expression $K_B = mR$.
Resuming, the first macroscopic fields (density, momentum, kinetic energy) can be computed in this way:

$$(\rho, \rho u, E)^T = \langle f\phi(v)\rangle, \quad \text{where } \phi(v) = \left(m, mv, \frac{1}{2}mv^2\right)^T, \ \langle g\rangle = \int_{\mathbb{R}^N} g(v)\, dv. \tag{1.5}$$

1.2.2 Collision invariants and Maxwellian equilibria

The macroscopic moments considered in (1.5) are relevant to molecular properties which are conserved by collisions, the so called *collision invariants*. Hereafter, we assume that $f \in \mathcal{B}$, where $\mathcal{B}$ denotes the space of admissible functions for the distribution function f. Essential properties of the elements of $\mathcal{B}$ are positivity and integrability. From one case to another, smooth properties will be specified.

We consider a class of function $\phi(v)$, smooth respect to v, and we compute the weak form of collision operator $Q(f,f)$

$$\int_{\mathbb{R}^N} Q(f,f)\phi(v)\, dv. \tag{1.6}$$

We observe that, if $\phi(v)$ is a molecular property, (1.6) represents the production of this molecular property due to collisions. For any test function $\phi(v)$ it can be proved [13] that

$$\int_{\mathbb{R}^N} Q(f,f)\phi(v)\, dv =$$

$$-\frac{1}{4}\int_{\mathbb{R}^N\times\mathbb{R}^N\times\mathbb{S}^2} B(v,w,\Omega)[f(v')f(w') - f(v)f(w)][\phi(v') + \phi(w') - \phi(v) - \phi(w)]\, d\Omega\, dw\, dv \tag{1.7}$$

where we have omitted the explicit dependence from t and x for the sake of simplicity.
In particular, we can choose 1, v, and v^2 as test function. Due to the microscopic mass, momentum and energy conservation (1.3) one can obtain easily that

$$\int_{\mathbb{R}^N} Q(f,f)\, dv = 0,$$

$$\int_{\mathbb{R}^N} Q(f,f)\, v\, dv = 0,$$
$$\int_{\mathbb{R}^N} Q(f,f)\, v^2\, dv = 0, \tag{1.8}$$

in others words, there is no production of mass, momentum and energy due to collisions. The molecular properties which do not vary through collisions are called collision invariants, according to the following definition

Definition 1.1. Each test function $\phi(v)$ which satisfies

$$\phi(v) + \phi(w) = \phi(v') + \phi(w') \quad \forall (v, w, \Omega) \in \mathbb{R}^N \times \mathbb{R}^N \times \mathbb{S}^2 \tag{1.9}$$

is called collision invariant.

The following results can be proved [13]

Theorem 1.2.1. *Let $\phi \in C^0$ be a collision invariant. Then there exist unique a, $c \in \mathbb{R}$, and $b \in \mathbb{R}^N$ such that*

$$\phi(v) = a + b \cdot v + cv^2. \tag{1.10}$$

Lemma 1.2.2 (Boltzmann's lemma)**.** *Let $W[f]$ be the function*

$$W[f] = \int_{\mathbb{R}^N} \ln f Q(f,f)\, dv. \tag{1.11}$$

Then $W[f]$ satisfies the following two properties:

- $W[f] \leq 0 \quad \forall f \in \mathcal{B}$,
- $W[f] = 0 \Leftrightarrow f(v')f(w') = f(v)f(w) \quad \forall (v, w, \Omega) \in \mathbb{R}^N \times \mathbb{R}^N \times \mathbb{S}^2$,

where v' and w' are given by (1.4.)

Proof. By (1.7) for $\phi(v) = \ln f$ we have

$$-W[f] =$$
$$= \frac{1}{4} \int_{\mathbb{R}^N \times \mathbb{R}^N \times \mathbb{S}^2} B(v,w,\Omega)[f(v')f(w') - f(v)f(w)][\ln(f(v')f(w')) - \ln(f(v)f(w))]\, d\Omega\, dw\, dv$$
$$= \frac{1}{4} \int_{\mathbb{R}^N \times \mathbb{R}^N \times \mathbb{S}^2} B(v,w,\Omega) \ln\left(\frac{f(v')f(w')}{f(v)f(w)}\right)\left(\frac{f(v')f(w')}{f(v)f(w)} - 1\right) f(v)f(w)\, d\Omega\, dw\, dv,$$

where $B(v,w,\Omega)$ and f are positive. Because the function $g(x) = (x-1)\ln x$ with $x \geq 0$ satisfies

- $g(x) \geq 0 \quad \forall x > 0$,

- $g(x) = 0 \Leftrightarrow x = 1$,

the thesis is proved. □

Definition 1.2. The distribution functions $f \in \mathcal{B}$ such that

$$Q(f, f)(v) = 0, \quad \forall v \in \mathbb{R}^N$$

are said equilibrium distributions.
Through Boltzmann's lemma 1.2.2 it is possible to state the following equivalence:

$$f \text{ is a collision equilibrium} \Leftrightarrow \ln(f) \text{ is a collision invariant.}$$

Thanks to Theorem 1.2.1 we get:

$$f \text{ is a collision equilibrium} \Leftrightarrow \exists\, a,\, c \in \mathbb{R}, \text{and } b \in \mathbb{R}^N \text{ such that} \ln f(v) = a + b \cdot v + cv^2$$

$$\Leftrightarrow \exists\, a,\, c \in \mathbb{R}, \text{and } b \in \mathbb{R}^N \text{such that } f(v) = e^{a+b\cdot v+cv^2}.$$

The last expression characterizes all the possible collision equilibria. Since f must be integrable, c must be strictly negative. Computing the macroscopic fields of the collision equilibria, we get

$$f(t, x, v) = M(\rho, u, T)(t, x, v) = \frac{\rho(t, x)}{(2\pi RT(t, x))^{N/2}} \exp\left(- \frac{|v - u(t, x)|^2}{2RT(t, x)} \right), \tag{1.12}$$

where ρ, u and T are the macroscopic density, velocity and temperature. The functions (1.12) are the so-called Maxwellian distributions. If (1.12) does not depend on x and t we have an absolute Maxwellian, otherwise a local Maxwellian. The H-theorem, given in the next section, will focus on the trend to equilibrium of the distribution function, solution of the Boltzmann equation.

1.2.3 H-theorem.

In this paragraph we investigate the effects of the collisions on the time evolution of the distribution function. The H-theorem is one of the most important results in this framework. It is based on the introduction of a function, the *H function,* which is directly related to the irreversibility of the physical process and to the entropy of the system. We focus on the effects of the collisions and then we consider the Boltzmann equation in a spatially uniform state ($\nabla_x f = 0$) with no external forces

$$\frac{\partial f}{\partial t} = Q(f, f). \tag{1.13}$$

Let $H[f] : \mathcal{B} \to \mathbb{R}$ be the H-function defined as follow,

$$H[f] = \int_{\mathbb{R}^N} f(t,v)\ln(f(t,v))\,dv. \tag{1.14}$$

Definition (1.14) shows that the H function depends only on time t. The time derivative leads to

$$\begin{aligned}\frac{d}{dt}H[f](t) &= \frac{d}{dt}\int_{\mathbb{R}^N} f(t,v)\ln(f(t,v))\,dv = \int_{\mathbb{R}^N}\left(\frac{\partial f}{\partial t}\ln f + f\frac{1}{f}\frac{\partial f}{\partial t}\right)dv \\ &= \int_{\mathbb{R}^N}\ln f Q(f,f)\,dv + \frac{d}{dt}\int_{\mathbb{R}^N} f\,dv = W[f]. \end{aligned}\tag{1.15}$$

Therefore, thanks to the Boltzmann's lemma 1.2.2, the *Boltzmann H-theorem* states that

$$\frac{\partial H}{\partial t} \leq 0, \tag{1.16}$$

and the equality holds only if and only if f is a collision equilibrium, that is, a local Maxwellian.

Boltzmann's H-theorem implies that the H function is a Lyapunov function for the local Maxwellian.This stresses the importance of the Maxwellian distribution functions, because each state evolves in time towards them.

1.2.4 Entropy inequality

Instead of considering (1.13), if we take into account the complete Boltzmann equation (1.1), we obtain the entropy inequality by the same steps of the previous paragraph.

Let $\phi(v) = -R\ln(f) = -\frac{K_B}{m}\ln(f)$ be a test function. We define the entropy s as

$$s = \int_{\mathbb{R}^N} f(v)\phi(v)\,dv = -\frac{K_B}{\rho}\int_{\mathbb{R}^N} f\ln f\,dv = -\frac{K_B}{\rho}H, \tag{1.17}$$

where H is the H-function. Now, we define the entropy flux h and the entropy production Σ

$$h = -\frac{K_B}{m}\int_{\mathbb{R}^N} vf\ln(f)\,dv,$$

$$\Sigma = -\frac{K_B}{m}\int_{\mathbb{R}^N}\ln(f)Q(f,f)\,dv = -\frac{K_B}{m}W[f] \geq 0.$$

The weak form of (1.1) with $\phi(v) = -\frac{K_B}{m}\ln(f)$ is

$$\frac{\partial}{\partial t}(ns) + \nabla\cdot h = \Sigma.$$

Due to the Boltzmann's lemma and the entropy production expression, the last equation becomes

$$\frac{\partial}{\partial t}(n\,s) + \nabla\cdot h \geq 0 \tag{1.18}$$

that is the entropy inequality.

1.2.5 Fluid limit

By (1.8), if we multiply the Boltzmann equation by the collision invariants $\phi(v) = m$, mv, $\frac{1}{2}mv^2$ and integrate on velocity space we obtain

$$\frac{\partial}{\partial t}\int_{\mathbb{R}^N} f\phi(v)\,dv + \nabla_x\left(\int_{\mathbb{R}^N} vf\phi(v)\,dv\right) = 0. \tag{1.19}$$

These equations describe the balance of mass, momentum and energy. The system of five equations is not closed since it involves higher order moments of the distribution function f, in addition to ρ, u, and T.

Let L be a characteristic length of the problem, and λ the mean free path. From the comparison between λ and L we can deduce important information about the behavior of the gas. Let us define

$$Kn = \frac{\lambda}{L}.$$

The parameter Kn is called the *Knudsen number*. If $Kn \sim O(1)$, that is $L \sim \lambda$, the particles cover a relative long distance between two subsequent collisions and the evolution is governed mainly by the free flow, namely by the streaming operator in the Boltzmann equation. In this case we state that we are in a *rarefied regime*. On the contrary, if $Kn \to 0$, that is $\lambda << L$, the particles will undergo a great number of collisions on a macroscopic significant distance. This is the regime where the evolution is governed by collisions and it is called *hydrodynamic or fluid regime*. In order to point out the different scaling between the physical quantities in different regimes, it could be useful to consider the dimensionless scaled Boltzmann equation

$$\frac{\partial f}{\partial t} + v\cdot\nabla_x f = \frac{1}{Kn}Q(f,f) \tag{1.20}$$

where, for simplicity, we denote by the same symbols the physical dimensionless quantity used.

As $Kn \to 0$, the collisions become more and more important and (1.20) formally becomes $Q(f,f) \to 0$, and thus f approaches the local Maxwellian. In this case the higher order moments of the distribution function can be computed as function of ρ, u, and T and by (1.19) we obtain the closed system of compressible Euler equations

$$\frac{\partial \rho}{\partial t} + \nabla_x\cdot(\rho u) = 0$$

$$\frac{\partial \rho u}{\partial t} + \nabla_x\cdot(\rho u\otimes u + pI) = 0$$

$$\frac{\partial E}{\partial t} + \nabla_x \cdot (Eu + pu) = 0$$

$$p = \rho T, \quad E = \frac{N}{2}\rho RT + \frac{1}{2}\rho u^2$$

where p is the gas pressure and $\otimes$ denotes the tensor product.
The rigorous passage from the Boltzmann equation to the compressible Euler equations has been investigated by several authors. Among them we mention [12, 38]. Higher order fluid models, such as the Navier-Stokes model, can be obtained from the Boltzmann equation using the Chapman-Enskog and the Hilbert expansions.

1.3 BGK model

One of the main shortcomings in dealing with the Boltzmann equation is the complicated structure of the collision integral (1.2).
It is therefore not surprising that alternative, simpler expressions have been proposed for the collision term; they are known as collision models, and any Boltzmann-like equation where the Boltzmann collision integral is replaced by a collision model is called a model equation or a kinetic model [13].
The idea behind this replacement is that a large amount of detail of the collisions (which are contained in the collision term) is not likely to influence significantly the values of many experimentally measured quantities. That is, unless very refined experiments are devised, it is expected that the fine structure of the collision operator can be replaced by a blurred image, based upon a simpler operator which retains only the qualitative and average properties of the true collision operator.
The most widely known collision model is usually called the Bhatnagar, Gross and Krook (BGK, 1954) model [8], although Welander proposed it independently [58]. The idea behind the BGK model is that the essential features of a collision operator are:

- the true collision term satisfies Eq. (1.8). Hence the BGK collision term must also satisfy them;
- moreover, the BGK model must satisfy the *Boltzmann H-theorem* (1.16), with equality holding if, and only if, f is a Maxwellian.

As we have seen in section 1.2.2, this second property expresses the tendency of the gas to a Maxwellian distribution. The simplest way of taking this feature into account seems to assume that the average effect of collisions is to change the distribution function f by an amount proportional to the departure of f from a Maxwellian $M[f]$. So, if ε is a constant

with respect to v, the BGK model reads as the following initial value problem

$$\begin{aligned} &\frac{\partial f}{\partial t} + v \cdot \nabla_x f = Q_{BGK}[f] \equiv \frac{1}{\varepsilon}(\mathcal{M} - f), \quad (t, x, v) \in \mathbb{R}^+ \times \mathbb{R}^D \times \mathbb{R}^N \\ &f(0, x, v) = f_0(x, v), \end{aligned} \tag{1.21}$$

where D and N denote the dimension of the physical and velocity spaces respectively, and ε is the relaxation time, that is of the order of the Knudsen number; $\mathcal{M}$ denotes a local Maxwellian. Therefore it has the same form of (1.12), but it depends on auxiliary parameters $\tilde{\rho}$, $\tilde{u}$ and $\tilde{T}$. His expression is:

$$\mathcal{M} = \frac{\tilde{\rho}}{\left[2\pi R\tilde{T}\right]^{N/2}} \exp\left(- \frac{(v - \tilde{u})^2}{2R\tilde{T}} \right). \tag{1.22}$$

The free parameters $\tilde{\rho}$, $\tilde{u}$ and $\tilde{T}$, are introduced in such a way that the BGK relaxation operator satisfies the main properties of the collision operator $Q(f, f)$. First of all, the collision operator of the Boltzmann equation satisfies (1.8), therefore, also for the relaxation operator $Q_{BGK}[f]$, the functions 1, v and v^2 must be collision invariants. In this way, the new operator does not have production of mass, momentum and energy. Thus, it is needed that the weak form of $Q_{BGK}[f]$ vanishes for $\phi(v) = 1$, v and v^2, that is

$$\int_{\mathbb{R}^N} (1, v, v^2)\mathcal{M}(v)\, dv = \int_{\mathbb{R}^N} (1, v, v^2) f\, dv. \tag{1.23}$$

By (1.23) we obtain $\tilde{\rho} = \rho$, $\tilde{u} = u$ and $\tilde{T} = T$, namely auxiliary parameters are the true moments of the distribution function f, and therefore

$$\mathcal{M} = M(\rho, u, T)(t, x, v) = \frac{\rho}{(2\pi RT(t, x))^{N/2}} \exp\left(- \frac{|v - u(t, x)|^2}{2RT(t, x)} \right). \tag{1.24}$$

The relaxation time ε, in general, can be a function of the local state of the gas. For instance, it can be inversely proportional to the density and depending on the temperature [4]:

$$\varepsilon^{-1} = A(T)\rho,$$

and hence varying with both time and space coordinates. Throughout the thesis, first in chapter 3, it is assumed to be a fixed constant for simplicity. However, when we will consider gas mixtures, the collision frequencies may vary with both time and space coordinates.

The BGK model (1.21) with $\mathcal{M}$ given by (1.24) is a consistent approximation of the Boltzmann equation. Indeed, it satisfies the main properties of the Boltzmann equation

[8, 58], such as conservation of mass, momentum and energy, as well as entropy dissipation and equilibrium solutions.
The equilibrium solutions are clearly Maxwellians, indeed

$$Q_{BGK}[f] = 0 \Leftrightarrow f = M[f].$$

The H-theorem is satisfied also for the BGK model. Indeed the Boltzmann's lemma can be easily proved:

$$\int_{\mathbb{R}^N} Q_{BGK}[f](v) \ln f(v)\, dv \leq 0. \tag{1.25}$$

Proof.

$$\int_{\mathbb{R}^N} Q_{BGK}[f](v) \ln f(v)\, dv = \int_{\mathbb{R}^N} \ln f(v) \Big(M[f](v) - f(v) \Big)\, dv =$$

$$= \int_{\mathbb{R}^N} \Big(\ln f(v) - \ln M[f](v) \Big) \Big(M[f](v) - f(v) \Big)\, dv =$$

$$= \int_{\mathbb{R}^N} \ln \frac{f(v)}{M[f](v)} \left(\frac{f(v)}{M[f](v)} - 1 \right) M[f](v)\, dv \leq 0,$$

where we used

$$\int_{\mathbb{R}^N} \ln(M[f]) \Big(M[f] - f \Big)\, dv = 0$$

because f and $M[f]$ have the same macroscopic fields.
The last inequality holds because the function $(x-1)\ln x$ is always positive except in $x = 1$ where it vanishes. Therefore, we can conclude that

$$\int_{\mathbb{R}^N} Q_{BGK}[f](v) \ln f(v)\, dv \leq 0 \quad \forall f \in \mathcal{B},$$

and

$$\int_{\mathbb{R}^N} Q_{BGK}[f](v) \ln f(v)\, dv = 0 \quad \Leftrightarrow f(v) = M[f](v).$$

□

As a consequence, the H-theorem and the entropy inequality are satisfied also for the BGK model.

We observe that the nonlinearity of the BGK relaxation operator is much worse than the nonlinearity of the collision term $Q(f, f)$. In fact, the latter is simply quadratic in f, while the former contains f in both the numerator and the denominator of an exponential (ρ, u and T appearing in $M[f]$ are functions of f).
The main advantage in using the BGK collision term is that for any given problem one can deduce integral equations for the macroscopic variables ρ, u and T. These equations

are strongly nonlinear, but simplify some iteration procedures and make the treatment of interesting problems feasible on a high speed computer.
The BGK model contains the most basic features of the Boltzmann collision integral, but has some shortcomings. Some of them can be avoided by suitable modifications, at the expense, however, of the simplicity of the model. A first modification can be introduced in order to allow the collision frequency to depend on the molecular velocity. This modification is suggested, for instance, for physical models, such as rigid spheres, where ε varies with the molecular velocity and this variation is expected to be important at high molecular velocity. Formally the modification is quite simple, but some problems arise. All the basic properties are retained, but to ensure the conservation of mass, momentum and energy, the density, velocity and temperature that now appear in the Maxwellian $M[f]$ are not the local density, velocity and temperature of the gas, but some fictitious local parameter, different from ρ, u and T, which allow us to ensure conservation properties. Analogous considerations will be done when BGK models for gas mixtures will be introduced, in Chapter 5.
A different kind of correction to the BGK model is obtained when we want to adjust the model to give the same Navier-Stokes equations as the full Boltzmann equation; in fact, the BGK model gives the value $Pr = 1$ for the Prandtl number (the ratio between the conductivity and the viscosity), a value that is not in agreement with both the true Boltzmann equation and the experimental data for a monatomic gas (which agree in giving $Pr \simeq \frac{2}{3}$). In order to have a correct Prandtl number, further adjustable parameters are required. Without going into details, this problem can be fixed by resorting to the so-called ES-BGK model [29], but in the present thesis we shall restrict to the classical BGK model.

These two aspects, the lower computational complexity and possibility to reproduce the hydrodynamic limit, explain the interest in the BGK models over the last years. Without expecting to be exhaustive, we refer for instance to [41, 57, 42, 60, 37, 3, 39] and the references therein for a more in-depth analysis of the various aspects (theoretical and numerical) of BGK models.

1.4 Chu reduction

An interesting simplification that can be introduced into the BGK equation concerns, for 1D problem in space, the possibility to describe problems in 3D velocity space by means of a system of two equations in one-dimensional velocity space. The idea is known as *Chu reduction* [15] and can be applied under suitable symmetry assumptions.

We consider the BGK equation (1.21) with $N = 3$ in a domain with axial symmetry with respect to an axis (say, $x_1 \equiv x$), in the sense that all transverse spatial gradients vanish, and the gas is drifting only in the axial direction. In such cases, distribution functions $f(t, x, \mathrm{v})$ depend on the full velocity vector $\mathrm{v} = (v_1, v_2, v_3)$ (i.e molecular trajectories are three-dimensional) but dependence on the azimuthal direction around the symmetry axis is such that all transverse components of the macroscopic velocity u vanish (i.e. $u_2 = u_3 = 0$). Let us introduce the new unknowns

$$g_1(t, x, v) = \int_{\mathbb{R}^2} f(t, x, \mathrm{v})\, dv_2 dv_3, \quad g_2(t, x, v) = \int_{\mathbb{R}^2} (v_2^2 + v_3^2) f(t, x, \mathrm{v})\, dv_2 dv_3, \tag{1.26}$$

each depending only on one space and one velocity variable $v = v_1$. Multiplication of (1.21) by 1 and $(v_2^2 + v_3^2)$ and integration with respect to $(v_2, v_3) \in \mathbb{R}^2$ yields then the following system of BGK equations for the unknown vector $g = (g_1, g_2)$, coupled with initial conditions

$$\begin{gathered} \frac{\partial g_i}{\partial t} + v \frac{\partial g_i}{\partial x} = \frac{1}{\varepsilon}(M[f]_i - g_i), \quad (t, x, v) \in \mathbb{R}_+ \times \mathbb{R} \times \mathbb{R}, \\ g_i(0, x, v) = g_{i,0}(x, v), \quad i = 1, 2. \end{gathered} \tag{1.27}$$

The BGK system (1.27) describes a relaxation process towards the vector Maxwellians $(M[f]_1, M[f]_2)$, which is obtained by Chu transform of (1.24) with $N = 3$ and has the form

$$(M[f]_1, M[f]_2) = (M[f]_1, 2RT\, M[f]_1),$$

where

$$M[f]_1 = \frac{\rho(t, x)}{\sqrt{2\pi RT(t, x)}} \exp\left(- \frac{(v - u(t, x))^2}{2RT(t, x)} \right).$$

The macroscopic moments of the distribution function f, needed to evaluate $M[f]_1$ are given in terms of g_1 and g_2 as:

$$\rho = \int_{\mathbb{R}} g_1\, dv, \qquad u = \frac{1}{\rho} \int_{\mathbb{R}} v g_1\, dv,$$
$$3RT = \frac{1}{\rho} \left[\int_{\mathbb{R}} (v - u)^2 g_1\, dv + \int_{\mathbb{R}} g_2\, dv \right].$$

The following relation holds:

$$\int_{\mathbb{R}} (v - u)^2 (M[f]_1 - g_1)\, dv + \int_{\mathbb{R}} (M[f]_2 - g_2)\, dv = 0. \tag{1.28}$$

Indeed

$$3RT\rho = \int_{\mathbb{R}} (v - u)^2 M[f]_1\, dv + 2RT \int_{\mathbb{R}} M[f]_1\, dv,$$

and also

$$3RT\rho = \int_{\mathbb{R}} (v - u)^2 g_1\, dv + \int_{\mathbb{R}} g_2\, dv.$$

Taking the difference we obtain (1.28).

Chapter 2

Basic numerical methods for evolutionary PDEs

In this chapter we will briefly recall some tools used in this thesis for the numerical solution of the BGK equation. The semi-Lagrangian technique is inspired by the method of characteristics for first order systems of linear PDEs. In order to derive a numerical method from this general idea, several ingredients should be put together, mainly a technique for ordinary differential equations to track characteristics, and a reconstruction technique to recover pointwise values of the numerical solution. To this end, in the first part of this chapter we present one-step and multi-step methods for ODEs, with particular attention to Runge-Kutta and BDF methods. Then we present non oscillatory interpolation techniques, such as ENO and WENO, needed in the numerical treatment of discontinuous solution of evolutionary PDEs. Finally, the basic ideas of semi-Lagrangian schemes for PDEs are presented.

2.1 Runge-Kutta methods for ODEs

We begin this section by introducing the generic numerical scheme for ODEs of first order[1]. We have to numerically solve the following problem

$$y' = g(t, y), \quad g : \mathbb{R} \times \mathbb{R}^m \to \mathbb{R}^m$$

$$y(0) = y_0,\ t \in [0, T]. \tag{2.1}$$

This problem is well posed when $g(t, y)$ is a Lipschitz function with respect to y, uniformly in t. Fixed a time step Δt, the continuous interval $[0, T]$ is replaced by a discrete point set

[1] A higher order equation may be always written as a first order system.

$\{t^n\}$ defined by $t^n = n\Delta t$, $n \in \mathbb{N}$. The numerical solution in this points will be denoted by $y^n \simeq y(t^n)$.
A numerical method is an equation that, starting from the discrete values $\{y^{n+1-j},\ j = 0, ...k,\ k \in \mathbb{N}\}$, allows to evaluate the discrete solution at time t^{n+1}. If k, the so-called step-number, is equal to 1 the method is one-step, otherwise it is called a multi-step method. In detail, we will examine Runge-Kutta schemes, that are a class of one-step methods, and the Backward Differentiation Formulas (BDF) schemes, that belong to the multi-step methods family.

2.1.1 One-step methods for ODEs

The main feature of a one-step method is that the numerical solution y^{n+1} depends only on the numerical solution at the previous time step. So, a one-step method can be formulated as follows,

$$y^{n+1} = y^n + \Delta t \Phi(t^n, y^n, y^{n+1}; \Delta t, g), \tag{2.2}$$

where Φ represents the numerical method. If Φ does not depend by y^{n+1} the method is explicit, else it is implicit.
Of course a good numerical method must be able to converge to the exact solution of the problem, in the limit of the time step length approaching to zero.
Definition 2.1. The method defined by (2.2) is convergent in $t \in [0, T]$ if

$$\lim_{\Delta t \to 0} |y^n - y(t)| = 0.$$

The method is called convergent in $[0, T]$ if is convergent $\forall t \in [0, T]$.
Of course convergence must be required for every numerical method. Here we introduce briefly a necessary condition to get it. To this aim we have to introduce the concept of consistency.
Let $\sigma(t, \Delta t)$ be the error obtained applying (2.2) to the exact solution in t with step Δt,

$$y(t + \Delta t) = y(t) + \Delta t \Phi(t, y(t); \Delta t, g) + \sigma(t, \Delta t).$$

The local truncation error is defined as

$$d(t, \Delta t) = \frac{\sigma(t, \Delta t)}{\Delta t}.$$

Definition 2.2. A method Φ is consistent with the ODEs (2.1) in $[0, T]$ if $d(h) \to 0$ as $\Delta t \to 0$ where

$$d(h) = max_{0 \le t \le T} |d(t, \Delta t)|.$$

Definition 2.3. A method is of order of consistency p if $d(h) = O(h^p)$.

Theorem 2.1.1. *If the function $\Phi(t, y; \Delta t)$ defines a consistent method in $[0, T]$ of order p, and if it is Lipschitz $\forall h \leq h_0$, $h_0 > 0$, then the method is convergent in $[0, T]$ with order p.*

2.1.2 Runge-Kutta methods

Runge-Kutta methods are an important family of implicit and explicit methods, which are used in temporal discretization for the approximation of solutions of ordinary differential equations.
In general, given a integer ν (number of stages), a ν-stage Runge-Kutta (RK) method has the following form:

$$k_i = g(t^n + c_i \Delta t, y^n + \sum_{j=1}^{\nu} a_{ij} k_j) \quad i = 1, ..., \nu$$

$$y^{n+1} = y^n + \Delta t \sum_{i=1}^{\nu} b_i k_i. \tag{2.3}$$

In other words, a RK method is completely characterized through its Butcher's table

$$\begin{array}{c|c} c & A \\ \hline & b^T \end{array}$$

where $A = (a_{ij})$ is a $\nu \times \nu$ matrix and $c = (1, \cdots, c_\nu)^T$ and $b = (b_1, \cdots, b_\nu)^T$ are vectors. k_i are called RK fluxes. When $a_{ij} = 0$ for $i \geq j$ we have an explicit method (ERK). If $a_{ij} = 0$ for $i > j$ and at least one $a_{ii} \neq 0$, we have a diagonal implicit RK (DIRK) method.In all other cases we speak of an implicit (IRK) method.
Usually, the coefficients satisfy the following relations:

$$\sum_{i=1}^{\nu} b_i = 1 \quad \text{and} \quad c_i = \sum_{i=1}^{\nu} a_{ij} \quad i = 1, ..., \nu.$$

The first is a consistency condition and ensures that at least first order accuracy is achieved; the second one greatly simplifies the derivation of order conditions for high order methods.

Definition 2.4. A Runge-Kutta method (2.3) has order p if for sufficiently smooth problems (2.1)

$$|y(t_0 + \Delta t) - y^(1)| \leq C h^{p+1},$$

i.e., if the Taylor series for the exact solution $y(t_0 + \Delta t)$ and for y^1 coincide up to (and including) the term h^p.

To recover the order conditions about the coefficients of the Butcher's table we have to compare the Taylor series for the exact and numerical solution. This part is very technical and we refer to [27] for more details. Here are listed the conditions to achieve order 1, 2 and 3.

- First order condition:

$$\sum_{i=1}^{\nu} b_i = 1. \tag{2.4}$$

- Second order condition:

$$\sum_{i=1}^{\nu} b_i c_i = \frac{1}{2}. \tag{2.5}$$

- Third order conditions:

$$\sum_{j=1}^{\nu}\sum_{i=1}^{\nu} b_i a_{ij} c_j = \frac{1}{6}, \qquad \sum_{i=1}^{\nu} b_i c_i^2 = \frac{1}{3}. \tag{2.6}$$

Of course to obtain second and third order the conditions for the smaller order must be satisfied. Thus, to obtain third order we have four conditions. The number of the conditions grows with p. The construction of higher order RK formulas is not an easy task. For instance, to achieve order 4, 5, 6, the number of conditions is respectively 8, 17, 37. Thus, to build a high order method one can increase the number ν of stages, but in this way also the computational cost increases. Hence, one always tries to minimize the number of intermediate stage.
Let us focus now on the stability properties of the RK methods.

2.1.3 Stability analysis for Runge-Kutta methods

Explicit methods

We consider the famous Dahlquist test equation

$$y' = \lambda y, \quad y_0 = 1, \quad z = \Delta t \lambda. \tag{2.7}$$

Using a simple explicit Euler's method to solve (2.7) we have

$$y^{n+1} = R(z) y^n$$

with

$$R(z) = 1 + z.$$

Hence it is immediate to observe that the numerical solution y^{n+1} is bounded if the argument z lies in the region

$$S = \{z \in \mathbb{C} : |R(z)| < 1\} = \{z \in \mathbb{C} : |z + 1| \leq 1\}$$

which is the circle of radius 1 and center $(-1, 0)$ on the complex plane. The function $R(z)$ is called the stability function of the method. It can be interpreted as the numerical solution after one step for (2.7). The set

$$S = \{z \in \mathbb{C} : |R(z)| < 1\} \tag{2.8}$$

is called the stability domain of the method.
The following theorem can be proved:
Theorem 2.1.2. *If an explicit RK methods is of order p, then*

$$R(z) = 1 + z + \frac{z^2}{2!} + \cdots + \frac{z^p}{p!} + O(z^{p+1})$$

and if $p = \nu$

$$R(z) = 1 + z + \frac{z^2}{2!} + \cdots + \frac{z^\nu}{\nu!}. \tag{2.9}$$

Implicit methods

Now, if we use the simple implicit Euler's method to solve (2.7) we have

$$R(z) = \frac{1}{1 + z}.$$

This time, the stability domain is the exterior of the circle with radius 1 and center $(+1, 0)$. The stability domain thus covers the entire negative half-plane and a large part of the positive half-plane as well. The implicit Euler method is thus more stable than the explicit one.
Proposition 2.1.3. *The ν-stage implicit RK method*

$$k_i = g(t^n + c_i \Delta t, y^n + \sum_{j=1}^{\nu} a_{ij} k_j) \quad i = 1, ..., \nu$$

$$y^{n+1} = y^n + \Delta t \sum_{i=1}^{\nu} b_i k_i$$

applied to (2.7) yields $y^{n+1} = R(z)y^n$ *with*

$$R(z) = 1 + zb^T (I - zA)^{-1} e,$$

where $e = (1, ..., 1)^T$.

Moreover, can be proved that for implicit method the stability function satisfies

$$R(z) = \frac{det(I - zA + zeb^T)}{dat(I - zA)}. \tag{2.10}$$

It is to observe immediately that the stability function is rational with numerator and denominator of degree $\leq \nu$.
The Dahlquist equation is stable if the eigenvalues λ lie on the entire complex half-plane $\mathbb{C}^-$.
Definition 2.5. A numerical method is said A-stable if the stability domain S is such that $S \supseteq C^-$.
A RK method with (2.10) as stability function is A-stable if and only if

$$|R(iy)| \leq 1, \ \forall y \in \mathbb{R}$$

and $R(z)$ is analytic for $Re\, z < 0$.
We have to notice that, by (2.9), an A-stable method must be implicit.

2.1.4 L-stability

Although some methods admit a stability region that coincides exactly with the negative half-plane, not always these represent the best solution. This is due to the behavior of the rational function $R(z)$ when $z \to \infty$ in case of stiff problems. This phenomena can be avoided if L-stability is required,
Definition 2.6. A numerical method is said L-stable if it is A-stable and

$$\lim_{z \to \infty} R(z) = 0.$$

A useful tool to construct an L-stable Runge-Kutta method is given by the following theorem:
Theorem 2.1.4. *If an implicit Runge-Kutta method with nonsingular A satisfies one of the following conditions:*

$$a_{\nu j} = b_j, \quad j = 1, ..., \nu, \tag{2.11}$$

$$a_{i1} = b_1, \quad i = 1, ..., s,$$

then $R(\infty) = 0$. This makes A-stable methods L-stable.
Methods satisfying (2.11) are called *stiffly accurate.*

2.2 Multi-step methods

The birth of multi-step methods is due mainly to J. C. Adams [27, 28]. In contrast to one-step methods, where the numerical solution is obtained solely from the differential equation and the initial value, a multi-step approach consists of two parts: firstly, a starting procedure which provides $y^1, \cdot, y^{n-1}$ at time $t^1, \cdot, t^{n-1}$, and, secondly, a multi-step formula to obtain an approximation to the exact solution $y(t^n)$. There are several possibilities for obtaining the starting values. Adams actually computed them using Taylor series expansion of the exact solution. Another possibility is to use any one-step method, e.g. a Runge-Kutta method. It is also usual to start with low-order multi-step methods and very small step size.
Two family of multi-step methods can be considered. One is based on numerical integration of the integral equation of (2.1) using some qradrature formula. The other one is based on interpolation. The Adams methods belong to the former, instead, the Backward Differentiation Formulas (BDF) methods belong to the latter one.

2.2.1 Adams methods

We suppose that the solution is known at time $t^n, \cdots, t^{n-q}$ and we wants the numerical solution y^{n+1} at time t^{n+1}. We consider (2.1) in integrated form,

$$y(t^{n+k}) = y(t^{n-j}) + \int_{t^{n-j}}^{t^{n+k}} g(t, y(t))\, dt. \tag{2.12}$$

On the right hand of (2.12) appears the unknown solution $y(t)$. But since the approximations $y^n, \cdots, y^{n-q}$ are known, the values $g_i = g(t^i, y^i)$ for $i = n-q, \cdots, n$ are also available and it is natural to replace the function $g(t, y(t))$ in (2.12) by the interpolation polynomial of degree q through the points (t^i, y^i), for $i = n-q, \cdots, n$. Skipping the technical steps, available in [27], one obtain the following general form for the Adams multi-steps methods

$$y^{n+k} = y^{n-j} + \Delta t \sum_{i=0}^{q} \beta_i g_{n-i}. \tag{2.13}$$

Varying the values of k and j, the Adams methods achieve different features and names:

- $j = 0$, $k = 1$: explicit Adams or Adams-Bashforth methods;
- $j = 1$, $k = 0$: implicit Adams or Adams-Moulton methods;
- $j = 1$, $k = 1$: Nyström methods (explicit methods);
- $j = 2$, $k = 0$: Milne methods (implicit methods).

2.2.2 BDF methods

The Backward Differentiation Formulas (BDF) methods are linear implicit multi-step methods that, for a given function and time, approximate the derivative of that function using information from already computed times by interpolation, thereby increasing the accuracy of the approximation. These methods are especially used for the solution of stiff differential equations.

Assume that the approximation $y^{n+1-q}, ..., y^n$ to the exact solution of (2.1) are known. In order to derive a formula for y^{n+1}, we consider the polynomial $p(t)$ which interpolates the values $\{(t^i, y^i) \,|\, i = n-q+1, ..., n+1\}$. The unknown value y^{n+1} will now be determined in such a way that the polynomial $p(t)$ satisfies the differential equation at t^{n+1}, i.e.

$$q'(t^{n+1}) = g(t^{n+1}, y^{n+1}).$$

Skipping the details, present in [27], the general form of the BDF method is

$$\sum_{i=0}^{q} \alpha_i y_{n+1-i} = \Delta t g(t^{n+1}, y^{n+1}). \tag{2.14}$$

For the sake of completeness we give the formulas related to $q = 1, 2, 3$:

$$q = 1, \quad y^{n+1} - y^n = \Delta t g(t^{n+1}, y^{n+1}), \tag{2.15}$$

$$q = 2, \quad \frac{3}{2} y^{n+1} - 2y^n + \frac{1}{2} y^{n-1} = \Delta t g(t^{n+1}, y^{n+1}), \tag{2.16}$$

$$q = 3, \quad \frac{11}{6} y^{n+1} - 3y^n + \frac{3}{2} y^{n-1} - \frac{1}{3} y^{n-2} = \Delta t g(t^{n+1}, y^{n+1}). \tag{2.17}$$

2.2.3 Local error and order conditions

The general theory of multi-step methods studies the following difference equation

$$\sum_{i=0}^{q} \alpha_i y_{n+i} = \Delta t \sum_{i=0}^{q} \beta_i g_{n+i}, \tag{2.18}$$

which includes all previously considered methods as special cases.

Definition 2.7. The local error $d(y, t, \Delta t)$ of the multi-step method (2.18) is defined by

$$d(y, t, \Delta t) = |y(t^{n+1}) - y^{n+1}|,$$

where $y(t)$ is the exact solution of (2.1) and y^{n+1} the numerical solution obtained from (2.18).

Once the local error of a multistep method is defined, one can introduce the concept of order in the same way as for one-step methods.

Definition 2.8. The multi-step method (2.18) is said to be of order p if for all sufficiently regular functions $y(t)$, we have

$$d(y, t, \Delta t) = O(\Delta t^{p+1}).$$

Our next aim is to characterize the order of a multi-step method in terms of the free parameters α_i and β_i. Dahlquist was the first to observe the fundamental role of the polynomials

$$\rho(z) = \sum_{i=0}^{q} \alpha_i z^i, \quad \sigma(z) = \sum_{i=0}^{q} \beta_i z^i.$$

They will be called the generating polynomials of the multi-step method (2.18).

Theorem 2.2.1. *The multi-step method (2.18) is of order p, if and only if one of the following equivalent conditions is satisfied:*

- $\sum_{i=0}^{q} \alpha_i = 0$ *and* $\sum_{i=0}^{q} \alpha_i i^k = k \sum_{i=0}^{q} \beta_i i^{k-1}$ *for* $k = 1, \cdots, p$;
- $\rho(e^{\Delta t}) - \Delta t \sigma(e^{\Delta t}) = O(\Delta t^{p+1})$ *for* $\Delta t \to 0$;
- $\dfrac{\rho(z)}{\ln z} - \sigma(z) = O((z-1)^p)$ *for* $z \to 1$.

Remark 1. The conditions for a multi-step method to be of order 1, which are usually called consistency conditions, can also be written in the form

$$\rho(1) = 0, \quad \rho'(1) = \sigma(1).$$

2.2.4 Stability and the first Dahlquist barrier

High order and a small local error are not sufficient for a useful multi-step method. The numerical solution can be unstable even though the step size Δt is taken very small. The essential part is the behavior of the solution as $n \to \infty$ (or $\Delta t \to 0$) with $n\Delta t$ fixed. From (2.18) for $\Delta t \to 0$ we obtain

$$\alpha_q y^{n+q} + \alpha_{q-1} y^{n+q-1} + \cdots + \alpha_0 = 0. \tag{2.19}$$

This can be interpreted as the numerical solution of the method (2.18) for the differential equation

$$y' = 0.$$

We put $y^j = z^j$ in (2.19), divide by z^n, and find that z must be a root of $\rho(z)$.

Lemma 2.2.2. *Let $z_1, \cdots, z_l$ be the roots of $\rho(z)$, of respective multiplicity $m_1, \cdots, m_l$. Then the general solution of (2.19) is given by*

$$y^n = p_1(n)z_1^n + \cdots + p_l(n)z_l^n \tag{2.20}$$

where the $p_j(n)$ are polynomials of degree $m_j - 1$.

Formula (2.20) shows us that for boundedness, and therefore stability, of y^n, as $n \to \infty$, we need that the roots of $\rho(z)$ lie in the unit disc and that the roots on the unit circle are simple.

Definition 2.9. The multi-step method (2.18) is called zero-stable if the generating polynomial $\rho(z)$ satisfies the root conditions; i.e.

- The roots of $\rho(z)$ lie on or within the unit circle;
- The roots on the unit circle are simple.

The following theorem can be proved about the relation between the stability of multi-step methods and accuracy order.

Theorem 2.2.3. *The k-step BDF formula (2.14) is stable for $q \leq 6$, and unstable for $q \geq 7$.*

Theorem 2.2.4 (The first Dahlquist barrier)**.** *The order p of a stable linear q-step method satisfies*

- *$p \leq q + 2$ if q is even,*
- *$p \leq q + 1$ if q is odd,*
- *$p \leq q$ if $\beta_q/\alpha_q \leq 0$ (in particular if the method is explicit.)*

2.2.5 A-Stability for multi-step methods

If we applied method (2.18) to the Dahlquist's test function $y' = \lambda y$ we obtain

$$(\alpha_k - \mu\beta_k)y^{n+k} + \cdots + (\alpha_0 - \mu\beta_0)y^n = 0, \quad \mu = \lambda\Delta t. \tag{2.21}$$

The characteristic equation of the difference equation (2.21) is therefore

$$\rho(z) - \mu\sigma(z) = 0, \tag{2.22}$$

which depends on the complex parameter μ. The difference equation (2.21) has stable solutions iff all roots of (2.22) are ≤ 1 in modulus. In addition, multiple roots must be strictly smaller than 1. We therefore formulate

Definition 2.10. The set S of $\mu \in \mathbb{C}$ such that all roots $z_j(\mu)$ of (2.22) satisfy $|z_j(\mu)| \leq 1$ and multiple roots satisfy $|z_j(\mu)| < 1$, is called the stability domain or region of absolute stability of method (2.18).

Definition 2.11. A multi-step method of the form (2.18) is A-stable if $S \supseteq \mathbb{C}^-$.
BDF methods are A-stable only for $q \leq 2$, see [28]. For $q = 3, 4, 5$ and 6, we see that the methods loose more and more stability, even if for $q = 3$ only a very small part of $\mathbb{C}^-$ in not included in the region of the absolute stability. For $q \geq 7$, as we know, the formulas are unstable anyway.

2.3 High order non oscillatory reconstruction

The new class of numerical methods to solve the BGK model of the Boltzmann equation, that we will introduce in Chapter 3, is based on a semi-Lagrangian formulation of (1.21)-(1.24). As we will see in the next sections, this formulation permits in principle to solve the problem along characteristics, by tracking them back until the initial time. The feet of characteristics generally will not be grid nodes, so interpolation is needed to reconstruct the distribution function from the values on the grid nodes. In this section we are going to introduce the numerical reconstruction adopted.
In order to obtain high order accuracy and to ensure the shock capturing properties of the proposed schemes near the fluid regime, a suitable nonlinear reconstruction technique for the computation of the numerical solution outside grid points is required. The numerical technique used, developed in [11], is based on a ENO (Essential Non-Oscillatory) technique reconstruction. As the name suggests, their development is due to the necessity to reconstruct a function, given by a discrete set of data, which exhibits discontinuity. In this case in fact classical high order Lagrange interpolation methods are oscillatory. Of course, these oscillations lead to numerical instability. Different ways have been proposed in the past to solve this problem. One consists in the introduction of artificial viscosity to reduce the oscillations, but this affects the solutions of the problems. Another way consists in the use of slope limiters [34]. In this case the goal was to eliminate the oscillations completely. The greater disadvantage of this method is that accuracy decreases to first order near the discontinuity. ENO (essentially non oscillator) and WENO (weighted ENO) methods [53] prevent formation of oscillations, still guaranteeing high order accuracy. Both methods are based on the reconstruction of piecewise smooth functions by choosing the interpolation points on smooth side of the function.

The original ENO and WENO techniques proposed by Shu [53], starting from the cell averages values of the unknown function, aims to reconstruct the unknown function at cell boundaries. Since we are interested in reconstruction for a generic point of the grid, we refer to WENO reconstruction developed by Carlini, Ferretti and Russo [11] by reporting

the general framework for its implementation. In the following sections we introduce this techniques.

2.3.1 The ENO approximation

Let us assume there is a smooth function $u(x)$, and we know only its cell averages $\{\bar{u}_j\}$. Then we want to construct in each cell j a polynomial p_j of a given degree $m-1$ (i.e. $p_j \in \Pi_{m-1}$)

$$p_j(x) = u(x) + O(\Delta x^m). \tag{2.23}$$

In particular, we shall be interested in evaluating this polynomial at cell boundaries:

$$u^-_{j+1/2} = p_j(x_{j+1/2}),$$

$$u^+_{j-1/2} = p_j(x_{j-1/2}).$$

Such polynomial is constructed as follows. Take m adjacent cells, that include cell j. Let these cells be denoted by $j-r, j-r+1, \cdots, j+s$ with $r+s+1=m$, $r,s \geq 0$. Then impose that

$$\langle p_j \rangle_l = \langle u \rangle_l = \frac{1}{\Delta x} \int_{x_{l-1/2}}^{x_{l+1/2}} u(x)\, dx,\ l = j-r, \cdots, j+s. \tag{2.24}$$

These m independent conditions uniquely determine a polynomial of degree $m-1$. Let us show that indeed this polynomial satisfies condition (2.23). This is easily shown by defining

$$U(x) \equiv \int_a^x u(\tilde{x})\, d\tilde{x},$$

a primitive of $u(x)$. The left bound a is not relevant. We choose it so that $a = x_{j_a-1/2}$. At the right edge of cell i one has:

$$U(x_{i+1/2}) = \Delta x \sum_{j=j_a}^{i} \bar{u}_j.$$

Let $P_j(x) \in \Pi_m$, and let $P_j(x_{i+1/2}) = U(x_{i+1/2})$, $i = j-r-1, \cdots, j+s$. These $m+1$ conditions uniquely determine $P_j \in \Pi_m$. Furthermore, from interpolation theory, one has

$$P(x) = U(x) + O(\Delta x^{m+1}),$$

and therefore

$$p(x) = P'(x) = U'(x) + O(\Delta x^m) = u(x) + O(\Delta x^m).$$

Polynomial $p(x)$ therefore satisfies (2.23) and (2.24).
There are m such polynomials. For example, for a polynomial of degree 2 one can choose

cells $j-2, j-1, j$, or $j-1, j, j+1$, or $j, j+1, j+2$. Which one should be chosen for the reconstruction? This is exactly where ENO comes into play. First, observe that for a given stencil, polynomial $P(x)$ can be computed using the divided difference of the function $U(x)$:

$$U[x_{i-1/2,x_{i+1/2}}] = \frac{U(x_{i+1/2}) - U(x_{i-1/2})}{x_{i+1/2} - x_{i-1/2}} = \bar{u}_i,$$

therefore first and higher order divided differences of U can be computed by $\{\bar{u}_j\}$, without using function U explicitly. Likewise, computation of $p(x)$ can be performed using divided differences that make use only of $\{\bar{u}_j\}$. The main purpose of the primitive function $U(x)$ is to find the proper stencil. The idea of ENO construction is the following. Take cell j, and construct a linear function between point $(x_{j-1/2}, U(x_{j-1/2}))$ and $(x_{j+1/2}, U(x_{j+1/2}))$. Let us call it $P_1(x)$. Then add one point, either to the left obtaining

$$R(x) = P_1(x) + U[x_{j-3/2}, x_{j-1/2}, x_{j+1/2}](x - x_{j-1/2})(x - x_{j+1/2}),$$

or on the right, obtaining

$$R(x) = P_1(x) + U[x_{j-1/2}, x_{j+1/2}, x_{j+3/2}](x - x_{j-1/2})(x - x_{j+1/2}).$$

Then choose the one which is less oscillatory, i.e. the one with the smallest second derivative. Therefore, extend your stencil by:

$$r \to r+1 \text{ if } |U[x_{j-3/2}, x_{j-1/2}, x_{j+1/2}]| < |U[x_{j-1/2}, x_{j+1/2}, x_{j+3/2}]|,$$

or

$$s \to s+1 \text{ if } |U[x_{j-3/2}, x_{j-1/2}, x_{j+1/2}]| > |U[x_{j-1/2}, x_{j+1/2}, x_{j+3/2}]|.$$

Then one can repeat the procedure by adding one more point to the stencil, either to the left or to the right, comparing the size of the next divided difference. The net effect of this procedure will be to choose a stencil that uses the smooth part of the function in the reconstruction.

For a given degree $m-1$, there are m possible stencils. For each of them there are two sets of coefficients [53], $\{c_{ri}\}$, $\{\tilde{c}_{ri}\}$ that compute $u^-_{j+1/2}$ and $u^+_{j-1/2}$ as a linear combination of cell averages on the stencil. These coefficients can be computed once and used later. Once the stencil is chosen (i.e. r is defined) by the ENO procedure, then one knows which set of coefficients c_{ri} one has to use. The expression for $u^-_{j+1/2}$ and $u^+_{j-1/2}$ for each choice of the stencil are of the form

$$u^-_{j+1/2} = \sum_{i=0}^{m-1} c_{ri}\bar{u}_{j-r+1},$$

$$u^+_{j-1/2} = \sum_{i=0}^{m-1} \tilde{c}_{ri}\bar{u}_{j-r+1}.$$

2.3.2 The WENO approximation

In the ENO reconstruction one chooses a stencil with m nodes to construct a polynomial of degree $m-1$, in order to reach an accuracy of $O(\Delta x^m)$ in the cell. However, the total number of points involved is $2m-1$. With all these points, a much more accurate reconstruction is possible. Suppose, for the sake of argument, that $m=3$, and that we use a parabola to reconstruct the function $u(x)$ in the cell j. Let q_k denotes the parabola obtained by matching the cell average in cells $k-1, k, k+1$, i.e. $q_k(x)$ is obtained by imposing

$$\langle q_k \rangle_l = \bar{u}_l, \quad l = k-1, k, k+1.$$

Then for our polynomial $p_j \in \Pi_2$ we can use either q_{j-1}, q_j, or q_{j+1}. Each choice would give us third order accuracy. We could also choose a convex combination of q_k,

$$p_j = \omega_{-1}^j q_{j-1} + \omega_0^j q_j + \omega_1^j q_{j+1},$$

with $\omega_{-1}^j + \omega_0^j + \omega_1^j = 1$, $\omega_l^j \geq 0, l = -1, 0, 1$. Every such convex combination would provide at least third order accuracy.
We can choose the weights according to the following requirements:

i) in the region of regularity of $u(x)$ the values of the weights are chosen in such a way to have a reconstruction of the function at some particular point with higher order of accuracy. Typically we need high order accuracy at points $x_j + \frac{\Delta x}{2}$ and $x_j - \frac{\Delta x}{2}$. With two more degrees of freedom it is possible to obtain fifth order accuracy at point $x_{j+1/2}$ (instead of third order).
We shall denote by C_{-1}^+, C_0^+, C_1^+ the constants that provide high order accuracy at point $x_{j+1/2}$:

$$p_j(x_{j+1/2}) = \sum_{k=-1}^{1} C_k^+ q_{j+k}(x_{j+1/2}) = u(x_{j+1/2}) + O(h^5),$$

and C_k^-, $k = -1, 0, 1$ the corresponding constants for high order reconstruction at point $x_{j-1/2}$,

$$p_j(x_{j-1/2}) = \sum_{k=-1}^{1} C_k^- q_{j+k}(x_{j-1/2}) = u(x_{j-1/2}) + O(h^5).$$

The value of these constants can be computed, and are given by

$$C_1^+ = C_{-1}^- = \frac{3}{10}, \quad C_0^+ = C_0^- = \frac{3}{5}, \quad C_{-1}^+ = C_1^- = \frac{1}{10}.$$

ii) in the region near a discontinuity, one should make use only of the values of the cell averages that belong to the regular part of the profile.

This is obtained by making the weights depend on the regularity of the function in the corresponding cell. In WENO scheme this results in setting

$$\alpha_k^j = \frac{C_k}{(\beta_k^j + \delta)^2}, \quad k = -1, 0, 1,$$

and

$$\omega_k^j = \frac{\alpha_k^j}{\sum_l \alpha_l^j},$$

with δ a properly small parameter, usually of order 10^{-6}. Here β_k are the so called *smoothness indicators,* and are used to measure the smoothness or, more precisely, the roughness of the function, by measuring some weighted norm of the function and its derivatives. Typically

$$\beta_k^j = \sum_{l=1}^{2} \int_{x_{j-1/2}}^{x_{j+1/2}} \Delta x^{2l-1} \left(\frac{d^l q_{j+k}(x)}{dx^l} \right)^2 dx, \; k = -1, 0, 1.$$

The integration can be carried out explicitly, obtaining

$$\beta_{-1} = \frac{13}{12}(\bar{u}_{j-2} - 2\bar{u}_{j-1} + \bar{u}_j)^2 + \frac{1}{4}(\bar{u}_{j-2} - 4\bar{u}_{j-1} + 3\bar{u}_j)^2,$$

$$\beta_0 = \frac{13}{12}(\bar{u}_{j-1} - 2\bar{u}_j + \bar{u}_{j+1})^2 + \frac{1}{4}(\bar{u}_{j-1} - \bar{u}_{j+1})^2,$$

$$\beta_1 = \frac{13}{12}(\bar{u}_j - 2\bar{u}_{j+1} + \bar{u}_{j+2})^2 + \frac{1}{4}(3\bar{u}_j - 4\bar{u}_{j+1} + \bar{u}_{j+2})^2.$$

With three parabolas one obtains a reconstruction that gives up to fifth order accuracy in smooth region, and that degrades to third order near discontinuities. A detailed description of ENO and WENO reconstruction can be found in the Chapter 4 of [53].

2.3.3 General WENO reconstruction

In the previous sections the WENO reconstruction method has been introduced. This allows us to obtain a non oscillatory high order interpolation near particular points of the computational grid, the cell boundary. Now the question concerns the WENO method for a generic point of the grid. To this aim we refer to a recent result by Carlini, Feretti and Russo [11]. In the following two sections we present as the second-third (WENO23) and the third-fifth (WENO35) order interpolation work.

2.3.4 Second-third order WENO interpolation (WENO23)

We suppose that $\{u_i\}$ is given in each grid point x_i. To construct a third order interpolation we start from two polynomials of degree two, so that

$$I[V^n](x) = \omega_L p_L(x) + \omega_R p_R(x),$$

where $p_L(x)$ and $p_R(x)$ are second order polynomials relevant to nodes x_{j-1}, x_j, x_{j+1} and x_j, x_{j+1}, x_{j+2}, respectively, see Fig. 2.1. The two linear weights C_L and C_R are first degree

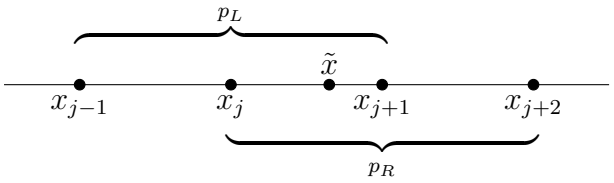

Figure 2.1: To reconstruct the unknown function in $\tilde{x}$ we need the polynomials p_L and p_R.

polynomials in x, and according to the general theory outlined so far, they read as

$$C_L = \frac{x_{j+2} - x}{3\Delta x}, \quad C_R = \frac{x - x_{j-1}}{3\Delta x};$$

the expressions of α_L, α_R, ω_L and ω_R may be easily recovered from the general form. The smoothness indicators have the following explicit expressions

$$\beta_L = \frac{13}{12}u_{j-1}^2 + \frac{16}{3}u_j^2 + \frac{25}{12}u_{j+1}^2 - \frac{13}{3}u_{j-1}u_j + \frac{13}{6}u_{j-1}u_{j+1} - \frac{19}{3}u_j u_{j+1},$$

$$\beta_R = \frac{13}{12}u_{j+2}^2 + \frac{16}{3}u_{j+1}^2 + \frac{25}{12}u_j^2 - \frac{13}{3}u_{j+2}u_{j+1} + \frac{13}{6}u_{j+2}u_j - \frac{19}{3}u_j u_{j+1}, \tag{2.25}$$

where

$$\alpha_k(x) = \frac{C_k(x)}{(\beta_k + \delta)^2} \tag{2.26}$$

(with δ a properly small parameter, usually of order 10^{-6}), and then the nonlinear weights read as

$$\omega_k = \frac{\alpha_k(x)}{\sum_l \alpha_l(x)}. \tag{2.27}$$

2.3.5 Third-fifth order WENO interpolation (WENO35)

To construct a fifth order interpolation we start from three polynomials of third degree:

$$I[V^n](x) = \omega_L p_L(x) + \omega_C p_C(x) + \omega_R p_R(x),$$

where the third order polynomials $p_L(x)$, $p_C(x)$ and $p_R(x)$ are constructed, respectively, on x_{j-2}, x_{j-1}, x_j, x_{j+1}, on x_{j-1}, x_j, x_{j+1}, x_{j+2}, and on x_j, x_{j+1}, x_{j+2}, x_{j+3}. The weights C_L, C_C and C_R are second degree polynomials in x, and have the form

$$C_L = \frac{(x - x_{j+2})(x - x_{j+3})}{20\Delta x^2}, \quad C_C = -\frac{(x - x_{j-2})(x - x_{j+3})}{10\Delta x^2},$$

$$C_R = \frac{(x - x_{j-2})(x - x_{j-1})}{20\Delta x^2},$$

while the smoothness indicators β_C and β_R have the expressions

$$\begin{aligned}\beta_C = {} & \frac{61}{45}u_{j-1}^2 + \frac{331}{30}u_j^2 + \frac{331}{30}u_{j+1}^2 + \frac{61}{45}u_{j+2}^2 - \frac{141}{20}u_{j-1}u_j + \frac{179}{30}u_{j-1}u_{j+1} \\ & - \frac{293}{180}u_{j-1}u_{j+2} - \frac{1259}{60}u_j u_{j+1} + \frac{179}{30}u_j u_{j+2} - \frac{141}{20}u_{j+1}u_{j+2}, \\ \beta_R = {} & \frac{407}{90}u_j^2 + \frac{721}{30}u_{j+1}^2 + \frac{248}{15}u_{j+2}^2 + \frac{61}{45}u_{j+3}^2 - \frac{1193}{60}u_j u_{j+3} + \frac{439}{30}u_j u_{j+2} \\ & - \frac{683}{180}u_j u_{j+3} - \frac{2309}{60}u_{j+1}u_{j+2} + \frac{309}{30}u_{j+1}u_{j+3} - \frac{553}{60}u_{j+2}u_{j+3},\end{aligned}$$

and β_L can be obtained using the same set of coefficients of β_R in a symmetric way (that is, replacing the indices $j-2, \cdots, j+3$ with $j+3, \cdots, j-2$) and α_k and ω_k are computed as in (2.26) and in (2.27).

2.4 Semi-Lagrangian schemes

The semi-Lagrangian technique for the approximation of first-order partial differential equations is based on the method of characteristics for advection equation, which accounts for the flow of information in the model equation.

At the numerical level, the semi-Lagrangian approximation mimics the method of characteristics, looking for the foot of the characteristic curve passing through every node, and following this curve for a single time step. This procedure provides methods which are unconditionally stable with respect to the choice of the time step. In this section we present this approach through some model problems.

A basic and very intuitive example to show as the semi-Lagrangian formulation works is the linear advection equation:

$$u_t(t,x) + f(t,x) \cdot u_x(u,x) = g(t,x), \quad (t,x) \in (t_0,T) \times \mathbb{R}. \tag{2.28}$$

Here, $f : (t_0,T) \times \mathbb{R} \to \mathbb{R}$ is the drift term and $g : (t_0,T) \times \mathbb{R} \to \mathbb{R}$ is the source term. We look for a solution $u : (t_0,T) \times \mathbb{R} \to \mathbb{R}$ satisfying the initial condition

$$u(t_0,x) = u_0(x), \quad x \in \mathbb{R}. \tag{2.29}$$

This is a classical model describing the transport of a scalar field, e.g. the distribution of a pollutant emitted by one of more sources (represented by g), and transported by a water stream or a wind (represented by f).
The physical interpretation is better clarified through the method of characteristics which provides an alternative characterization of the solution. In the simplest case, for $g(t,x) = 0$ and $f(t,x) = c$ (constant) the solution is given by the well known representation formula

$$u(t,x) = u_0(x - c(t - t_0)) \quad (t,x) \in (t_0, T) \times \mathbb{R}. \tag{2.30}$$

In fact, assume that a regular solution u exists. Differentiating u with respect to t along a curve of the form $(t, y(t))$, we obtain

$$\frac{d}{dt}u(t, y(t)) = u_x(t, y(t)) \cdot \dot{y}(t) + u_t(t, y(t)), \tag{2.31}$$

so that, since u solves the advection equation, the total derivative (2.31) will identically vanish along the curves which satisfy

$$\dot{y}(t) = c.$$

Such curves have the physical meaning of flow lines along which the scalar field u is transported. They are known as *characteristics* and, in this particular case, are straight lines. Then, to assign a value to the solution at a point (t,x) it suffices to follow the unique line passing through (t,x) until it crosses the x-axis at the point $z = x - c(t - t_0)$, z being the foot of the characteristic. Since the solution is constant along this line, we get expression (2.30). Conversely, it is easy to check that a function of x and t in the form (2.30) satisfies with (2.28) $f(t,x) = c$ and $g(t,x) = 0$, provided u_0 is differentiable.

2.4.1 Simple semi-Lagrangian examples of approximation schemes

Now we try to give some basic ideas (in a single space dimension) about the approximation schemes for the model problems introduced above, the linear advection equation at constant speed c (to fix ideas, we assume that $c > 0$):

$$\begin{cases} u_t + cu_x = 0 & (t,x) \in (0,T) \times \mathbb{R} \\ u(0,x) = u_0(x) & x \in \mathbb{R}. \end{cases} \tag{2.32}$$

The more classical method to construct an approximation of (2.32) is to build a uniform grid in space and time (a lattice) with constant steps Δx and Δt, covering the domain of the solution:

$$\left\{ (t^n, x_j) = (n\Delta t, j\Delta x),\ n \in \mathbb{N},\ n \le \frac{T}{\Delta t},\ j \in \mathbb{Z} \right\}.$$

The basic idea behind all finite difference approximation is to replace every derivative by an incremental ratio. Thus, one obtains a finite dimensional problem whose unknowns are the values of the numerical solution at all the nodes of the lattice, so that the value u_j^n associated to the node (t^n, x_j) should be regarded as an approximation of $u(t^n, x_j)$. For the time derivative, it is natural to choose the forward incremental ratio

$$u_t(t,x) = \frac{u(t+\Delta t, x) - u(t,x)}{\Delta t}$$

which allows, starting from the solution at the initial time t_0, to compute explicitly the approximations for increasing times $t^k > t_0$. Writing the forward incremental ratio in time at (t^n, x_j), we get

$$u_t(t^n, x_j) \simeq \frac{u_j^{n+1} - u_j^n}{\Delta t}. \tag{2.33}$$

For the approximation of u_x we have several possibilities, like

$$u_x(t^n, x_j) \simeq \frac{u_{j+1}^n - u_j^n}{\Delta x} \quad \text{(right finite difference)}$$

$$u_x(t^n, x_j) \simeq \frac{u_j^n - u_{j-1}^n}{\Delta x} \quad \text{(left finite difference)}$$

$$u_x(t^n, x_j) \simeq \frac{u_{j+1}^n - u_{j-1}^n}{2\Delta x} \quad \text{(centered finite difference)}$$

which are all based on the values at the nodes (t^n, x_k).
In this case , the choice of the approximation for u_x crucially affects the convergence of the numerical solution to the exact solution. Although centered finite difference would in principle provide a more accurate approximation of the space derivative, given the time derivative approximation (2.33), the only choice which leads to a convergent scheme [33, 34] is to use the left incremental ratio if $c > 0$, the right incremental ratio if $c < 0$, which corresponds to the so-called upwind scheme. In conclusion, for $c > 0$, we obtain a scheme in the form

$$\frac{u_j^{n+1} - u_j^n}{\Delta t} + c\frac{u_j^n - u_{j-1}^n}{\Delta x} = 0. \tag{2.34}$$

A different way to construct the approximation of (2.32) is to consider the advection term as a directional derivative and write

$$cu_x(t^n, x_j) \simeq -\frac{u^n(x_j - c\delta) - u_j^n}{\delta}$$

where δ is a small positive parameter, and u^n denotes an extension of the numerical solution (at time t^n) to be computed outside the grid points. Coupling the forward finite

difference in time with this approximation we get

$$\frac{u_j^{n+1} - u_j^n}{\Delta t} - \frac{u^n(x_j - c\delta) - u_j^n}{\delta} = 0,$$

and finally, choosing $\delta = \Delta t$, we obtain the scheme

$$u_j^{n+1} = u^n(x_j - c\Delta t). \tag{2.35}$$

This is the semi-Lagrangian scheme for (2.32), which could also be deduced from a discretization of the representation formula (2.30). Contrary to finite difference approach, semi-Lagrangian schemes use points which may not be grid nodes ($x_j - c\Delta t$ in our example), thus the corresponding values of the numerical solution need to be reconstructed by some interpolation technique. In section 2.3 we have already presented the high order interpolation techniques used to achieve high order semi-Lagrangian numerical schemes developed in chapter 3.

2.4.2 CFL condition for semi-Lagrangian schemes

In 1928, long time before the theory of convergence of numerical schemes for PDEs had become an established matter, Courant, Friedrichs and Lewy published a paper in which the concept of *domain of dependence* [33, 34, 48] was singled out as a key point for the convergence of numerical schemes. To sketch the general idea, we first define the *analytical domain of dependence* $D_d(t,x)$ of the solution u at a point (t,x), as the smallest set such that, if the initial condition u_0 of (2.32) is changed on the set $\mathbb{R}^d \setminus D_d(t,x)$, $u(t,x)$ remains unchanged. The discrete counterpart of this set is the *numerical domain of dependence* $D_d^\Delta(t,x)$, for a point $(t,x) = (t^n, x_i)$ in the space-time grid, which is the set of all nodes x_j such that $u_0(x_j)$ affects the value u_i^n.

The Courant, Friedrichs and Lewy (CFL) condition states that, for any point (t,x), the condition that the analytical domain of dependence must be included in the numerical domain of dependence, is a necessary condition for stability.
The proof of the CFL condition is very simple: if the analytical domain of dependence is not included in the numerical one, then there exist a subset of $D_d(t,x)$ which have non intersection with $D_d^\Delta(t,x)$. Therefore, since any change in the value of u_0 in this subsets modifies the value of $u(t,x)$ but not the value of the numerical approximation, the scheme cannot be convergent.
On the other hand, by the Lax equivalence theorem (which was stated about thirty years later) [33, 34] the CFL condition is also a necessary condition for stability. Indeed, since a consistent scheme is convergent if and only if it is stable, if a consistent scheme violates

the CFL condition, then this scheme is unstable.

One of the most interesting advantages of the numerical schemes based on a semi-Lagrangian formulation is that they allow to achieve stability without strict restrictions on the time step.
If we look at the upwind scheme (2.34), that can be written in the following way:

$$u_j^{n+1} = u_j^n - c\frac{\Delta t}{\Delta x}(u_j^n - u_{j-1}^n), \tag{2.36}$$

we can observe that the numerical domain of dependence is composed by x_j and x_{j-1}. The analytical one depends on the choice of the time step. A relative big time step could take the foot of characteristic with velocity $c > 0$ outside the grid cell $[x_{j-1}, x_j]$, and therefore could violate the CFL condition. So, intuitively, the CFL condition for the upwind scheme states that

$$\frac{c\Delta t}{\Delta x} < 1 \;\Leftrightarrow\; \Delta t < \frac{\Delta x}{c}. \tag{2.37}$$

The stability of the scheme can be checked in various ways. A rigorous one that can be used, since the equation and method are linear, is Fourier analysis. We look for a solution of the form

$$u_j^n = \rho^n e^{ij\xi}, \tag{2.38}$$

where $i = \sqrt{-1}$ denotes the imaginary unit. Assume $c > 0$. Then, substituting (2.38) in (2.36) we have

$$\begin{aligned}\rho &= 1 - \frac{\Delta t}{\Delta x}c(1 - e^{i\xi}) \\ &= 1 - \lambda(1 - cos\xi) - i\lambda \sin\xi,\end{aligned}$$

where $\lambda = c\Delta t/\Delta x$. Performing the calculations one has

$$|\rho|^2 = 1 - 2\lambda(1 - \lambda)(1 - cos\xi).$$

Because $1 - cos\xi \geq 0$ and $\lambda > 0$, it is $|\rho|^2 < 1$ if $1 - \lambda > 0$, and therefore if $\lambda < 1$ that is the same of (2.37).
So, if we introduce the Courant number, denoted by CFL, the upwind scheme is stable if

$$\Delta t = CFL\frac{\Delta x}{c},$$

where CFL< 1.

In the same way, we can compute the CFL condition for the semi-Lagrangian scheme for the advection equation expressed by (2.35). As we can see, in this case the numerical

domain of dependence is composed by x_j and by the foot of the characteristics $x_j - c\Delta t$. Therefore, in this case, the numerical domain of dependence is not fixed, but depends on c and Δt. In this way the analytical domain of dependence will be always included in the numerical one, and to achieve numerical stability there is no need for restrictions on time step choice.

This is the more relevant feature of numerical schemes based on a semi-Lagrangian formulation. The possibility to choose CFL numbers greater than one or more, without losing stability properties, makes them very interesting from a computational point of view, because the computational cost decreases substantially.

Chapter 3

Semi-Lagrangian schemes applied to BGK equation

In this chapter we develop and test high order numerical schemes for the BGK equation, based on a semi-Lagrangian formulation. This chapter is an extended version of the paper [24], submitted for publication.

3.1 Lagrangian formulation and first order scheme

Initially, we shall restrict to the BGK equation in one space and velocity dimension (namely $D = N = 1$ in (1.21),(1.24)). In the Lagrangian formulation, the time evolution of $f(t, x, v)$ along the characteristic lines is given by the following system:

$$\begin{aligned} &\frac{df}{dt} = \frac{1}{\varepsilon}(M[f] - f), \\ &\frac{dx}{dt} = v, \\ &x(0) = \tilde{x}, \;\; f(0, x, v) = f_0(x, v), \qquad t \geq 0, \;\; x, \, v \in \mathbb{R}. \end{aligned} \tag{3.1}$$

For simplicity, we assume constant time step Δt and uniform grid in physical and velocity space, with mesh spacing Δx and Δv respectively, and denote the grid points by $t^n = n\Delta t$, $x_i = x_0 + i\Delta x$, $i = 0, \cdots, N_x$, $v_j = j\Delta v$, $j = -N_v, \cdots, N_v$, where $N_x + 1$ and $2N_v + 1$ are the number of grid nodes in space and velocity, respectively, so that $[x_0, x_{N_x}]$ is the space domain. We also denote the approximate solution $f(t^n, x_i, v_j)$ by f_{ij}^n.
Relaxation time ε is typically of the order of the Knudsen number, defined as the ratio between the molecular mean free path length and a representative macroscopic length;

thus, the Knudsen number can vary in a wide range, from order greater than one (in rarefied regimes) to very small values (in fluid dynamic regimes).
For this reason, if we want to capture the fluid-dynamic limit, we have to use an L-stable scheme in time. An implicit first order L-stable semi-Lagrangian scheme (Fig. 3.1) can be achieved in this simple way

$$f_{ij}^{n+1} = \tilde{f}_{ij}^{n} + \frac{\Delta t}{\varepsilon}(M[f]_{ij}^{n+1} - f_{ij}^{n+1}). \tag{3.2}$$

The quantity $\tilde{f}_{ij}^{n} \simeq f(t^n, x_i - v_j\Delta t, v_j)$ can be computed by suitable reconstruction from $\{f_{\cdot j}^{n}\}$; linear reconstruction will be sufficient for first order scheme, while higher order reconstructions, such as ENO or WENO [11], may be used to achieve high order avoiding oscillations. The convergence of this first order scheme has been studied in [49].
$M[f]_{ij}^{n+1}$ is the Maxwellian constructed with the macroscopic moments of f^{n+1}:

$$M[f]_{ij}^{n+1} = M[f](x_i, v_j, t^{n+1}) = \frac{\rho_i^{n+1}}{\sqrt{2\pi R T_i^{n+1}}} exp\Big(- \frac{(v_j - u_i^{n+1})^2}{2RT_i^{n+1}} \Big).$$

This formula requires the computation of the discrete moments of f^{n+1}, through a numerical approximation of the integrals in (1.5). This is obtained in the following standard way[1]:

$$\begin{aligned}
\rho_i^{n+1} &= \sum_{j=-N_v}^{N_v} f_{ij}^{n+1}\Delta v, \\
u_i^{n+1} &= \frac{1}{\rho_i^{n+1}} \sum_{j=-N_v}^{N_v} v_j f_{ij}^{n+1}\Delta v, \\
E_i^{n+1} &= \sum_{j=-N_v}^{N_v} \frac{1}{2} v_j^2 f_{ij}^{n+1}\Delta v.
\end{aligned} \tag{3.3}$$

From now on, we will denote formulas in (3.3) with the more compact notation: $\mathsf{m}[f_{i\cdot}^{n+1}] = (\rho_i^{n+1}, (\rho u)_i^{n+1}, E_i^{n+1})$, where, in general, $\mathsf{m}[f]$ will indicate the approximated macroscopic moments related to the distribution function f.

[1] Computing the moments using this approximation of the integrals has the consequence that the discrete Maxwellian $M_{ij}^{n+1} = \frac{\rho_i^{n+1}}{\sqrt{2\pi R T_i^{n+1}}} exp(-\frac{(v_j - u_i^{n+1})^2}{2RT_i^{n+1}})$ does not have the same discrete moments as f_{ij}^{n+1}. The discrepancy is very small if the distribution function is smooth and the number of points in velocity space is large enough, because midpoint rule is spectrally accurate for smooth functions having (numerically) compact support. However, for small values of N_v, such discrepancy can be noticeable. To avoid this drawback, Mieussens introduced a discrete Maxwellian [37, 36]. The computation of the parameters of such Maxwellian requires the solution of a non linear system. A comparison between the continuous and discrete Maxwellian can be found, for example, in [2]. Here we shall neglect this effect, and assume that, using eq. (3.3), M_{ij}^{n+1} and f_{ij}^{n+1} have the same moments with sufficient approximation.

Now it is evident that Equation (3.2) cannot be immediately solved for f_{ij}^{n+1}. It is a non linear implicit equation because the Maxwellian depends on f^{n+1} itself through its moments. To solve this implicit step one can act as follows. Let us take the moments of equation (3.2); this is obtained at the discrete level multiplying both sides by $\phi_j \Delta v$, where $\phi_j = \{1, v_j, v_j^2\}$ and summing over j as in (3.3). Then we have

$$\sum_j (f_{ij}^{n+1} - \tilde{f}_{ij}^n)\phi_j = \frac{\Delta t}{\varepsilon} \sum_j (M[f]_{ij}^{n+1} - f_{ij}^{n+1})\phi_j,$$

which implies that

$$\sum_j f_{ij}^{n+1}\phi_j \simeq \sum_j \tilde{f}_{ij}^n \phi_j,$$

because, by definition, the Maxwellian at time t^{n+1} has the same moments as f^{n+1} and we assume that equations (3.3) is accurate enough. This in turn gives

$$\mathsf{m}[f_{i\cdot}^{n+1}] \simeq \mathsf{m}[\tilde{f}_{i\cdot}^n]. \tag{3.4}$$

Once the Maxwellian at time t^{n+1} is known using the approximated macroscopic moments $\mathsf{m}[\tilde{f}_{i\cdot}^n]$, the distribution function f_{ij}^{n+1} can be explicitly computed

$$f_{ij}^{n+1} = \frac{\varepsilon \tilde{f}_{ij}^n + \Delta t M_{ij}^{n+1}}{\varepsilon + \Delta t}. \tag{3.5}$$

This approach has already been used in [49, 50, 51], and in [42] in the context of Eulerian schemes.

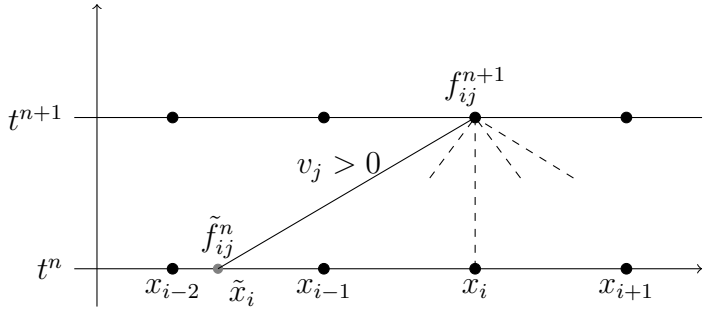

Figure 3.1: Representation of the implicit first order scheme. The foot of the characteristic does not lie on the grid, and some interpolation is needed to compute $\tilde{f}_{ij}^n$.

3.2 High order Runge-Kutta methods

The scheme of the previous section corresponds to implicit Euler applied to the BGK model in characteristic form. High order discretization in time can be obtained by Runge-Kutta or BDF methods.
In [50, 51], the relaxation operator has been dealt with an L-stable diagonally implicit Runge-Kutta scheme [28]. DIRK schemes are completely characterized by the triangular $\nu \times \nu$ matrix $A = (a_{lk})$, and the coefficients vectors $c = (1, \cdots, c_\nu)^T$ and $b = (b_1, \cdots, b_\nu)^T$, which are derived by imposing accuracy and stability constraints as described in Section 2.1.2 [28].
DIRK schemes can be represented through the Butcher's table

$$\begin{array}{c|c} c & A \\ \hline & b^T \end{array}$$

Here we consider the following DIRK schemes

$$\text{RK2} = \begin{array}{c|cc} \alpha & \alpha & 0 \\ 1 & 1\text{-}\alpha & \alpha \\ \hline & 1\text{-}\alpha & \alpha \end{array}, \qquad \text{RK3} = \begin{array}{c|ccc} \frac{1}{2} & \gamma & 0 & 0 \\ (1+\gamma)/2 & (1-\gamma)/2 & \gamma & 0 \\ 1 & 1-\delta-\gamma & \delta & \gamma \\ \hline & 1-\delta-\gamma & \delta & \gamma \end{array}$$

which are a second and third order L-stable schemes, respectively [5]. The coefficient α is

$$\alpha = 1 - \frac{\sqrt{2}}{2},$$

while γ is the middle root of $6x^3 - 18x^2 + 9x - 1$, $\gamma \simeq 0.4358665215$, and $\delta = 3/2\gamma^2 - 5\gamma + 5/4 \simeq -0.644363171$. Both RK schemes have the property that the last row of the matrix A equals b^T, therefore the numerical solution is equal to the last stage value. Such schemes are called "stiffly accurate". An A-stable scheme which is stiffly accurate is also L-stable, as seen in section 2.1.4 [28]. Applying the DIRK schemes to the characteristic formulation of the BGK equation (3.1), the numerical solution is obtained as

$$f_{ij}^{n+1} = f_{ij}^{(\nu,n)} + \Delta t \sum_{\ell=1}^{\nu} b_\ell K_{ij}^{(\nu,\ell)}, \tag{3.6}$$

where

$$K_{ij}^{(\nu,\ell)} = \frac{1}{\varepsilon}(M[F_{ij}^{(\nu,\ell)}] - F_{ij}^{(\nu,\ell)})$$

denote the RK fluxes on the characteristics $x = x_i + v_j(t - t^{n+1})$, and

$$F_{ij}^{(\nu,\ell)} = f_{ij}^{(\nu,n)} + \Delta t \sum_{k=1}^{\ell} a_{\ell k} K_{ij}^{(\ell,k)}$$

are the stage values; the first index of the pair (ν, ℓ) indicates that we are along the ν-th characteristic and the second one denotes that we are computing the ℓ-th stage value. Moreover $f_{ij}^{(\nu,n)} \equiv f(t^n, x_i - c_\nu \Delta t v_j, v_j)$.

In a standard DIRK method, the ℓ-th stage value, say $F_{ij}^{(\nu,\ell)}$, is evaluated by solving an implicit equation involving only $F_{ij}^{(\nu,\ell)}$, since the previous stage values have already been computed, due to the triangular structure of the matrix A. In our case this is not so easy, because if the point corresponding to stage ℓ along the characteristics is not a grid point, it is not possible to compute the moments of the Maxwellian at that point in space-time; indeed, after multiplying by ϕ_j and summing on j, the elements of the sum are computed in variable space points, so we cannot take advantage of the useful properties of the collision invariants. For this reason, we need two kinds of stage values: the stage value along the characteristics, $F_{ij}^{(\nu,\ell)}$, and the stage values on the grid, $F_{ij}^{(\ell,\ell)}$ (see Figure 3.2 and 3.3).
Second and third order RK schemes are described below.

3.2.1 Second order Runge-Kutta method

The general form of RK2 is (see Fig. 3.2)

$$f_{ij}^{n+1} = f_{ij}^{(2,n)} + \Delta t(b_1 K_{ij}^{(2,1)} + b_2 K_{ij}^{(2,2)}). \tag{3.7}$$

First we compute $F_{ij}^{(1,1)}$ in the grid node by

$$F_{ij}^{(1,1)} = \frac{\varepsilon f_{ij}^{(1,n)} + \Delta t a_{11} M_{ij}^{(1,1)}}{\varepsilon + \Delta t a_{11}}.$$

The Maxwellian $M_{ij}^{(1,1)} = M[F_{ij}^{(1,1)}]$ can be evaluated by means of the macroscopic moments $\mathsf{m}[f_{i\cdot}^{(1,n)}]$, using an argument similar to the one adopted in (3.4). $f_{i,j}^{(1,n)} = f(t^n, x_i - c_1 v_j \Delta t, v_j)$ can be computed by a suitable WENO space reconstruction at time t^n [11]; in Section 2.3.3 we reported the WENO reconstructions adopted in these cases.

Once the implicit step is solved, the Runge-Kutta fluxes $K_{ij}^{(2,1)} = \frac{1}{\varepsilon}(M[F_{ij}^{(1,1)}] - F_{ij}^{(1,1)})$ are computed by high order interpolation on the intermediate nodes $\tilde{x}^{(3)}$ along the characteristics. Then the second stage value can be computed by

$$F_{ij}^{(2,2)} = f_{ij}^{(2,n)} + \Delta t\left(a_{21} K_{ij}^{(2,1)} + a_{22}\frac{1}{\varepsilon}(M[F_{ij}^{(2,2)}] - F_{ij}^{(2,2)})\right). \tag{3.8}$$

Equation (3.8) cannot be immediately solved because the Maxwellian depends on $F_{ij}^{(2,2)}$ itself. However, if we take the moments of both sides of equation (3.8), we can compute the

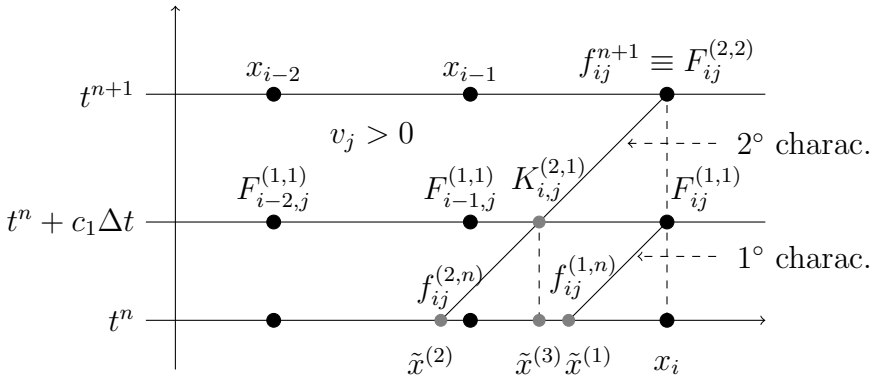

Figure 3.2: Representation of the RK2 scheme. The black circles denote grid nodes, the gray ones the points where interpolation is needed.

moments of $F_{ij}^{(2,2)}$ since the elements of the sum on j containing the Maxwellian $M[F_{ij}^{(2,2)}]$ are now on fixed space points. Indeed

$$\sum_j \left(F_{ij}^{(2,2)} - f_{ij}^{(2,n)} - \Delta t a_{21} K_{ij}^{(2,1)} \right) \phi_j = a_{22} \frac{\Delta t}{\varepsilon} \sum_j \left(M[F_{ij}^{(2,2)}] - F_{ij}^{(2,2)} \right) \phi_j = 0,$$

thus the moments are given by $\mathsf{m}[F_{i\cdot}^{(2,2)}] = \mathsf{m}[f_{i\cdot}^{(2,n)} + \Delta t a_{21} K_{i\cdot}^{(2,1)}]$, so we can compute $M[F_{ij}^{(2,2)}]$, and solve the implicit step for $F_{ij}^{(2,2)}$.
Notice that $f_{ij}^{n+1} = F_{ij}^{(2,2)}$, because the scheme is stiffly accurate, i.e the last row of the matrix A is equal to the vector of weights.

3.2.2 Third order Runge-Kutta method

The RK3 scheme works in a similar way, and Fig. 3.3 shows the procedure.

Algorithm (RK3)

- Calculate $f_{i,j}^{(1,n)} = f(t^n, \tilde{x}^{(1)} = x_i - c_1 v_j \Delta t, v_j)$, $f_{i,j}^{(2,n)} = f(t^n, \tilde{x}^{(2)} = x_i - c_2 v_j \Delta t, v_j)$, $f_{i,j}^{(3,n)} = f(t^n, \tilde{x}^{(4)} = x_i - v_j \Delta t, v_j)$ by interpolation from $f_{\cdot j}^n$;
- Calculate $F_{ij}^{(1,1)}$ in the grid node using the technique (3.4), (3.5), with Δt replaced by $c_1 \Delta t$. Given $F_{ij}^{(1,1)}$, one can evaluate the Runge-Kutta fluxes $K_{ij}^{(1,1)} = \frac{1}{\varepsilon}\Big(M[F_{ij}^{(1,1)}] - F_{ij}^{(1,1)} \Big)$ in the grid nodes and then calculate $K_{ij}^{(2,1)}$ and $K_{ij}^{(3,1)}$ by interpolation from $K_{\cdot j}^{(1,1)}$ in $\tilde{x}^{(3)} = x_i - (c_2 - c_1) v_j \Delta t$ and $\tilde{x}^{(5)} = x_i - (1 - c_1) v_j \Delta t$, respectively;

- Calculate $F_{ij}^{(2,2)}$ in the grid node using RK2 scheme described in the previous section with time step $c_2\Delta t$. Given $F_{ij}^{(2,2)}$, one can evaluate $K_{ij}^{(2,2)} = \frac{1}{\varepsilon}\left(M[F_{ij}^{(2,2)}] - F_{ij}^{(2,2)}\right)$ in the grid nodes and then calculate $K_{ij}^{(3,2)}$ by interpolation from $K_{\cdot j}^{(2,2)}$ in $\tilde{x}^{(6)} = x_i - (1-c_2)v_j\Delta t$;
- Now one can update f_{ij}^{n+1} using (3.6), taking into account that the method is stiffly accurate and using the properties of the collision invariants to solve the implicit step.

Summary of the Runge-Kutta schemes

Three schemes based on RK are tested:

- scheme RK2W23: uses WENO23 for the interpolation and RK2, as described above, for time integration;
- scheme RK3W23: uses WENO23 for the interpolation and RK3, as described above, for time integration;
- scheme RK3W35: uses WENO35 for interpolation and RK3 for time integration.

Remark.

In practice, the Runge-Kutta fluxes can be computed from the internal stages. For example, using RK2, we have

$$K_{ij}^{(1,1)} = \frac{1}{\varepsilon}(M[F_{ij}^{(1,1)}] - F_{ij}^{(1,1)}) = \frac{F_{ij}^{(1,1)} - f_{ij}^{(1,n)}}{\Delta t a_{11}}.$$

The latter expression can be used in the limit $\varepsilon \to 0$, with no constraint on the time step.

3.3 BDF methods

In this section we present a new family of high order semi-Lagrangian schemes, based on BDF. The backward differentiation formulas are implicit linear multistep methods for the numerical integration of ordinary differential equations $y' = g(t, y)$, and they had been recalled in Section 2.2.2. Using the linear polynomial interpolating y^n and y^{n-1} one obtains the simplest first order BDF method (BDF1) that corresponds to backward Euler, used in Section 3.1.

Here the characteristic formulation of the BGK model, that leads to ordinary differential equations, is approximated by using BDF2 and BDF3 methods, in order to obtain

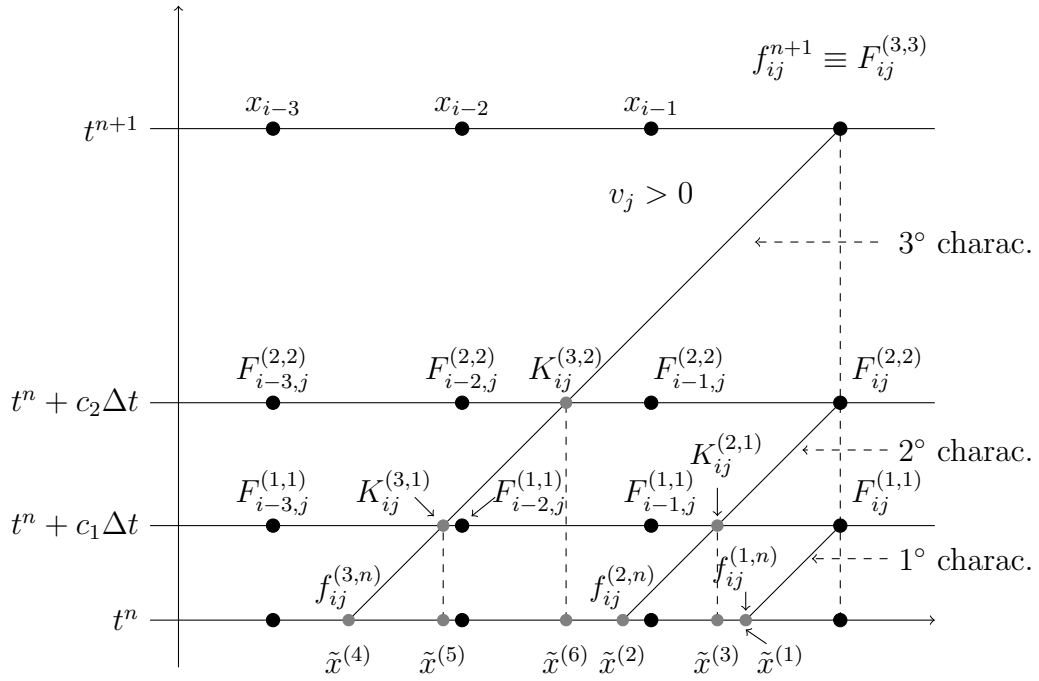

Figure 3.3: Representation of the RK3 scheme. The black circles denote grid nodes, the gray ones the points where interpolation is needed.

high order approximation. The relevant expressions, under the hypothesis that the time step Δt is fixed, are:

$$\text{BDF2} := \quad y^{n+1} = \frac{4}{3}y^n - \frac{1}{3}y^{n-1} + \frac{2}{3}\Delta t\, g(y^{n+1}, t^{n+1}), \tag{3.9}$$

$$\text{BDF3} := \quad y^{n+1} = \frac{18}{11}y^n - \frac{9}{11}y^{n-1} + \frac{2}{11}y^{n-2} + \frac{6}{11}\Delta t\, g(y^{n+1}, t^n). \tag{3.10}$$

Here we apply the BDF methods along the characteristics.

3.3.1 Second order BDF method.

The numerical approximation of the first equation in (3.1) is obtained as

$$\text{BDF2} := \quad f_{i,j}^{n+1} = \frac{4}{3}f_{ij}^{n,1} - \frac{1}{3}f_{ij}^{n-1,2} + \frac{2}{3}\frac{\Delta t}{\epsilon}(M[f]_{ij}^{n+1} - f_{ij}^{n+1}), \tag{3.11}$$

where $f_{i,j}^{n-(s-1),s} \simeq f(t^{n-(s-1)}, x_i - sv_j\Delta t, v_j)$, can be computed by suitable reconstruction from $\{f_{\cdot j}^{n-(s-1)}\}$; high order reconstruction will be needed for BDF2 and BDF3 schemes, and again we make use of the WENO techniques [11], recalled in Chapter 2, for accurate non oscillatory reconstruction.

To compute the solution f_{ij}^{n+1} from equations (3.11), also in this case one has to solve a non linear implicit equation. We can act as previously done for the backward Euler method, by taking advantage of the properties of the collision invariants. Thus we multiply both sides of the equation (3.11) by ϕ_j and sum over j, getting

$$\sum_j \left(f_{ij}^{n+1} - \frac{4}{3} f_{ij}^{n,1} + \frac{1}{3} f_{ij}^{n-1,2} \right) \phi_j = \frac{2\Delta t}{3\varepsilon} \sum_j (M[f]_{ij}^{n+1} - f_{ij}^{n+1}) \phi_j,$$

which implies that

$$\sum_j (f_{ij}^{n+1}) \phi_j = \sum_j \left(\frac{4}{3} f_{ij}^{n,1} - \frac{1}{3} f_{ij}^{n-1,2} \right) \phi_j,$$

so in Equation (3.11) we can compute $M[f_{ij}^{n+1}]$ with the usual procedure, adopting the approximated macroscopic moments

$$(\rho_i^{n+1}, (\rho u)_i^{n+1}, E_i^{n+1}) = \mathsf{m} \left[\frac{4}{3} f_{i\cdot}^{n,1} - \frac{1}{3} f_{i\cdot}^{n-1,2} \right]. \tag{3.12}$$

Once the Maxwellian $M[f_{ij}^{n+1}]$ is computed, the distribution function value f_{ij}^{n+1} can be easily obtained from schemes (3.11) for BDF2. The procedure for BDF2 is sketched in Fig. 3.4 and described in the following algorithm.

Algorithm (BDF2)

- Calculate $f_{ij}^{n-1,2} = f(t^{n-1}, \tilde{x}_2 = x_i - 2v_j\Delta t, v_j)$, $f_{ij}^{n,1} = f(t^n, \tilde{x}_1 = x_i - v_j\Delta t, v_j)$ by interpolation from $f_{\cdot j}^{n-1}$ and $f_{\cdot j}^{n}$ respectively;
- Compute the Maxwellian $M[f_{ij}^{n+1}]$ using (3.12) and upgrade the numerical solution f_{ij}^{n+1}.

A similar algorithm is obtained using BDF3, as we will see in the next subsection.

3.3.2 Third order BDF method.

The numerical solution of the BGK equation in (3.1) is obtained as

$$f_{i,j}^{n+1} = \frac{18}{11} f_{ij}^{n,1} - \frac{9}{11} f_{ij}^{n-1,2} + \frac{2}{11} f_{ij}^{n-2,3} + \frac{6}{11} \frac{\Delta t}{\epsilon} (M[f]_{ij}^{n+1} - f_{ij}^{n+1}), \tag{3.13}$$

where $f_{i,j}^{n-(s-1),s}$ can be computed by suitable reconstruction from $\{f_{\cdot j}^{n-(s-1)}\}$.

To compute the solution f_{ij}^{n+1} from equation (3.13) we need again to take moments of such equation

$$\sum_j \left(f_{ij}^{n+1} - \frac{18}{11} f_{ij}^{n,1} + \frac{9}{11} f_{ij}^{n-1,2} - \frac{2}{11} f_{ij}^{n-2,3} \right) \phi_j = \frac{6\Delta t}{11\varepsilon} \sum_j (M[f]_{ij}^{n+1} - f_{ij}^{n+1}) \phi_j,$$

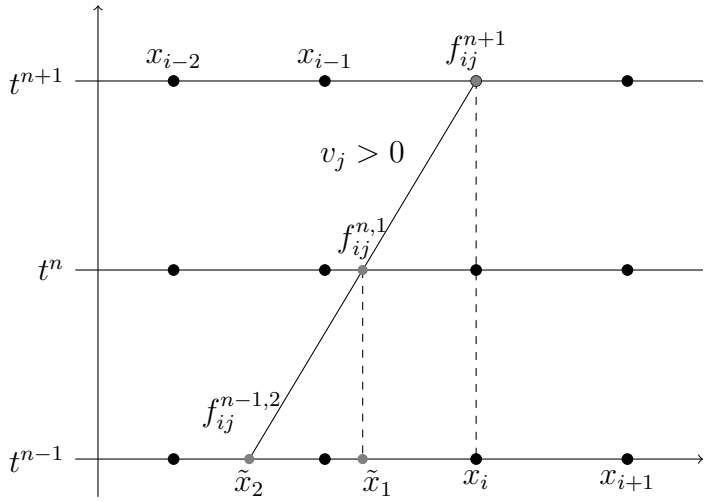

Figure 3.4: Representation of the BDF2 scheme. The black circles denote grid nodes, the gray ones the points where interpolation is needed.

which implies that

$$\sum_j (f_{ij}^{n+1})\phi_j = \sum_j \left(\frac{18}{11} f_{ij}^{n,1} - \frac{9}{11} f_{ij}^{n-1,2} + \frac{2}{11} f_{ij}^{n-2,3}\right)\phi_j,$$

so in Equation (3.13) we can compute $M[f_{ij}^{n+1}]$ with the usual procedure, adopting the approximated macroscopic moments

$$(\rho_i^{n+1}, (\rho u)_i^{n+1}, E_i^{n+1}) = m\left[\frac{18}{11} f_{i\cdot}^{n,1} - \frac{9}{11} f_{i\cdot}^{n-1,2} + \frac{2}{11} f_{i\cdot}^{n-2,3}\right]$$

Once the Maxwellian $M[f_{ij}^{n+1}]$ is computed, the distribution function value f_{ij}^{n+1} can be easily obtained from schemes (3.13) for BDF3. This procedure is sketched in Fig. 3.5.

To compute the starting values f_{ij}^1 for BDF2 and f_{ij}^1, f_{ij}^2 for BDF3 we have used, as predictor, Runge-Kutta methods of order 2 and 3, respectively.

Summary of the BDF schemes

Three schemes based on BDF are tested:

- scheme BDF2W23: uses WENO23 for the interpolation and BDF2, as described above, for time integration;

- scheme BDF3W23: uses WENO23 for the interpolation and BDF2, as described above, for time integration;
- scheme BDF3W35: uses WENO35 for interpolation and BDF3 for time integration.

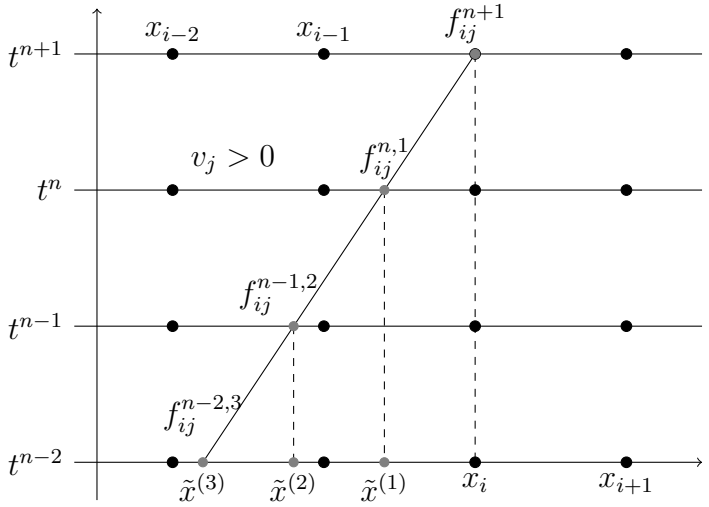

Figure 3.5: Representation of the BDF3 scheme. The black circles denote grid nodes, the gray ones the points where interpolation is needed.

At variance with Runge-Kutta methods, BDF methods do not need to compute intermediate stage values, and the implicit step for the Maxwellian is solved only once during a time step. Moreover, we have to interpolate in less out-of-grid points (for instance, we have to perform only 3 interpolations in a time step using BDF3, versus 6 interpolations needed to advance one time step using a DIRK method of order 3). This makes BDF methods very efficient from a computational point of view.

Remark

Using a scheme based on a Eulerian formulation, only one reconstruction is necessary at each time step, at variance with 3 or 6 reconstructions needed for the third order semi-Lagrangian BDF or Runge-Kutta methods, respectively. Nevertheless, semi-Lagrangian schemes are competitive against Eulerian ones, because the former do not have to fulfill the classical Courant restriction on the time step (CFL ≤ 1). In rarefied regime, for instance, it is possible to use CFL ≈ 10 with semi-Lagrangian schemes, and they turn out to be more efficient than Eulerian schemes. In the solution of Riemann problems in fluid regime semi-Lagrangian schemes work well using CFL $\leq 2-3$. In this case semi-Lagrangian and Eulerian schemes are comparable from a computational point of view. A more detailed study on this argument is under investigation.

3.4 Semi-lagrangian schemes without interpolation

As we can observe, the cost of the schemes presented above is mainly due to the interpolation, especially when we use high order interpolation techniques.
In order to reduce the computational cost we look for schemes that avoid interpolation. The key idea is to choose discretization parameters in such a way that all the characteristics connect grid points in space. This is obtained, for example, by choosing $\Delta v \Delta t = \Delta x$ (see Fig. 3.6).

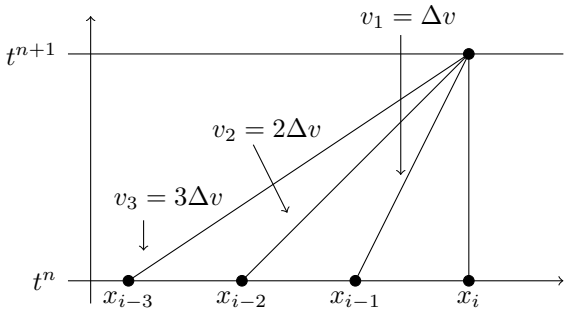

Figure 3.6: Implicit first order scheme without interpolation.

This choice corresponds to solve the equation at each characteristics by implicit Euler, thus resulting in a first order method in time. In order to increase the order of accuracy one can resort to BDF or RK time discretization. We have to observe that with the choice $\Delta v \Delta t = \Delta x$, which corresponds to have $CFL = N_v$, BDF2 and BDF3 can be easily applied in this setting. More difficult is the construction of higher order RK schemes that avoid interpolation.

3.4.1 Construction of suitable high order Runge-Kutta schemes which avoid interpolation

The use of higher order RK schemes requires indeed that the stage values lie on the grid as well. This is obtained by imposing $\Delta v \Delta t = s\Delta x$, $s \in \mathbb{N}$. In this case the coefficients of the vector c must be multiples of $1/s$. Moreover we need a L-stable scheme. We can easily recover a L-stable scheme building an A-stable stiffly accurate method, by Theorem 2.1.4, that is, imposing that the vector b is equal to the last row of the matrix A. Furthermore, looking for high order methods we have also to impose accuracy and stability constraints (2.4), (2.5) and (2.6) on the coefficients of the Butcher's table. If we satisfy all these conditions, we will have a high order L-stable DIRK scheme that avoids interpolation.

Looking for a second order scheme, we have examined the following possible choices for the vector c

1 $c = (1/2, 1)$, where $s = 2$;

2 $c = (1/3, 1)$, where $s = 3$;

3 $c = (2/3, 1)$, where $s = 3$.

Respectively, we obtain the following DIRK schemes:

$$T_1 = \begin{array}{c|cc} 1/2 & 1/2 & 0 \\ 1 & 1 & 0 \\ \hline & 1 & 0 \end{array} \qquad T_2 = \begin{array}{c|cc} 1/3 & 1/3 & 0 \\ 1 & 3/4 & 1/4 \\ \hline & 3/4 & 1/4 \end{array} \qquad T_3 = \begin{array}{c|cc} 2/3 & 2/3 & 0 \\ 1 & 3/2 & -1/2 \\ \hline & 3/2 & -1/2 \end{array}$$

Instead, looking for a third order scheme, we have examined the following possible choices for the the vector c

1 $c = (1/4, 1/2, 1)$;

2 $c = (1/4, 3/4, 1)$;

3 $c = (1/2, 3/4, 1)$;

Respectively, we obtain the following DIRK schemes:

$$A_1 = \begin{array}{c|ccc} 1/4 & 1/4 & 0 & 0 \\ 1/2 & 1/2 & 0 & 0 \\ 1 & 4/9 & 1/3 & 2/9 \\ \hline & 4/9 & 1/3 & 2/9 \end{array} \qquad A_2 = \begin{array}{c|ccc} 1/4 & 1/4 & 0 & 0 \\ 3/4 & 325/3 & -1291/12 & 0 \\ 1 & 5/9 & 1/3 & 1/9 \\ \hline & 5/9 & 1/3 & 1/9 \end{array}$$

$$A_3 = \begin{array}{c|ccc} 1/2 & 1/2 & 0 & 0 \\ 3/4 & 1/2 & 1/4 & 0 \\ 1 & 5/3 & -4/3 & 2/3 \\ \hline & 5/3 & -4/3 & 2/3 \end{array}$$

Here $s = 4$. With $s = 3$, that is $c = (1/3, 2/3, 1)$, the system of the constraints giving a third order L-stable DIRK scheme that avoids interpolation, have no solutions.
As we can notice, the scheme T_1 is the implicit midpoint scheme. It is well known that the midpoint scheme is not L-stable because its stability function is

$$R(z) = \frac{1 + z/2}{1 - z/2}$$

that does not fulfill Definition 2.6 as $z \to \infty$. The others schemes, T_2, T_3, A_1, A_2, A_3 are stiffly accurate by construction. By Theorem 2.1.4, if they are A-stable, they will be L-stable. In Fig. 3.7 the stability regions of such schemes are shown. Recalling that a Runge-Kutta scheme is A-stable if the A-stability region includes $\mathbb{C}^-$, by Fig. 3.7 we can deduce that only the schemes T_2 and A_3 are A-stable and therefore they are L-stable DIRK schemes avoiding interpolation of second and third order, respectively.
Using schemes that avoid the interpolation, the choice of the time step is determined by the other discretization steps, and the CFL number is fixed to sN_v for DIRK schemes, whereas is Nv for each BDF methods. This means that we have very large time step for DIRK schemes. The semi-Lagrangian nature of the family of schemes introduced in the previous sections, allows us to use large CFL numbers. Nonetheless, for example, choosing $N_v = 20$, the use of schemes with $s = 4$ leads to $CFL = 80$. In these cases, i.e. scheme A_3, some instabilities arise in the numerical solution, but using a fine space grid we are able to obtain good numerical solution. The high number of space points is not a computational problem, because these schemes does not require interpolation and for this reason are very efficient from a computational point of view. We notice that the BDF schemes do have not this problem because in this case $s = 1$. Moreover these schemes are very simple to implement and therefore each time step can be advanced very efficiently.
A comparison with more standard semi-Lagrangian methods that make use of interpolation will be presented in the Section 3.6 on numerical results. Numerical experiments show that schemes without interpolation can be cost-effective, especially for problems that do not require a fine mesh in velocity. In particular, BDF3 without interpolation appears to have the best performance in most tests.

3.5 Chu reduction model

The schemes presented before have been extended to treat problems in 3D in velocity, 1D in space, in slab geometry. The starting point is the Chu reduction [15] introduced in Section 1.4, which, under suitable symmetry assumption, allows to transform a 3D equation (in velocity) in a system of two equations 1D (in velocity), to which the schemes previously introduced can be applied.
The system of BGK equations to discretize is the following:

$$\frac{\partial g_i}{\partial t} + v\frac{\partial g_i}{\partial x} = \frac{1}{\varepsilon}(M[f]_i - g_i), \quad (t, x, v) \in \mathbb{R}_+ \times \mathbb{R} \times \mathbb{R}, \tag{3.14}$$

$$g_s(0, x, v) = g_{s,0}(x, v), \quad s = 1, 2.$$

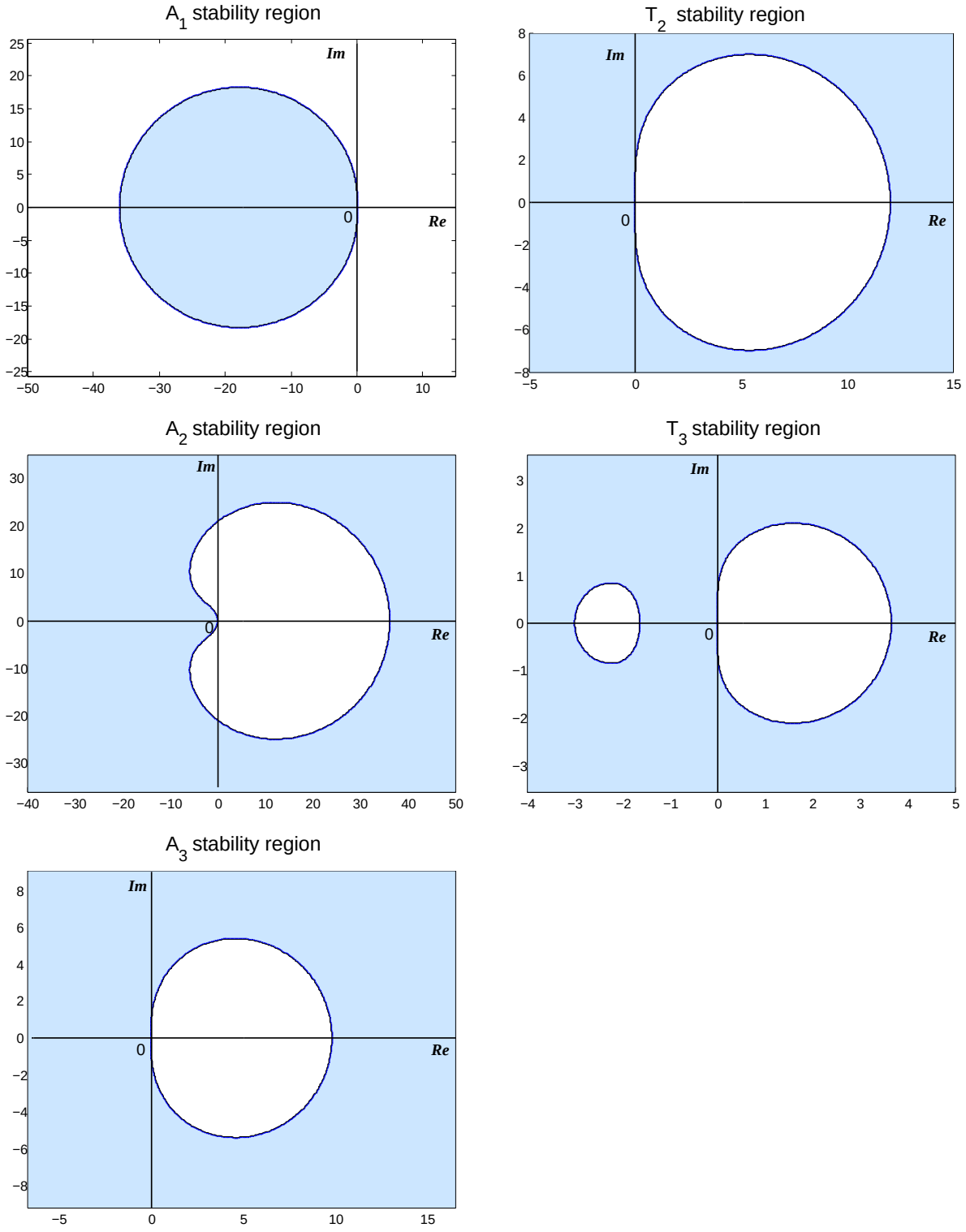

Figure 3.7: Stability regions (cyan regions) of DIRK methods avoiding interpolation. Left column: third order DIRK methods (from the top to bottom: A_1, A_2, A_3); right column: second order DIRK methods (from the top to bottom: T_2, T_3). The stability regions of A_3 and T_2 include $\mathbb{C}^-$, thus, schemes A_3 and T_2 are A-stable.

The discrete version of the first order implicit scheme of (3.14) is

$$g_{s,ij}^{n+1} = \tilde{g}_{s,ij}^{n} + \frac{\Delta t}{\varepsilon}(M_{s,ij}^{n+1} - g_{s,ij}^{n+1}) \quad s = 1, 2. \tag{3.15}$$

To solve the implicit step we have to compute $\mathsf{m}[g_{1,i\cdot}^{n+1}]$. The density ρ_i^{n+1} and the momentum $(\rho u)_i^{n+1}$ can be easily computed multiplying the first equation of (3.15) by 1 and v_j and summing over j. In this way we get

$$\rho_i^{n+1} = \Delta v \sum_j \tilde{g}_{1,ij}^{n}, \qquad (\rho u)_i^{n+1} = \Delta v \sum_j v_j \tilde{g}_{1,ij}^{n}.$$

To obtain the temperature T_i^{n+1}, instead, we have to multiply by $(v_j - u_j)^2$ and by 1 respectively the first and the second equation of (3.15), and than summing over j.
Now, using the discrete analogue of (1.28):

$$\Delta v \sum_j (v_j - u_j)^2 (M_{1,ij}^{n+1} - g_{1,ij}^{n+1}) + \Delta v \sum_j (M_{2,ij}^{n+1} - g_{2,ij}^{n+1}) = 0,$$

one can compute the temperature T_i^{n+1} in this way:

$$3R\rho_i^{n+1} T_i^{n+1} = \Delta v \sum_j (v_j - u_j)^2 \tilde{g}_{1,ij}^{n} + \Delta v \sum_j \tilde{g}_{2,ij}^{n}.$$

Once the new moments ρ_i^{n+1}, $(\rho u)_i^{n+1}$ and T_i^{n+1} are computed, we can solve the implicit step and upgrade the numerical solution.
In a very simple and similar way is possible to extend the high order numerical schemes introduced before.

3.6 Numerical tests

We have considered two types of numerical tests with the purpose of verifying the accuracy (test 1) and the shock capturing properties (test 2) of the schemes. Different values of the Knudsen number, represented by the relaxation parameter ε, have been investigated in order to observe the behavior of the methods varying from the rarefied ($\varepsilon \simeq 1$) to the fluid ($\varepsilon \simeq 10^{-6}$) regime. We use units for temperature such that $R = 1$.
In the first part of the section we consider the 1D model and we explore the choice of the optimal CFL. A comparison between semi-Lagrangian schemes with and without interpolation is also presented. The second part of the section is devoted to the results obtained by the method applied to the 1D space–3D velocity case in slab geometry (Chu reduction).

3.6.1 Test 1: regular velocity perturbation

This test has been proposed in [42]. Initial velocity profile is given by

$$u = 0.1\exp(-(10x-1)^2) - 2\exp(-(10x+3)^2), \quad x \in [-1,1].$$

Initial density and temperature profiles are uniform, with constant value $\rho = 1$ and $T = 1$. The initial condition for the distribution function is the Maxwellian, computed by given

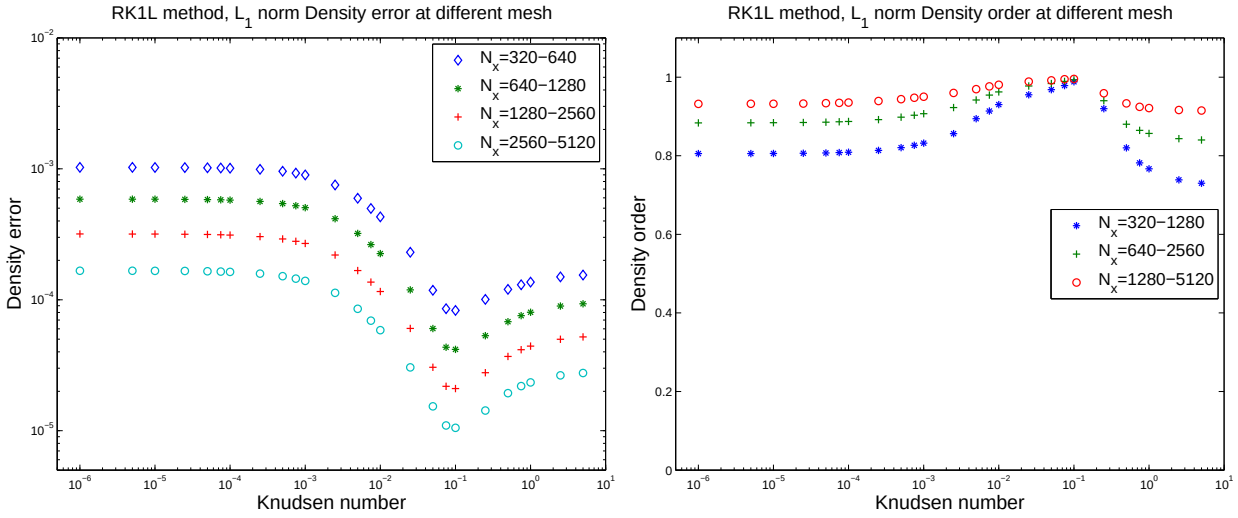

Figure 3.8: L_1 error and accuracy order of implicit Euler methods coupled with linear interpolation, varying ε, using periodic boundary conditions.

macroscopic fields. To check the accuracy order the solution must be smooth. Using periodic or reflective boundary conditions, we observe that some shocks appear in the solution around the time $t = 0.35$, so the accuracy order has been tested using a final time $t_f = 0.32$, that is large enough to reach thermodynamic equilibrium. In all tests $N_v = 20$ velocity points have been used, uniformly spaced in $[-10, 10]$. For the time step, we set $\Delta t = \text{CFL}\,\Delta x/v_{max}$ and we have used CFL$= 4$. The spatial domain is $[-1, 1]$.
We have compared the following method:

- First order implicit Euler coupled with linear interpolation (see Fig. 3.8);
- RK2W23 and BDF2W23 as second order methods (see Fig. 3.9);
- RK3W23 and RK3W35 (see Fig. 3.10), BDF3W23 and BDF3W35 (see Fig. 3.11) as third order methods;

The Figures 3.8-3.11 show the L_1 error and the rate of convergence related to macroscopic density of the schemes using periodic boundary conditions. The same behavior is observed when monitoring the error in mean velocity and in energy.

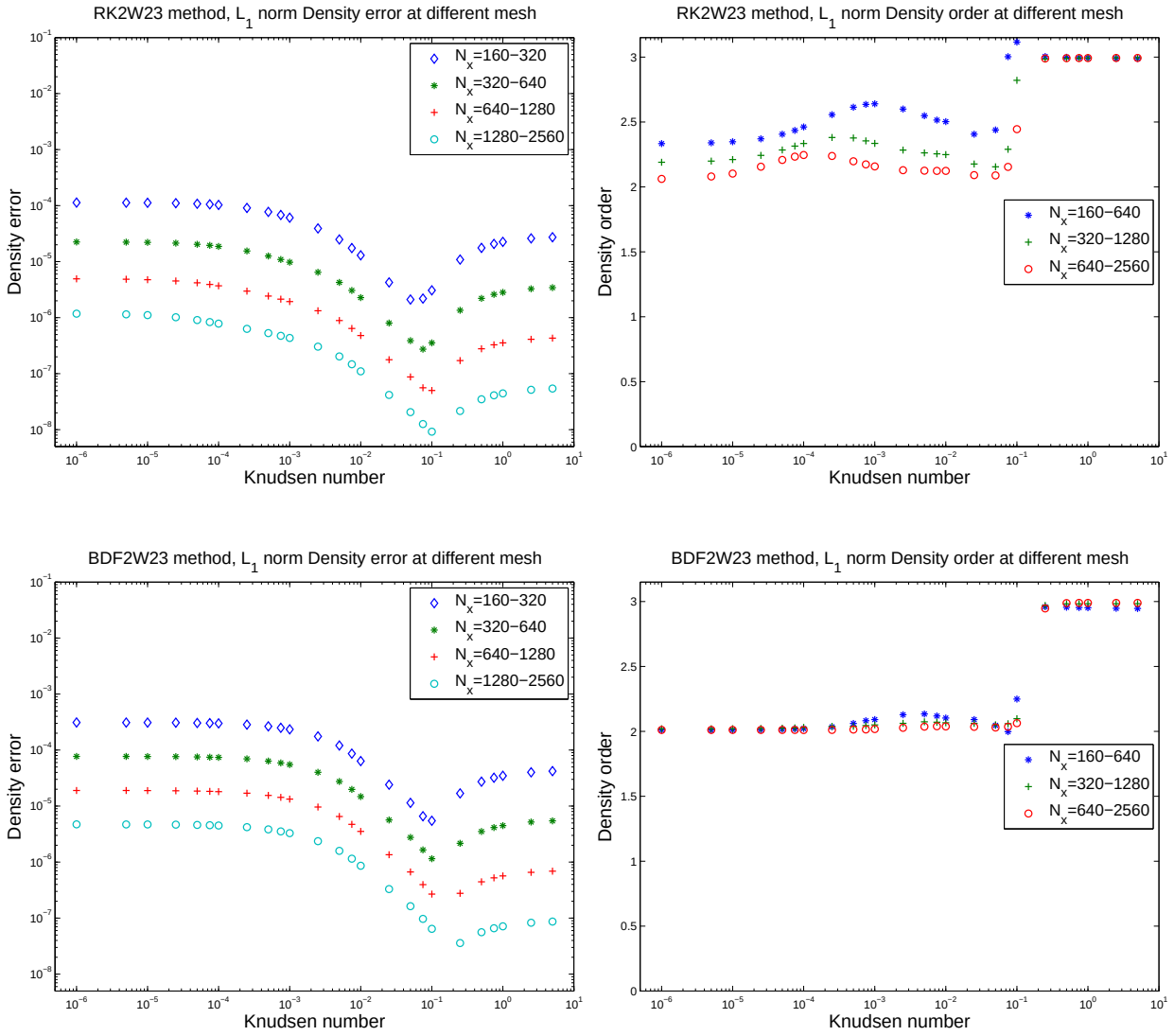

Figure 3.9: L_1 error and accuracy order of RK2W23 and BDF2W23, varying ε, using periodic boundary conditions.

Remarks

- In most regimes the order of accuracy is the theoretical one. More precisely all schemes maintain the theoretical order of accuracy in the limit of small Knudsen number, except RK3-based scheme, whose order of accuracy degrades to 2, with both WENO23 and WENO35 interpolation. Some schemes (RK2W23, RK3W35, BDF2W23, BDF3W35) present a spuriously high order of accuracy for large Knudsen number. This is due to the fact that for such large Knudsen number and small final

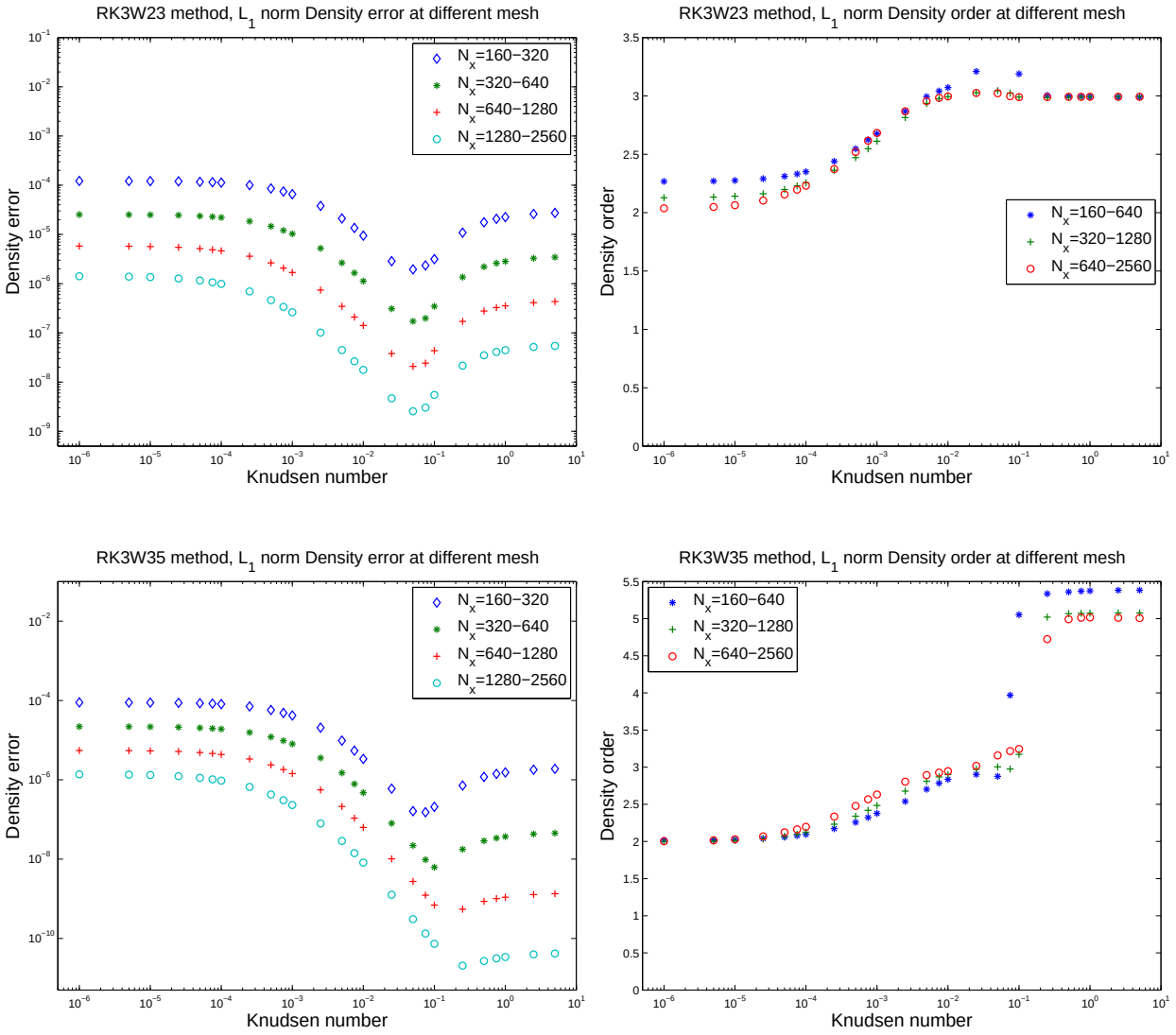

Figure 3.10: L_1 error and accuracy order of RK3W23 and RK3W35, varying ε, using periodic boundary conditions.

time most error is due to space discretization, which in such schemes is of order higher than time discretization. The most uniform accuracy is obtained by the BDF3W23 scheme.

- Most tests have been conducted with periodic boundary conditions. Similar results are obtained using reflecting boundary conditions (see Fig. 3.12). The numerical technique used to deal with reflecting boundary conditions is explained in detail in Chapter 4.

3.6.2 Optimal CFL

The semi-Lagrangian nature of the scheme allows us to avoid the classical CFL stability restriction. In this way, one can use large CFL numbers in order to obtain larger time step, thus lowering the computational cost. How much can we increase the CFL number without degrading the accuracy?
Consistency analysis of semi-Lagrangian schemes [18] shows that the error is composed by two part: one depending on the time integration and the other depending on the interpolation.

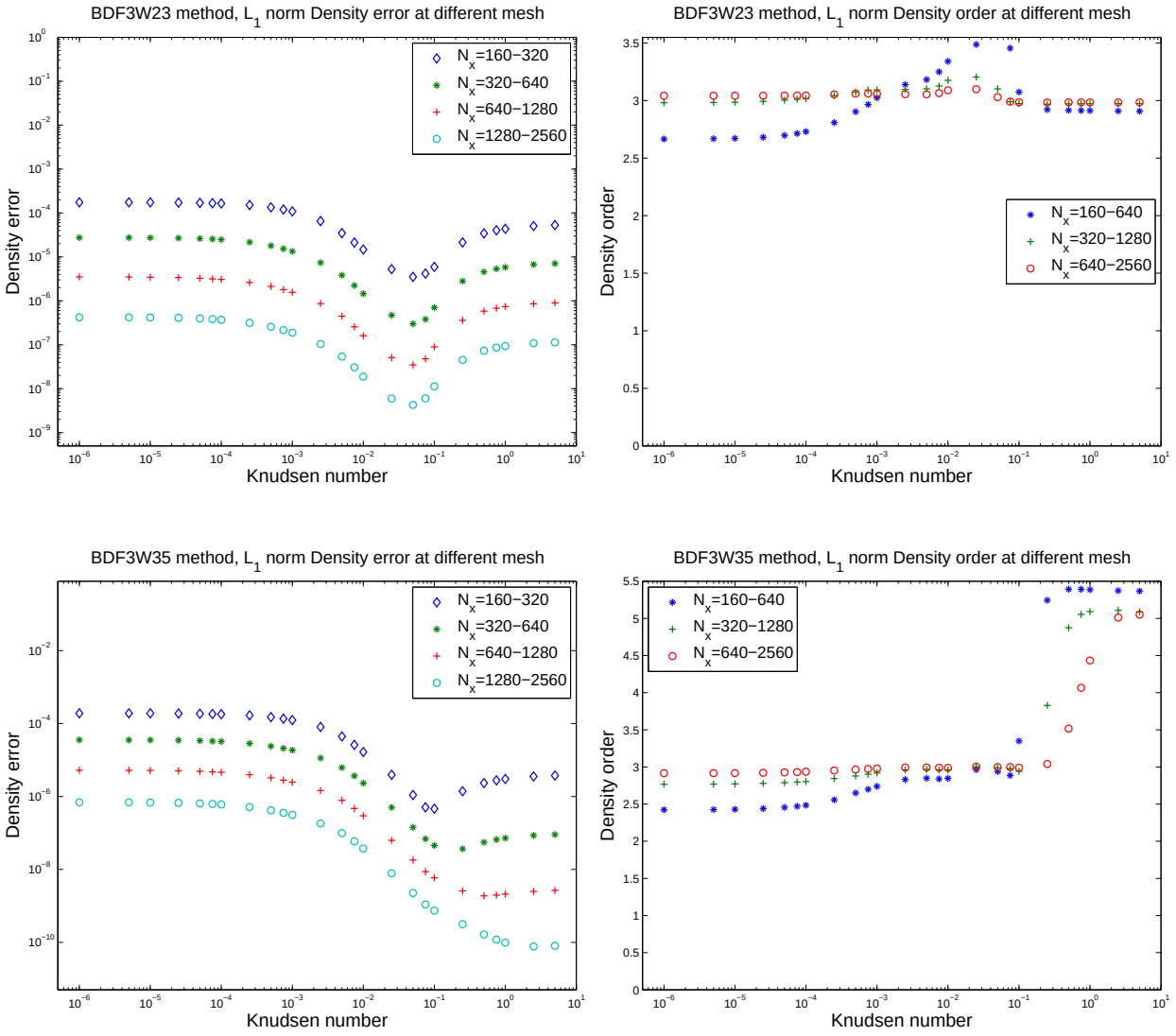

Figure 3.11: L_1 error and accuracy order of BDF3W23 and BDF3W35, varying ε, using periodic boundary conditions.

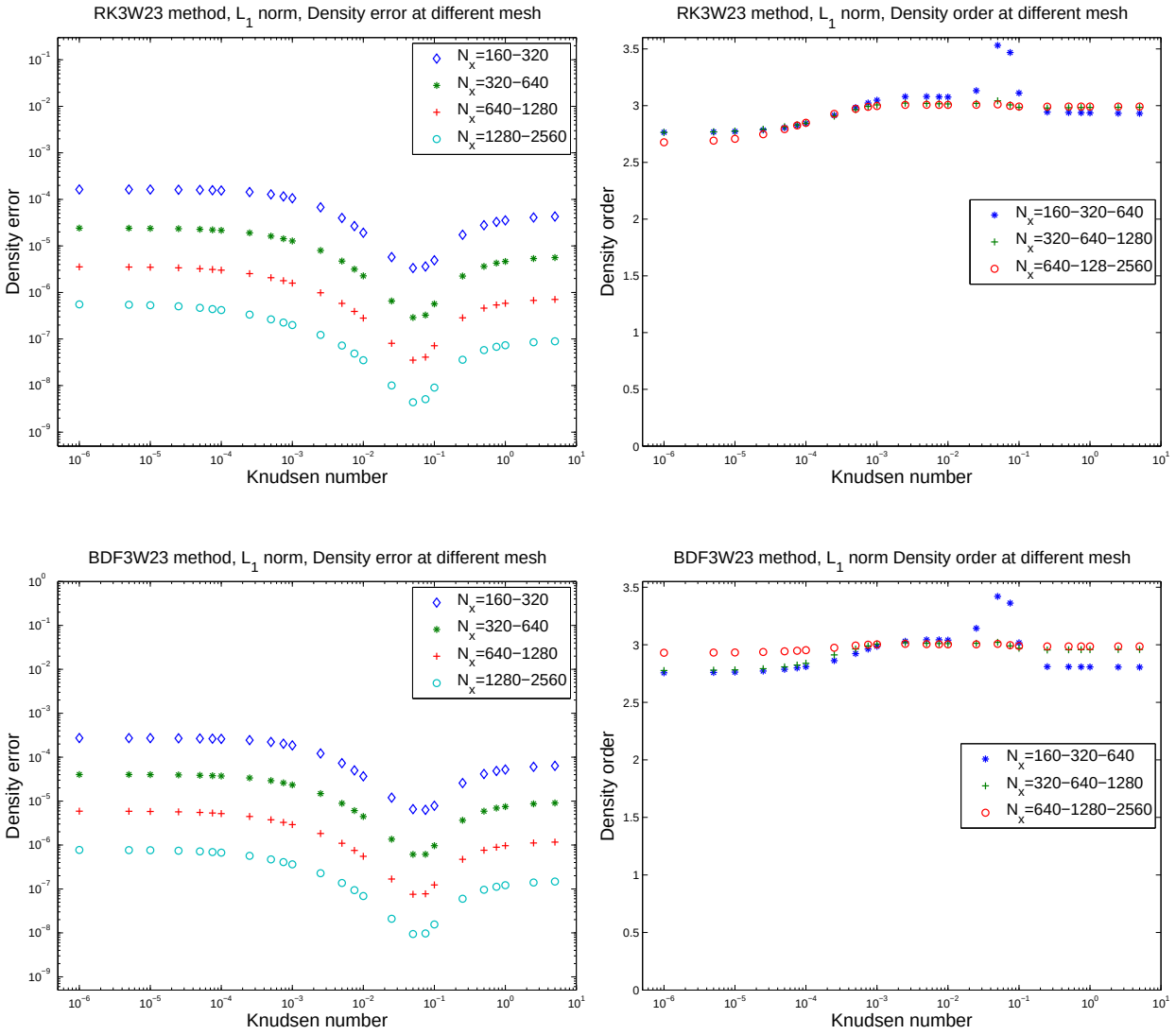

Figure 3.12: L_1 error and accuracy order of RK3 and BDF3 methods coupled with WENO23, varying ε, using reflective boundary conditions.

Therefore, if we use a small CFL number, the time step will be small and the error will be mainly due to the interpolation. On the other hand, if we use a big CFL number, the error will be mainly due to the time integration. This argument leads us to think that there is an optimal value of the CFL number, that allows us to minimize the error. The following Figures 3.13-3.14 show this behavior. Each picture shows the L_2 error of the macroscopic density of the previous smooth initial data, varying the CFL number from 0.05 to 20. The grid of the CFL values is not uniform because we want to work with constant time step until the final time, that for this test is set to 0.3. The Knudsen number is fixed to the

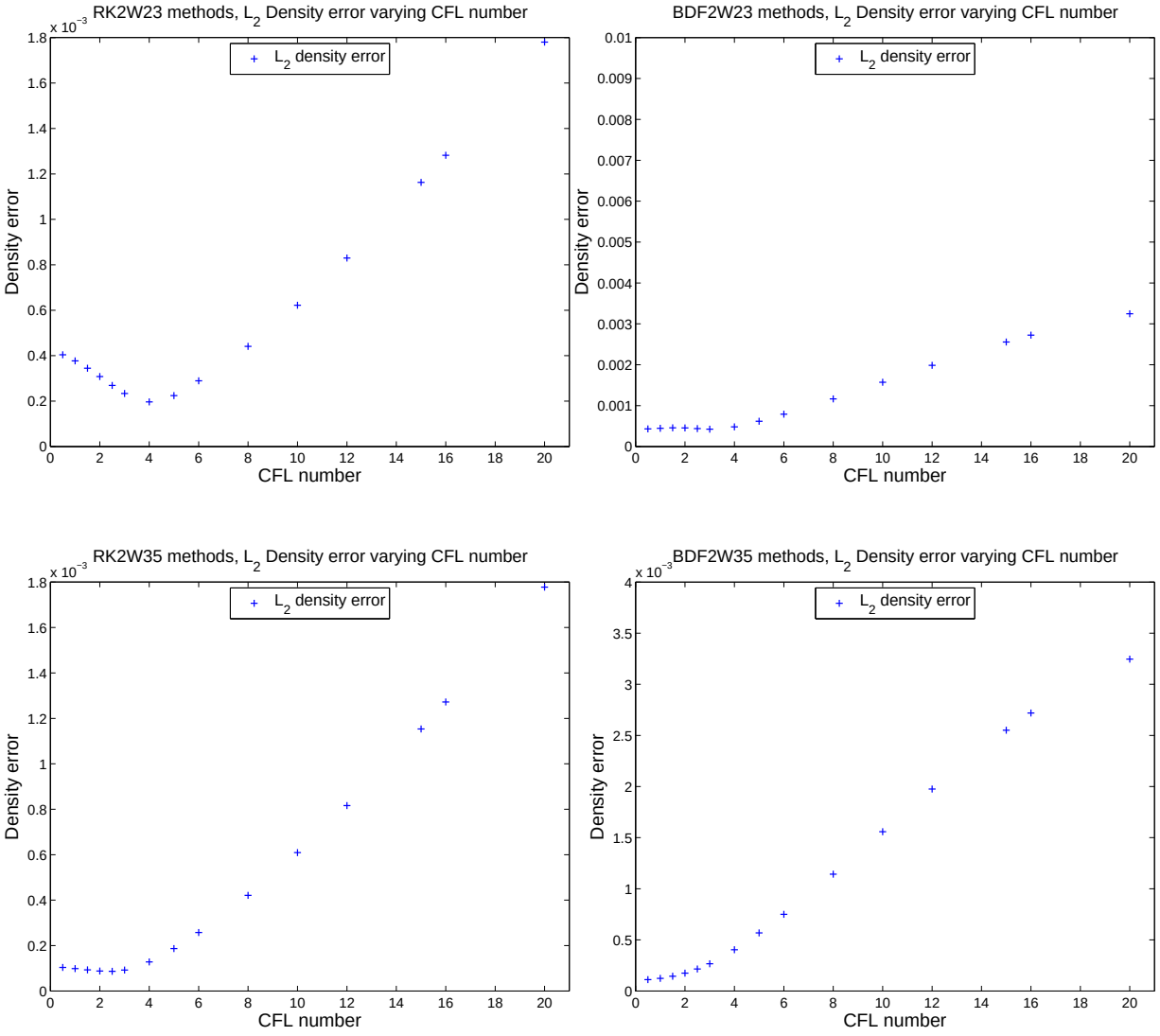

Figure 3.13: Optimal CFL number. Left RK2, right BDF2. From top to bottom: WENO23, WENO35.

value 10^{-4}.

When the accuracy in space is not much larger than in time, as in the case of RK2W23, RK3W23, BDF3W23, an evident optimal CFL number appears, since in such cases interpolation error and time discretization error balance.

If space discretization is much more accurate than time discretization, the optimal CFL number decreases. Note that with the same formal order of accuracy, the optimal CFL number is larger for schemes based on RK than for schemes based on BDF, because RK have a smaller error constant.

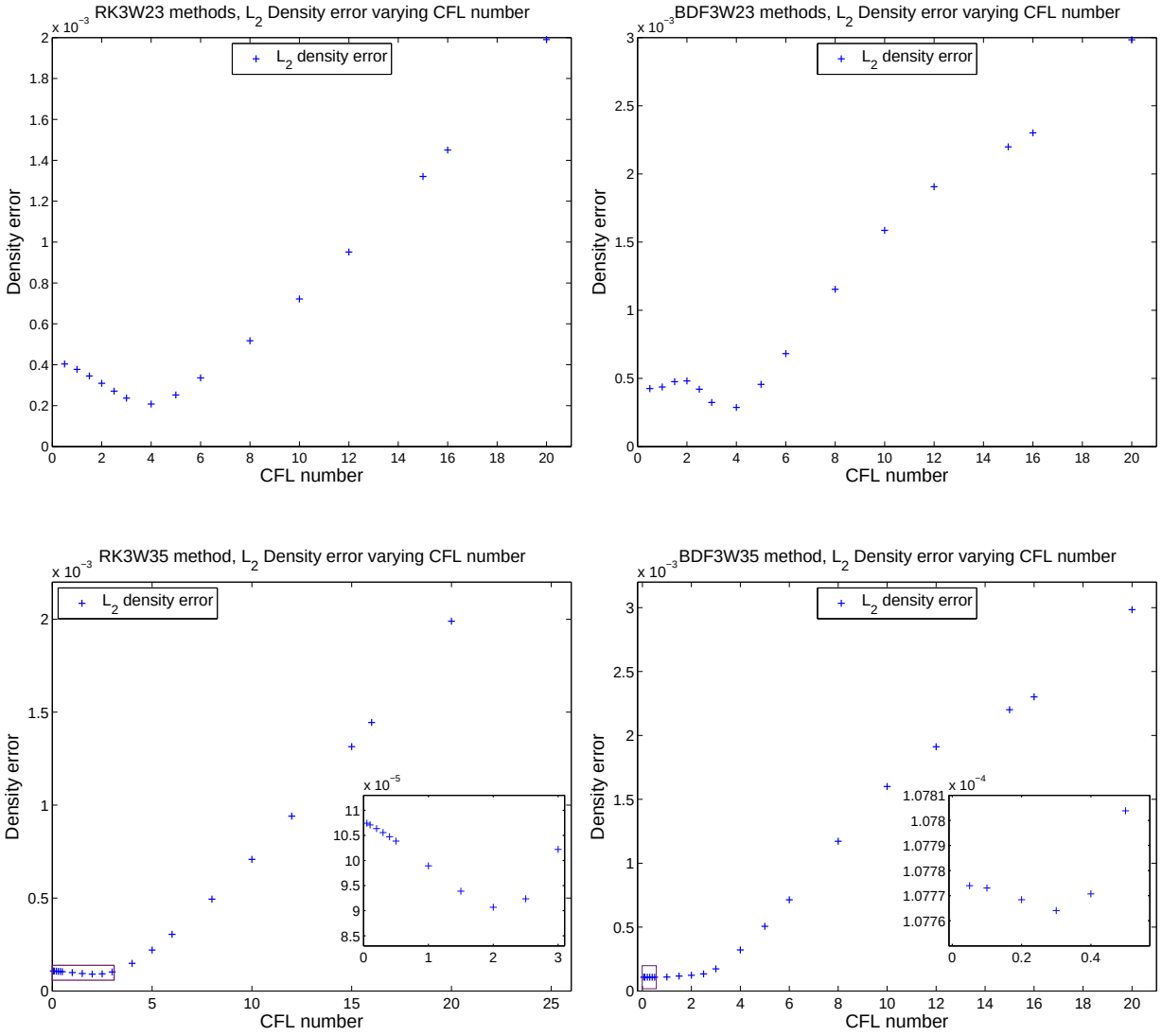

Figure 3.14: Optimal CFL number. Left RK3, right BDF3. From top to bottom: WENO23, WENO35.

3.6.3 Test 2: Riemann problem

This test allows us to evaluate the capability of our class of schemes in capturing shocks and contact discontinuities. In particular, we are interested in the behavior of the schemes in the fluid regime. Here we illustrate the results obtained for moments, i.e density, mean velocity and temperature profiles, for $\varepsilon = 10^{-2}$ and $\varepsilon = 10^{-6}$ (see Fig. 3.15-3.16). The spatial domain chosen is $[0, 1]$ and the discontinuity is taken at $x = 0.5$. Free-flow boundary conditions are assumed. The final time is 0.16. These tests have been performed using $N_v = 30$ velocity nodes, uniformly spaced in $[-10, 10]$. As shown in Fig. 3.15 and 3.16,

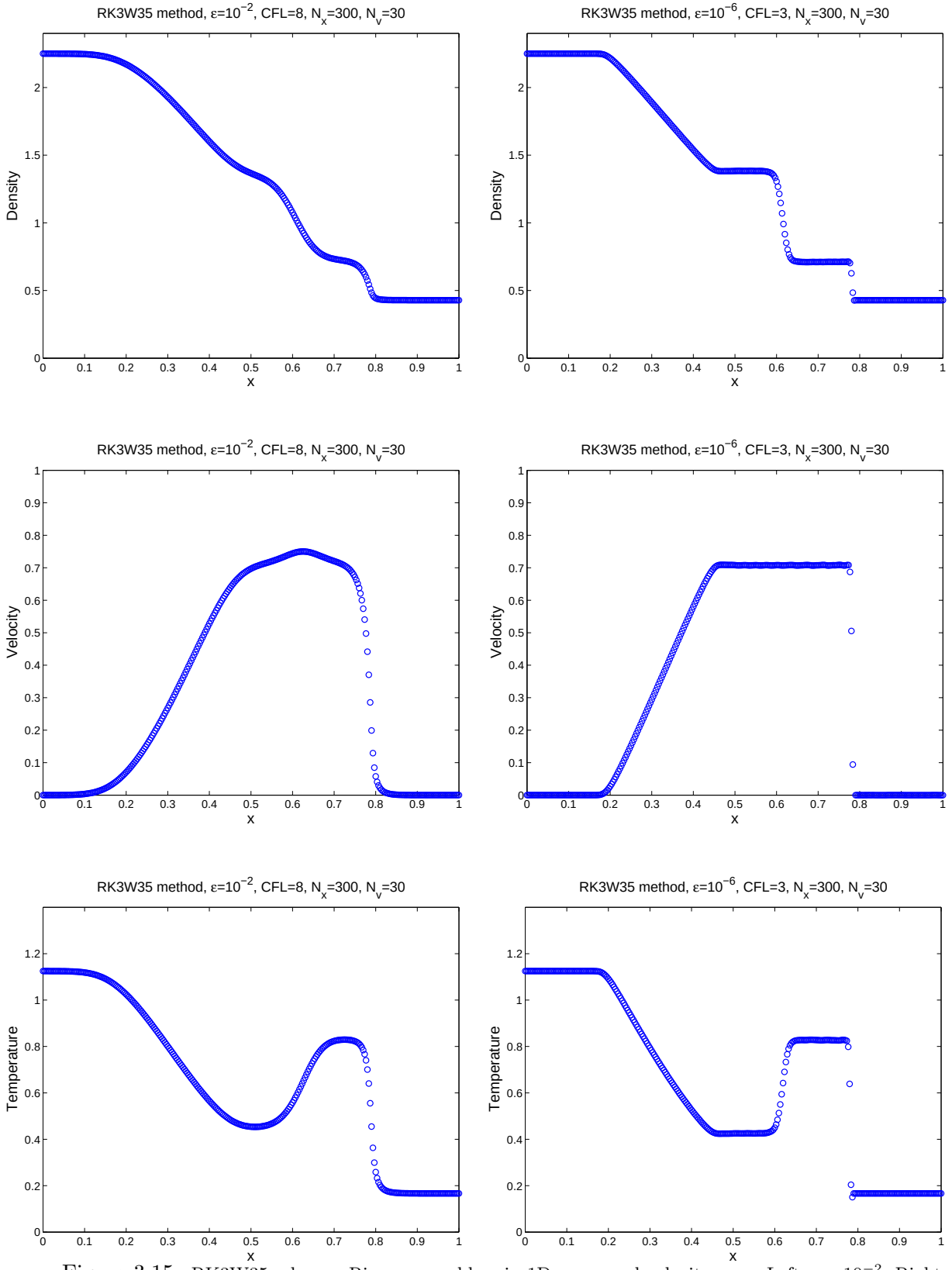

Figure 3.15: RK3W35 scheme. Riemann problem in 1D space and velocity case. Left $\varepsilon = 10^{-2}$; Right $\varepsilon = 10^{-6}$. From top to bottom: density, velocity and temperature.

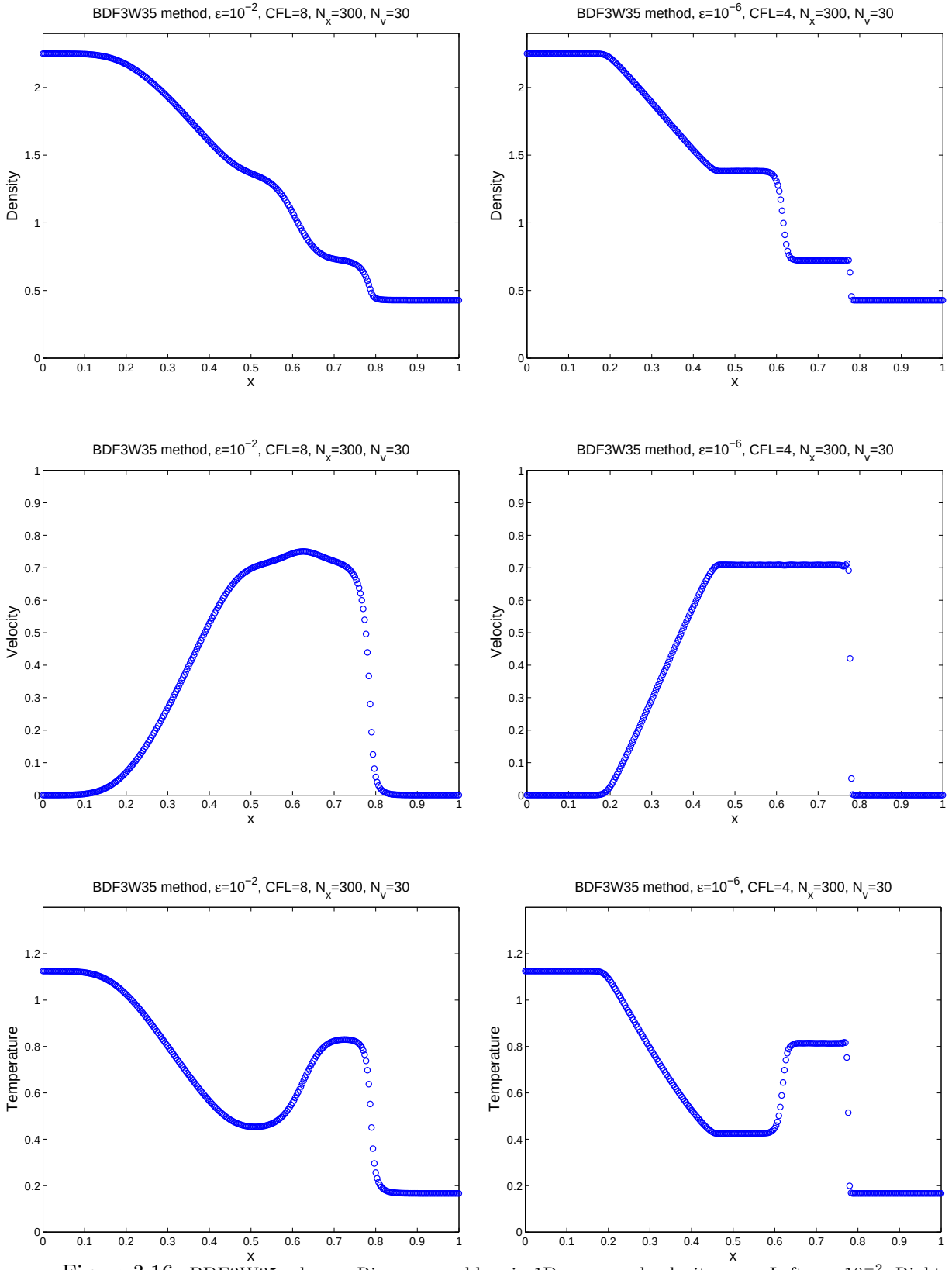

Figure 3.16: BDF3W35 scheme. Riemann problem in 1D space and velocity case. Left $\varepsilon = 10^{-2}$; Right $\varepsilon = 10^{-6}$. From top to bottom: density, velocity and temperature.

the schemes are able to capture the fluid dynamic limit for very small values of the relaxation time, relevant to regimes in which the evolution of the moments is governed by the Euler equations.

3.6.4 Semi-Lagrangian schemes without interpolation

As discussed in Sec. 3.4, semi-Lagrangian schemes avoiding interpolation are very advantageous from a computational point of view. In Figure 3.17 we compare the CPU time and

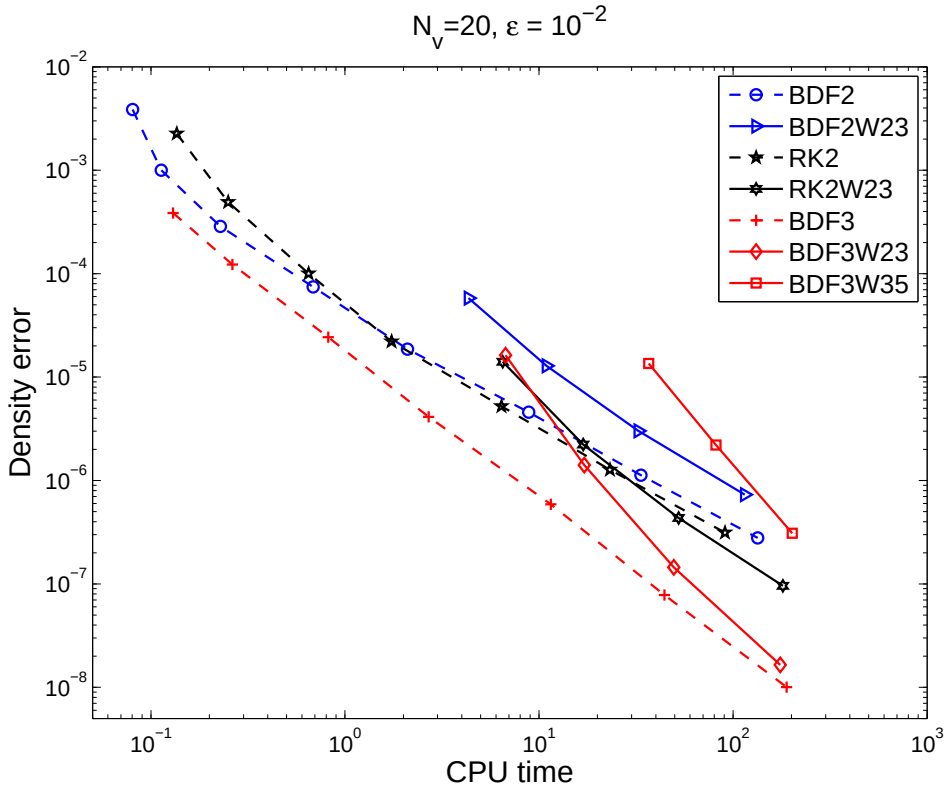

Figure 3.17: CPU time and L_1 error varying N_x.

the L_1 error of the schemes with and without interpolation. At third order of accuracy the relation between CPU time and error is better for the scheme without interpolation using $N_v = 20$. The relative effectiveness of such schemes with respect to the ones that require interpolation decreases when increasing the number of velocities, because the CFL depends on N_v in this case. However, these results are just indicative, as the schemes should be implemented efficiently. Figure 3.18 shows the error and accuracy order in L_1-norm relevant to schemes without interpolation. As we can observe, the theoretical accuracy order is reached as the spatial mesh becomes finer. Indeed, even if the CFL number is fixed to sN_v, Δt decreases when Δx decreases. We just want to remark that a

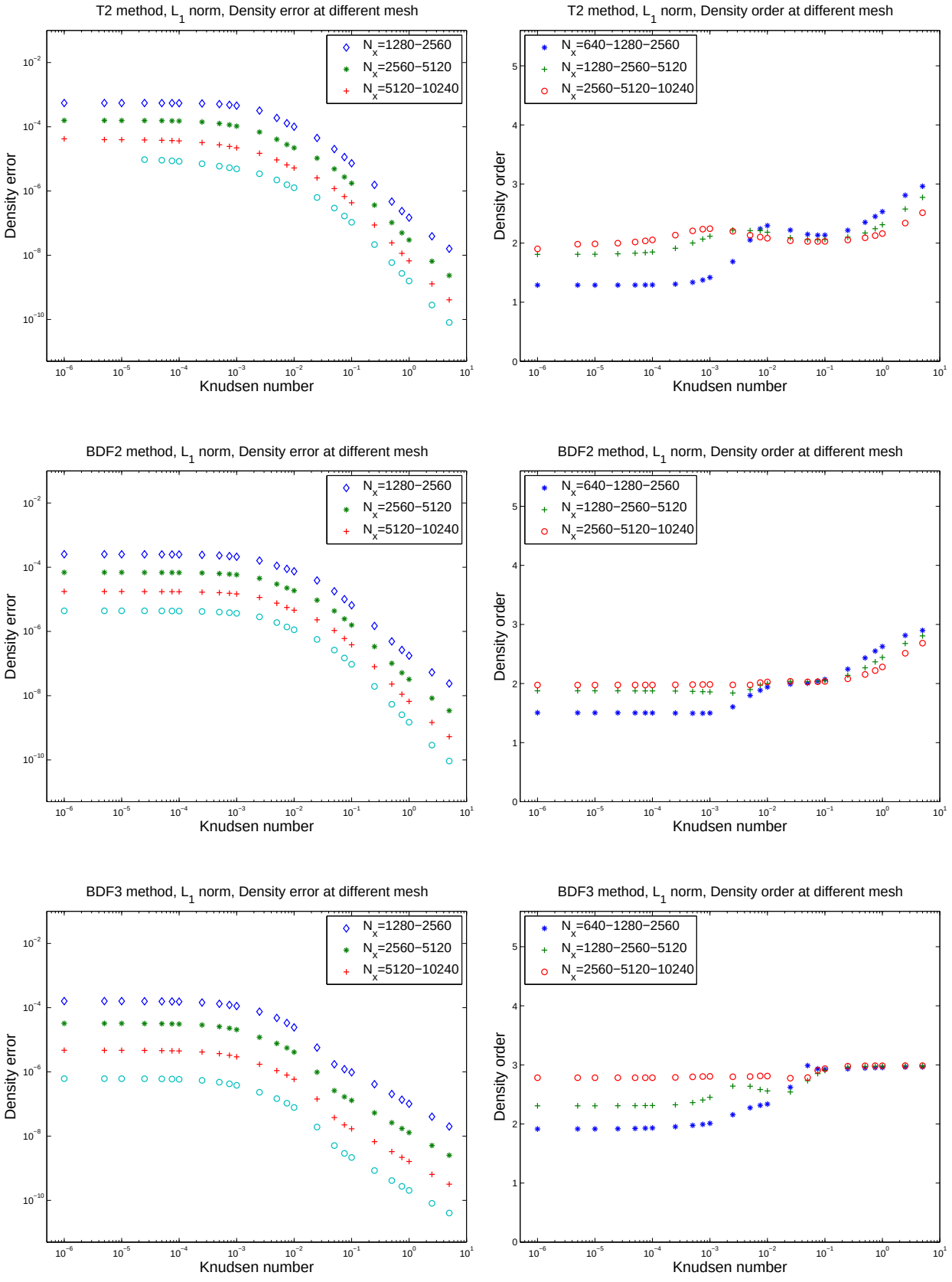

Figure 3.18: L_1 error and accuracy order of T2, BDF2 and BDF3 methods without interpolation, varying ε, using periodic boundary conditions related to the 1D problem.

spatial reconstruction is not needed, because the feet of the characteristics coincide with grid points, so no spatial error is introduced.

3.6.5 Numerical results - Chu reduction

Also for the problem $3D$ in velocity we have considered two numerical test, that are aimed at verifying the accuracy and the shock capturing properties of the schemes.

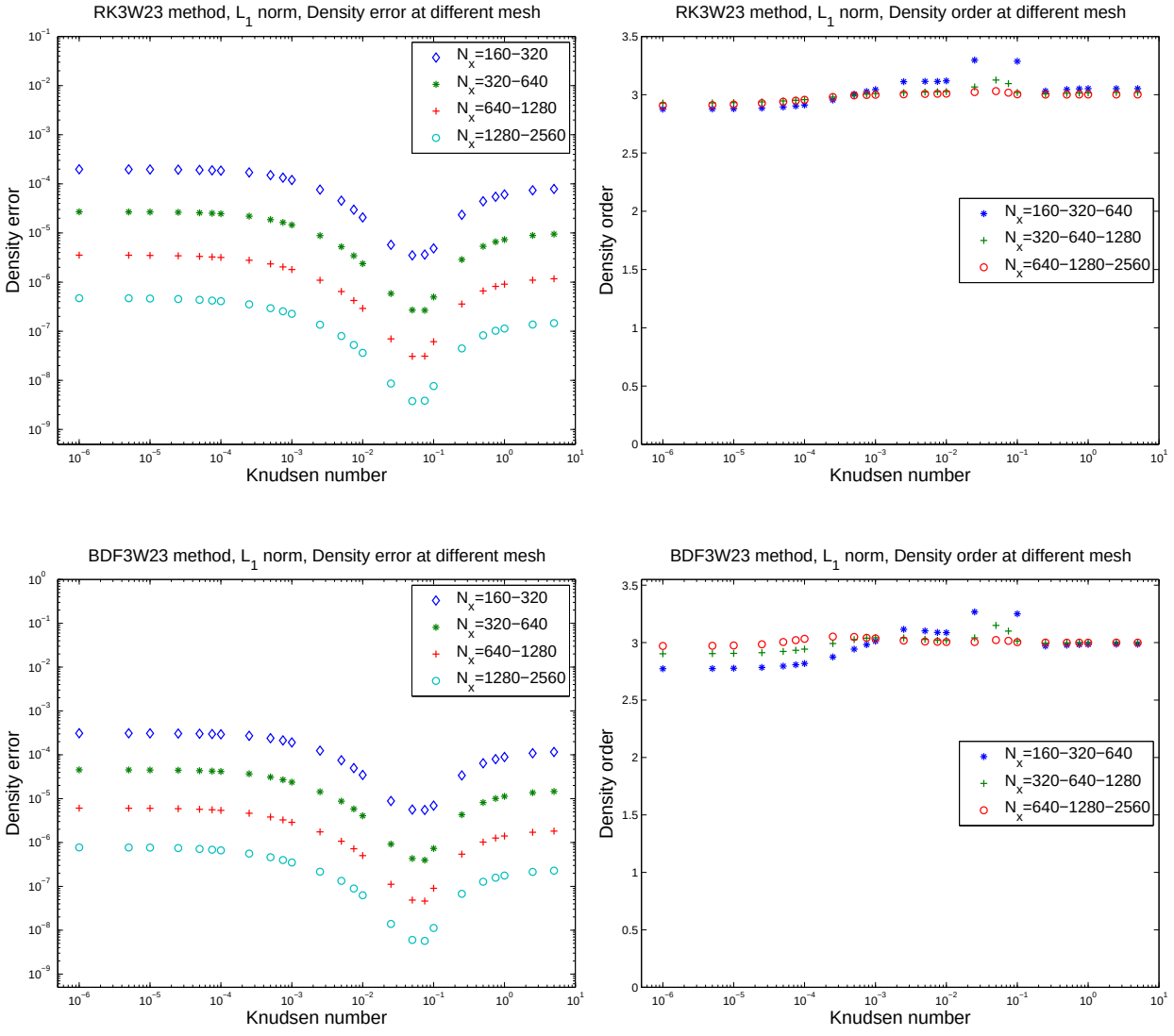

Figure 3.19: L_1 error and accuracy order of RK3 and BDF3 methods coupled with WENO23, varying ε, using reflective boundary conditions related to the 1D space–3D velocity problem.

Different values of the Knudsen number have been investigated in order to observe the behavior of the methods varying from the rarefied to the fluid regime. The initial data for

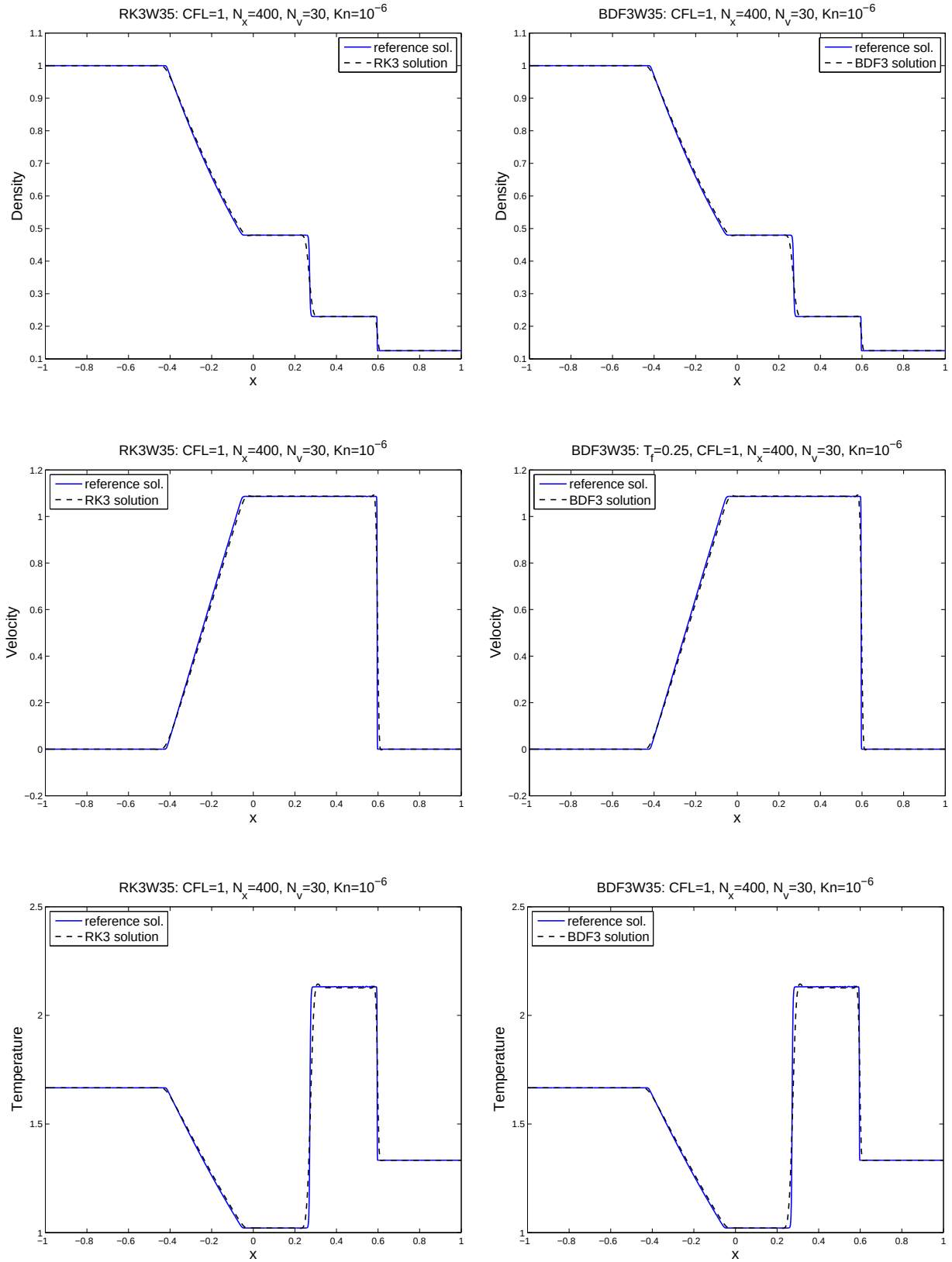

Figure 3.20: 1D space - 3D velocity case. Comparison with the gas dynamics solution. Left RK3W35; Right BDF3W35. From top to bottom: density, velocity and temperature.

test 1 are the same of the corresponding test problem $1D$ in velocity, whereas the data for the second one is a Maxwellian, having now the following initial macroscopic moments: $(\rho_L, u_L, T_L) = (1, 0, 5/3)$, $(\rho_R, u_R, T_R) = (1/8, 0, 4/3)$. As in the previous cases, free-flow boundary conditions are imposed. The final time is 0.25. This test has been performed using $N_v = 30$ velocity nodes uniformly spaced in $[-10, 10]$.
We will show only the order of accuracy related to the schemes RK3W23 and BDF3W23 (Fig. 3.19) using reflective boundary conditions, since we get essentially the same results of the 1D case. In this test CFL= 2 and the final time is 0.4. Regarding the Riemann problem we will show a comparison with the solution of the gas dynamics, for $\varepsilon = 10^{-6}$, see Fig. 3.20. As shown by the results, also in this case the scheme is able to capture the fluid dynamic limit for very small values of the relaxation time, relevant to regimes in which the evolution of the moments is governed by the Euler equations.

3.7 Hybrid order schemes

In the previous section we have seen that the high order numerical schemes proposed are able to capture the correct fluid limit as $\varepsilon \to 0$, also in presence of shock and contact discontinuities. In these cases we have used a small CFL number, for instance $CFL = 3, 4$, see Section 3.6.3. If we use higher CFL number, we observe that some instabilities arise near the shocks in the macroscopic fields' profiles. This is a drawback from a computational point of view because it forces the use of small time step. Numerical instabilities mainly come from the high order temporal discretization, and not from spatial interpolation. Indeed, numerical tests performed by coupling high order in time and low order in space, show the same behavior, and thus the responsible can not be the spatial interpolation.
To overcome these difficulties we have developed a hybrid scheme coupling low and high order schemes [44]. Indeed, we observe that the results obtained by means of the first order scheme, both in rarefied or fluid regime, do not present any oscillations, even if we use high CFL numbers. Thus, the basic idea of hybrid schemes is to use low order in the regions where the instabilities are present, and high order elsewhere. The instabilities are localized near the shocks, thus to choose when low order schemes must be used we resort to the smooth indicators β (2.25). The smooth indicators are zero if the function is constant and much greater as the function present discontinuities. In this way, fixed a tolerance tol, when $\beta > tol$ we use first order scheme, elsewhere high order. Fig. 3.21 and 3.22 show the numerical results using the same initial data of Section 3.6.3. The basic schemes used are RK2W23 and BDF2W23. The correction to low order is fixed to $\beta = 10^{-5}$.
As we can see by the numerical results, by means of this trick, we are able to use large

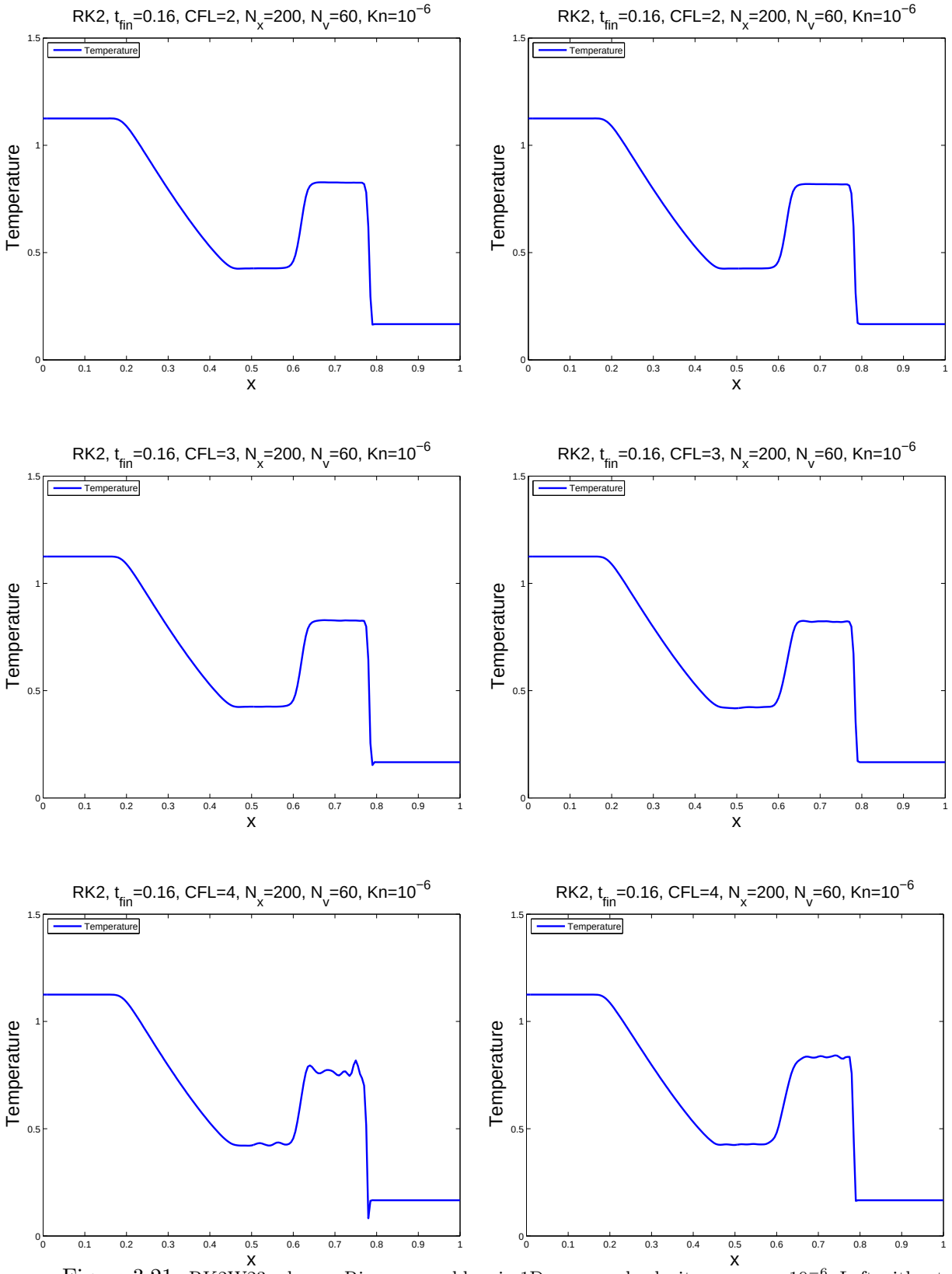

Figure 3.21: RK2W23 scheme. Riemann problem in 1D space and velocity case. $\varepsilon = 10^{-6}$. Left without correction; right hybrid scheme. From top to bottom CFL number equal to 2,3 and 4.

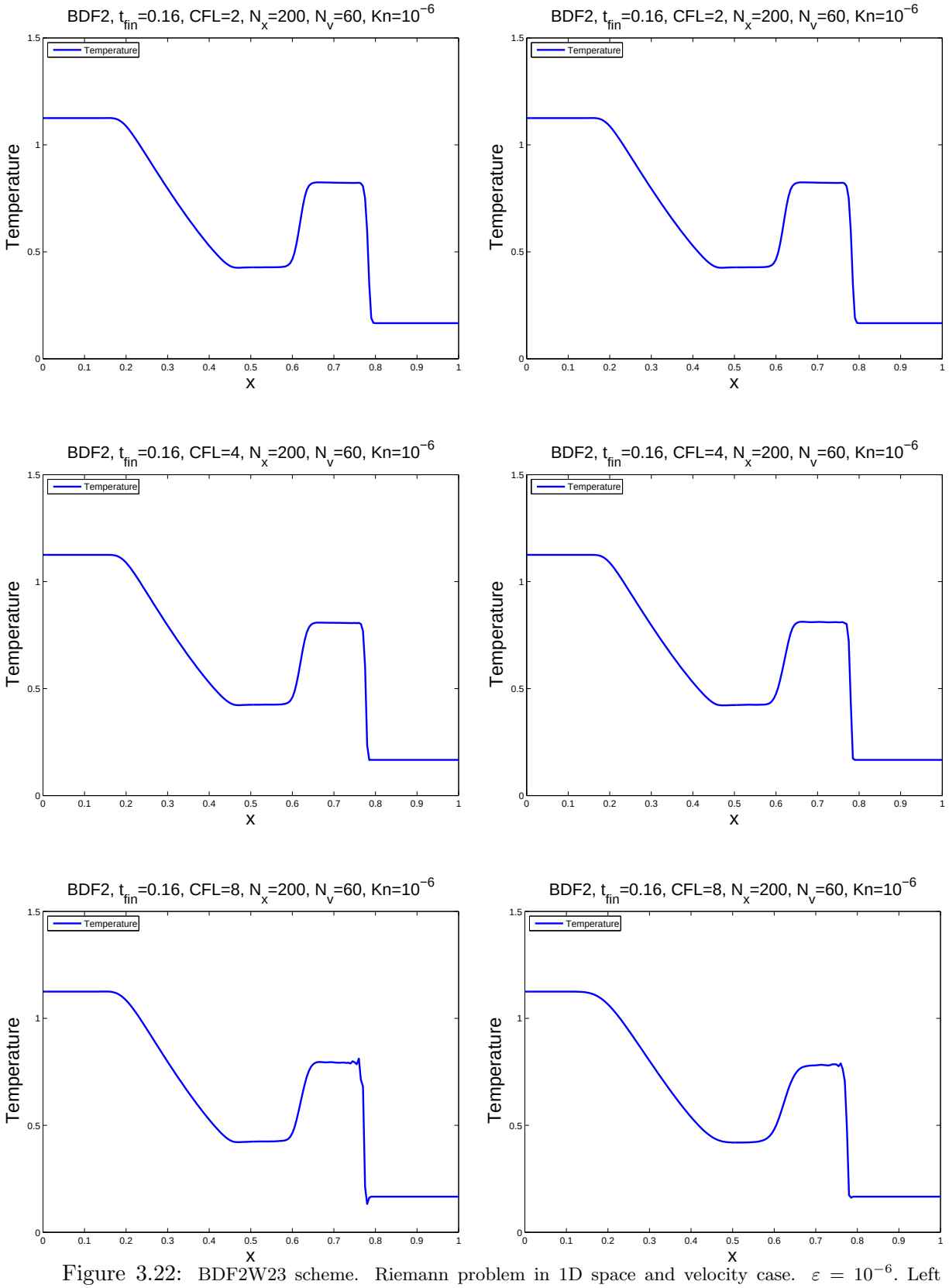

Figure 3.22: BDF2W23 scheme. Riemann problem in 1D space and velocity case. $\varepsilon = 10^{-6}$. Left without correction; right hybrid scheme. From top to bottom CFL number equal to 2,4 and 8.

	L_1-relative errors			L_1-orders			
N_x	Density	Velocity	Energy	Density	Velocity	Energy	Correct.
II order	**without**	**correction**					
20	-	-	-	-	-	-	0%
40	3.318e-03	2.648e-01	9.239e-03	-	-	-	0%
80	1.234e-03	1.179e-01	3.656e-03	1.426	1.167	1.337	0%
160	2.015e-04	2.057e-02	6.685e-04	2.614	2.519	2.451	0%
320	3.287e-05	2.901e-03	1.151e-04	2.616	2.826	2.538	0%
640	7.265e-06	5.260e-04	2.455e-05	2.178	2.463	2.229	0%
1280	1.806e-06	1.173e-04	5.842e-06	2.007	2.164	2.071	0%
II order	**with**	**correction**	$\beta \geq 10^{-3}$				
20	-	-	-	-	-	-	0.38%
40	3.265e-03	2.601e-01	9.074e-03	-	-	-	0%
80	1.234e-03	1.179e-01	3.656e-03	1.403	1.141	1.311	0%
160	2.015e-04	2.057e-02	6.685e-04	2.614	2.519	2.451	0%
320	3.287e-05	2.901e-03	1.151e-04	2.616	2.826	2.538	0%
II order	**with**	**correction**	$\beta \geq 10^{-4}$				
20	-	-	-	-	-	-	4.27%
40	3.438e-03	2.700e-01	9.076e-03	-	-	-	1.49%
80	1.449e-03	1.357e-01	4.264e-03	1.246	0.992	1.089	0.001%
160	2.022e-04	2.060e-02	6.691e-04	2.841	2.720	2.671	0%
320	3.287e-05	2.901e-03	1.151e-04	2.616	2.826	2.538	0%
640	7.265e-06	5.260e-04	2.455e-05	2.178	2.463	2.229	0%
II order	**with**	**correction**	$\beta \geq 10^{-5}$				
20	-	-	-	-	-	-	10.63%
40	2.750e-03	2.521e-01	8.514e-03	-	-	-	7.41%
80	2.305e-03	1.773e-01	5.593e-03	0.254	0.507	0.606	3.28%
160	6.610e-04	5.094e-02	1.762e-03	1.802	1.799	1.666	0.62%
320	6.866e-05	5.617e-03	2.185e-04	3.267	3.181	3.011	0.001%
640	7.254e-06	5.254e-04	2.454e-05	3.242	3.418	3.155	0%
1280	1.806e-06	1.173e-04	5.842e-06	2.005	2.163	2.070	0%

Table 3.1: RK2, $N_v = 40$, $Kn = 10^{-6}$, $CFL = 4$, $T_f = 0.16$, interpolation WENO23. Accuracy order obtained for different choices of the tolerance. The last column represents the percentage of points (x_i, v_j) where is used first order.

	L_1-relative errors			L_1-orders			
N_x	Density	Velocity	Energy	Density	Velocity	Energy	Correct.
II order	**without**	**correction**					
20	-	-	-	-	-	-	0%
40	3.147e-03	2.780e-01	1.006e-02	-	-	-	0%
80	1.838e-03	1.709e-01	5.742e-03	0.776	0.702	0.809	0%
160	4.321e-04	4.778e-02	1.507e-03	2.088	1.838	1.929	0%
320	1.050e-04	9.650e-03	3.818e-04	2.040	2.307	1.981	0%
640	2.774e-05	2.025e-03	9.573e-05	1.920	2.252	1.996	0%
1280	7.167e-06	4.686e-04	2.397e-05	1.952	2.111	1.997	0%
II order	**with**	**correction**	$\beta \geq 10^{-3}$				
20	-	-	-	-	-	-	0.7%
40	3.096e-03	2.727e-01	9.561e-03	-	-	-	0%
80	1.838e-03	1.709e-01	5.742e-03	0.752	0.674	0.735	0%
160	4.321e-04	4.778e-02	1.507e-03	2.088	1.838	1.929	0%
320	1.050e-04	9.650e-03	3.818e-04	2.040	2.307	1.981	0%
II order	**with**	**correction**	$\beta \geq 10^{-4}$				
20	-	-	-	-	-	-	5.05%
40	3.035e-03	2.697e-01	9.167e-03	-	-	-	1.55%
80	2.096e-03	1.816e-01	6.020e-03	0.533	0.570	0.606	0.001%
160	4.323e-04	4.778e-02	1.507e-03	2.277	1.926	1.997	0%
320	1.050e-04	9.650e-03	3.818e-04	2.041	2.307	1.980	0%
640	2.774e-05	2.025e-03	9.573e-05	1.920	2.252	1.996	0%
II order	**with**	**correction**	$\beta \geq 10^{-5}$				
20	-	-	-	-	-	-	10.37%
40	2.457e-03	2.628e-01	8.561e-03	-	-	-	7.39%
80	2.436e-03	1.910e-01	6.287e-03	0.012	0.460	0.445	3.27%
160	9.040e-04	7.314e-02	2.471e-03	1.430	1.385	1.347	0.63%
320	1.422e-04	1.273e-02	4.980e-04	2.668	2.521	2.310	0.001%
640	2.774e-05	2.025e-03	9.574e-05	2.357	2.652	2.379	0%
1280	7.167e-06	4.686e-04	2.397e-05	1.952	2.111	1.997	0%

Table 3.2: BDF2, $N_v = 40$, $Kn = 10^{-6}$, $CFL = 4$, $T_f = 0.16$, interpolation WENO23. Accuracy order obtained for different choices of the tolerance. The last column represents the percentage of points (x_i, v_j) where is used first order.

time step also in fluid regimes. Of course, one may ask: how much does accuracy order decrease? Tables 3.1 and 3.2 show the accuracy orders of the same hybrid schemes applied to a smooth initial data using different tolerance. We can observe a small degradation of the accuracy order. However, increasing the number of grid points, the schemes tend to avoid corrections to first order and high order is recovered. Therefore, we can conclude that, using large time step together order reduction, we lose a bit of accuracy, but we obtain a numerical scheme that does not present oscillation.

Chapter 4

Gas-surface interaction and boundary conditions

In many applications the gas moves in a region bounded by one or several solid bodies, and in these cases boundary conditions have to be prescribed to characterize the behavior of the gas near the wall. In the following sections we shall investigate the conditions which must be satisfied by the distribution function f at the boundary ∂D of the region D where the motion of the particles takes place. The theoretical investigations of the gas-wall interaction are exceedingly difficult because of the complexity of phenomena taking place at the wall.

In this thesis we refer to the boundary conditions proposed by Maxwell. In a appendix to a paper published in 1879 [13, 35] he discussed the problem of finding a boundary condition for the distribution function. As a first hypothesis he supposed the surface of a physical wall to be a perfectly elastic smooth fixed surface, having the apparent shape of the solid without any minute deviations. In this case the gas molecules are reflected in a specular way; therefore the gas cannot exert any stress on the surface, except in the direction of the normal. The condition read as:

$$f_s = f(t,x,v) = f(t,x,v-2n(n\cdot(v-v_b))), \quad x\in\partial D,\ (v-v_b)\cdot n>0, \tag{4.1}$$

where n is the unit vector normal to the surface at x and v_b is the velocity of the wall, which is non zero if we are dealing with a moving boundary.
Maxwell noticed that assumption (4.1), known as *specular reflection boundary condition,* means that the gas can exert any stress on the surface only in the direction of the normal. This assumption is extremely unrealistic and can only be used in particular cases, since in many situations the gas can exert stresses also in oblique directions to the surface, that

cannot be represented as perfectly reflected.
This is why he introduced another type of boundary conditions, corresponding to a more complex gas-solid interaction. As a second model for a real wall, Maxwell considers a stratum in which fixed elastic spheres are placed so far apart from one another that any one sphere is not sensibly protected by any other sphere from the impact of molecules. He also assumes the stratum to be so deep that every molecule which comes from the gas toward such wall must strike one or more of the spheres; when at last the molecule leaves the stratum of spheres and returns into the gas, its velocity must of course be directed from the surface toward the gas, but any magnitude and direction of the velocity will take place with the same probability. So, the boundary condition read as

$$f_d = f(t,x,v) = \frac{\rho_b}{2\pi RT_b} \exp\left(- \frac{|v - v_b|^2}{2RT_b} \right), \quad x \in \partial D, \; v \cdot n > 0, \tag{4.2}$$

where T_b is the temperature, ρ_b the density and v_b the velocity of the wall. This model is known as *diffusive reflection boundary condition.*

Finally there is also a more complicated intermediate situation which is devoted to

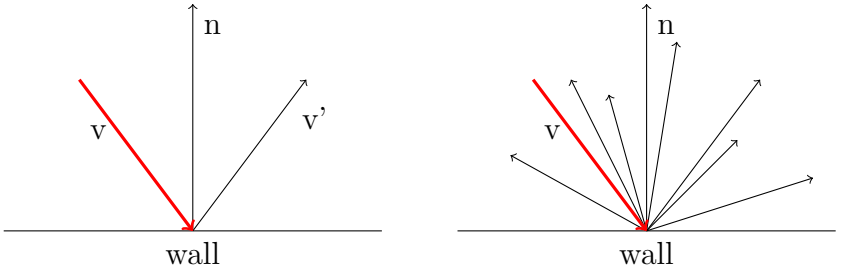

Figure 4.1: Left: specular conditions; Right: diffuse conditions.

be more physically realistic. Maxwell postulated that he prefers to treat the surface as something intermediate between a perfectly reflecting and perfectly absorbing surface, and, in particular, there is a fraction of the gas which accommodates to the temperature of the wall and another one which is reflected by the solid. The mixed boundary condition reads:

$$f(t,x,v) = (1-\alpha) f_s + \alpha f_d, \tag{4.3}$$

where $\alpha \in [0,1]$ is called the accommodation coefficient. It represents the tendency of the gas to accommodate to the wall. It means that the fraction $(1-\alpha)$ of molecules satisfies specular boundary conditions whereas a fraction α satisfies diffuse boundary conditions. If $\alpha = 0$ we have specular boundary condition and the re-emitted stream does not feel the boundary, while if $\alpha = 1$ we recover diffusive boundary condition, and in this case the re-emitted stream has completely lost its memory of the incoming stream (except for conservation of the number of molecules).

4.1 Numerical treatment of the boundary conditions

In this section we will investigate the numerical treatment of the boundary conditions. The techniques are exposed in the mono dimensional case and at the first order of accuracy in time. The extension to high order schemes is only matter of technicality and does not present conceptual difficulties.

4.1.1 Specular reflection

We assume that the boundary is static, i.e. $v_b = 0$ in (4.1). Each particle hitting the wall is immediately reflected by the wall with same tangential velocity and opposite normal velocity:

$$v_{refl} = v - 2n(n \cdot v)$$

where v_{refl} is the particle velocity after reflection and v the particle velocity before reflection. This holds true for each particle such that $v \cdot n > 0$. For $v \cdot n < 0$, the distribution function on the boundary is already known from the inner cell. The distribution function for the boundary points has to be computed only for $v \cdot n > 0$. Therefore the numerical

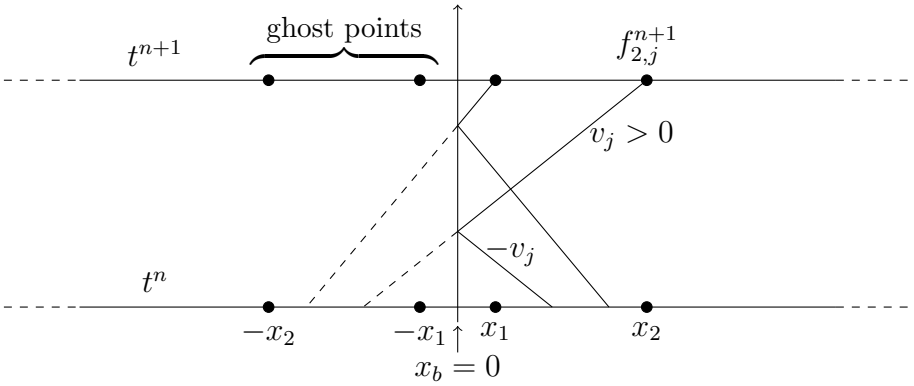

Figure 4.2: Discretization of specular reflective conditions.

discretization of the specular reflective condition is very easy. For the sake of simplicity we suppose that the wall is placed in $x_b = 0$. It is enough to consider some ghost points to extend the distribution function beyond the wall and use as many ghost points as the value of the CFL number. The ghost points will be placed symmetrically with respect to the wall, and if $-x_g$ is the ghost point symmetric to x_g the value of the distribution function on $-x_g$ will be $f_{g,-j}^n$, whereas in x_g one has $f_{g,j}^n$. In this way we can compute the feet of the characteristics by considering the extension of the impinging characteristics (dashed lines in Figure 4.2) beyond the wall without the need of considering the reflected characteristics. If we use a low order scheme in time as in Figure 4.2 a linear interpolation

is enough.
In an analogous way it is treated the extension to high order of accuracy. In this case the high order scheme will be coupled with a high order interpolation.

4.1.2 Diffusive condition

In this section we deal with the numerical approximation of solutions of kinetic BGK equations in a bounded domain with diffusive boundary conditions. We propose two techniques, the first is based on an iterative procedure, the second is a tentative to improve the first one, avoiding the iterative procedure. The techniques proposed do not make use of ghost points and for this reason are self–consistent procedures. We have to distinguish

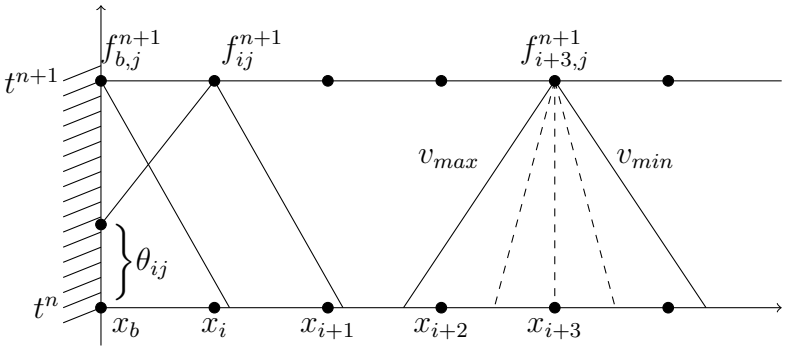

Figure 4.3: Discretization of diffusive conditions.

three types of spatial cells: those that are far enough from the wall, for which the characteristics fan does not ever touch the wall; the cells close enough to the wall, for which only a part of the fan of the characteristics touches the wall, and then the cell located at the wall, where a special treatment is needed.
First of all we compute the values of the distribution function at the wall. Let us assume that the boundary is located on the left, at position $x_b = 0$ with temperature T_b. We assume that the solution at time t^n:
$\left\{f^n_{ij}, i = 1, ..., N_x,\ j = -N_v, ..., N_v\right\}$ is known, together with and the density at $x_b = 0,\ \rho^n_b$.
The density ρ^{n+1}_{bj} is computed by imposing zero mass flux at $t = t^{n+1}$, $x_b = 0$, that is $\sum_j v_j f^{n+1}_{bj} = 0$, where

$$f^{n+1}_{bj} = \begin{cases} \rho^{n+1}_b \frac{\exp(-v_j^2/2T_b)}{(2\pi T_b)^{1/2}} & \text{if } v_j > 0, \\ \\ \tilde{f}^n_{ij} + \frac{\Delta t}{\varepsilon}(M^{n+1}_{bj} - f^{n+1}_{bj}) & \text{if } v_j < 0 \end{cases} \tag{4.4}$$

The Maxwellian M_{bj}^{n+1} cannot be computed in the usual way. We shall therefore use an iterative procedure. Let

$$f_{bj}^{(0)} = \begin{cases} \rho_b^{(0)} E_{bj} & \text{for } v_j > 0, \\ \\ \tilde{f}_{ij}^n = f(t^n, x_i - v_j \Delta t, v_j) & \text{for } v_j < 0 \end{cases}$$

with $E_{bj} = \exp(-v_j^2/2T_b)/(2\pi T_b)^{1/2}$. Imposing $\sum_j v_j f_{bj}^{(0)} = 0$ one determines $\rho^{(0)}$. Once $\rho^{(0)}$ is known, one computes the moments $m_\beta^{(0)} = \sum_j v_j^\beta f_{bj}^{(0)}$, $\beta = 0, 1, 2$. From the moments one computes the Maxwellian $M_{bj}^{(0)}$. Then one can iterate untill convergence:

$$f_{bj}^{(k)} = \begin{cases} \rho_b^{(k)} E_{bj} & \text{if } v_j > 0, \\ \\ \tilde{f}_{ij}^n + \frac{\Delta t}{\varepsilon}(M_{bj}^{(k-1)} - f_{bj}^{(k-1)}) & \text{if } v_j < 0 \end{cases}$$

Finally we set $f_{bj}^{n+1} = \lim_{k\to\infty} f_{bj}^{(k)}$ and $\rho_b^{n+1} = \lim_{k\to\infty} \rho_b^{(k)}$. Once the density at the new time t^{n+1} has been found, one can then compute the function at other grid points, as follows. Let us consider, for example, point x_i in the previous figure. Then one has:

$$f_{ij}^{n+1} = \begin{cases} \tilde{f}_{ij}^n + \frac{\Delta t}{\varepsilon}(M_{ij}^{n+1} - f_{ij}^{n+1}) & \text{if } \tilde{x}_{ij} = x_i - v_j \Delta t > 0, \\ \\ f_{\theta_{ij}} = \big(\theta_{ij}\rho_b^{n+1} + (1-\theta_{ij})\rho_b^n\big) E_{bj} & \text{if } \tilde{x}_{ij} < 0. \end{cases} \tag{4.5}$$

The geometrical factor $\theta_{ij} = 1 - x_i/(v_j \Delta t)$ can be computed for each velocity.
The Maxwellian M_{ij}^{n+1} may be computed by using an iterative procedure similar to the one used for the computation of ρ_b^{n+1}. Starting from

$$f_{ij}^{(0)} = \begin{cases} \tilde{f}_{ij}^n & \text{if } \tilde{x}_{ij} > 0, \\ \\ f_{\theta_{ij}} & \text{if } \tilde{x}_{ij} < 0, \end{cases}$$

one computes the moments $m_\beta^{(0)} = \sum_j v_j^\beta f_{ij}^{(0)}$ and then $M_{ij}^{(0)}$. Given $f_{ij}^{(k-1)}$, compute

$$f_{ij}^{(k)} = \begin{cases} \tilde{f}_{ij}^n + \frac{\Delta t}{\varepsilon}(M_{ij}^{(k-1)} - f_{ij}^{(k-1)}) & \text{if } \tilde{x}_{ij} > 0, \\ \\ f_{\theta_{ij}} + \frac{(1-\theta_{ij})\Delta t}{\varepsilon}(M_{ij}^{(k-1)} - f_{ij}^{(k-1)}) & \text{if } \tilde{x}_{ij} < 0. \end{cases}$$

Finally we set $f_{ij}^{n+1} = \lim_{k\to\infty} f_{ij}^{(k)}$.

The main drawback of this approach relies on the iterative loops. Indeed, the iteration may be slow if $\varepsilon << \Delta t$ because in the iteration one has:

$$f_{ij}^{(k)} = \begin{cases} \dfrac{\tilde{f}_{ij}^{n} + \frac{\Delta t}{\varepsilon} M_{ij}^{(k-1)}}{1 + \frac{\Delta t}{\varepsilon}} & \text{if } \tilde{x}_{ij} > 0, \\ \dfrac{f_{\theta_{ij}} + \frac{(1-\theta_{ij})\Delta t}{\varepsilon} M_{ij}^{(k-1)}}{1 + \frac{\theta_{ij}\Delta t}{\varepsilon}} & \text{if } \tilde{x}_{ij} < 0, \end{cases}$$

and the coefficient $\dfrac{\frac{\Delta t}{\varepsilon}}{1 + \frac{\Delta t}{\varepsilon}} = \dfrac{\Delta t}{\varepsilon + \Delta t}$ may be very close to 1.

An improvement can be achieved by the following technique that avoids iterative procedures. Let us assume that the boundary is located on the left, at position $x_b = x_L$ with

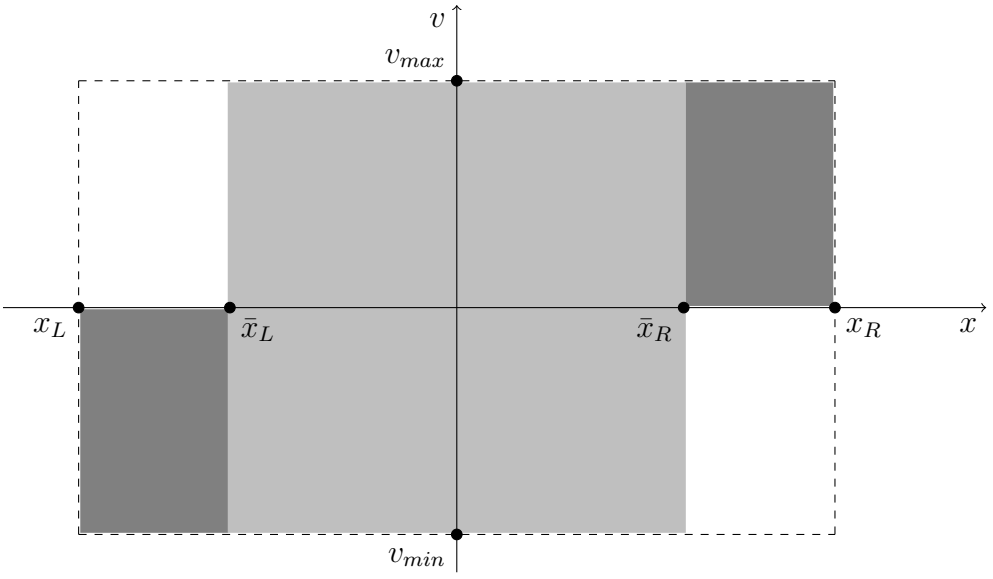

Figure 4.4: Mono dimensional phase space. The discretized distribution function is defined in $[x_L, x_R] \times [v_{min}, v_{max}]$. The distances $|x_L - \bar{x}_L|$ and $|x_R - \bar{x}_R|$ is $v_{max}\Delta t$. In the central region (ligth gray) the characteristics fan does not touch the boundary. In the dark gray regions (outflow region) we can extrapolate the distribution function from the central region. For the inflow region (white region) we use information coming from the wall.

temperature T_b. We assume that we know the solution at time t^n and the density at x_L, ρ_b^n.

First of all we can compute the distribution function at time t^{n+1} where the characteristics fan does not touch the wall (light gray region, Fig. 4.4) using the technique described in the previous chapter. Then one can compute the distribution function at the outflow region (dark gray region, Fig. 4.4), where $v \cdot n < 0$, for the spatial grid nodes whose characteristics fan touches the wall, by extrapolation. A natural way to extrapolate the distribution function is by means of Lagrange polynomials. However, when a shock goes out of the boundary, the high order extrapolation may lead to severe oscillations near the shock. To prevent this, we would like to have a lower order accurate but more robust extrapolation. Therefore, a WENO type extrapolation [19, 54] will be applied and described in the next section.

Now, we can compute the distribution function at the inflow boundary in a very simple way making a little modification to the expression (4.4). We define the distribution function at the boundary in this way:

$$f_{bj}^{n+1} = \begin{cases} f_{bj}^{n+1}(\text{obtained by extrap.}) & \text{if } v_j \cdot n < 0 \\ \\ \rho_b^{n+1} E_{bj} & \text{if } v_j \cdot n > 0. \end{cases} \tag{4.6}$$

The main difference between expressions (4.4) and (4.6) is that in expression (4.6) the Maxwellian at time t^{n+1} does not appear, therefore there is no need for iterative loops. The unknown is only ρ_b^{n+1}, that can be easily computed imposing zero mass flux at the boundary:

$$\rho_b^{n+1} = \frac{\sum_{v_j \cdot n < 0} v_j f_{bj}^{n+1}}{\sum_{v_j \cdot n > 0} v_j E_{bj}}. \tag{4.7}$$

As last, we have to update the distribution function at time t^{n+1} in the spatial grid nodes whose characteristics fan touches the wall at the inflow (white region, Fig. 4.4). In this case we define the distribution function in the following way:

$$f_{ij}^{n+1} = \begin{cases} f_{ij}^{n+1}(\text{obtained by extrap.}) & \text{if } v_j \cdot n < 0 \\ \\ f_{\theta_{ij}} & \text{if } v_j \cdot n > 0 \text{ and } \tilde{x}_{ij} < 0. \\ \\ \text{interpolation between} f_{\theta_{ij}} \text{and} & \\ f_{ij}^{n} \text{in the inner cells (light gray region)} & \text{if } v_j \cdot n > 0 \text{ and } \tilde{x}_{ij} > 0. \end{cases} \tag{4.8}$$

Also in this case the main difference between expressions (4.5) and (4.8) is that in expression (4.6) the Maxwellian at time t^{n+1} does not appear, therefore there is again no need

for iterative loops to compute the macroscopic moments of the Maxwellian.
The main advantage of the second technique is that the computational time does not increase as the relaxation parameter approaches to zero, but remains constant. Moreover, the formulation is self consistent (mass conservation is maintained), and the numerical technique explained in Fig. 4.4 has to be used only for few grid points near the boundary.

4.2 Inverse Lax-Wendroff technique

A good technique available in literature to treat diffusive boundary conditions due to Filbet and Yang [19], is the Inverse Lax-Wendroff method. This technique is useful when the numerical scheme foresees the employment of ghost points. In particular, it is applied to compute the values of f at the ghost points for the inflow boundary. In this case we cannot approximate f by an extrapolation, since the distribution function at the interior points cannot predict the inflow. Filbet and Yang in [19] extended the inverse Lax-Wendroff type procedure proposed in [55, 30, 59] for solving kinetic equations. At the left boundary x_L, a first order Taylor expansion gives

$$f_j(x) = f_{x_L,j} + (x - x_L)\frac{\partial f}{\partial x}\bigg|_{x=x_L} + O(\Delta x^2).$$

Hence a first order approximation of f at ghost points g is

$$f_{g,j} = f_{x_L,j} + (x_g - x_L)\frac{\partial f}{\partial x}\bigg|_{x=x_L}.$$

To obtain the values on the ghost points it is necessary to approximate the first spatial derivative. By reformulating the Boltzmann equation we have

$$\frac{\partial f}{\partial x}\bigg|_{x=x_L} = \frac{1}{v_x}\bigg(- \frac{\partial f}{\partial t} + \frac{1}{\varepsilon}Q(f,f)\bigg)\bigg|_{x=x_L}.$$

Now, instead of approximating the first spatial derivative, one has to compute the time derivative and the collision operator in $x = x_L$. An approximation of the time derivative and of the collision term can be computed explicitly using the values of f at previous time instants at the boundary. In the numerical test section a comparison between the technique proposed in this thesis and the inverse Lax-Wendroff method is investigated.

4.3 Numerical test

In this section, we present a variety of test cases in 1D showing the effectiveness of our method to get an accurate solution of the BGK equation set in a bounded domain with

diffusive boundary conditions. The numerical results have been obtained using BDF2 scheme coupled with the treatment at the boundary which not uses iterative procedure.

4.3.1 Smooth solutions

First of all, we consider a smooth initial data to compute the order of convergence in L^2 norm of our numerical methods. As smooth initial datum f_0 we consider the following

$$f_0(x,v) = \frac{\rho_0(x)}{2\pi} \exp\left(-\frac{v^2}{2}\right),\ x \in (-0.5, 0.5),\ v \in [-10, 10],$$

with a density $\rho_0(x) = 1 + 0.1\cos(2\pi x)$. We consider purely diffusive boundary conditions with a wall temperature $T_L = T_R = 1$. The solution is expected to be smooth for short time and then may develop a discontinuity at the boundary, which may propagate in the physical domain. We perform several numerical simulations on a time interval $[0, t_f]$ with $t_f = 1$, $N_v = 20$, CFL number equal to 4 and a grid space varying with $N_x = 40, 80, \ldots, 1280$. In Tables 4.1, 4.2 we compute the error and the accuracy order in L^2 norm of our numerical methods, varying the Knudsen number ε from rarefied to hydrodynamic regimes. The error is computed making the differences between two solution obtained by two different meshes, N_x and $2N_x$. We can clearly see the expected second order convergence in rarefied regime; as the Knudsen number approaches zero, the order decreases because some discontinuities arise near the wall. Moreover, we verify that our scheme is also second-order accurate at the boundary.

L_2 relative errors

N_x	$\varepsilon = 1$	$\varepsilon = 10^{-1}$	$\varepsilon = 5 \cdot 10^{-2}$	$\varepsilon = 10^{-2}$	$\varepsilon = 10^{-3}$	$\varepsilon = 5 \cdot 10^{-4}$	$\varepsilon = 10^{-4}$
80	2.803e-3	1.662e-3	2.234e-3	6.590e-3	1.583e-2	1.708e-2	1.823e-2
160	1.601e-3	5.328e-4	7.921e-4	2.885e-3	1.033e-2	1.222e-2	1.443e-2
320	7.076e-4	1.613e-4	2.541e-4	1.026e-3	4.909e-3	6.664e-3	9.753e-3
640	2.398e-4	4.556e-5	7.650e-5	3.540e-4	1.799e-3	2.782e-3	5.668e-3
1280	6.838e-5	1.213e-5	2.143e-5	1.246e-4	5.713e-4	9.143e-4	2.494e-3

L_2 orders

160	0.8074	1.6417	1.4960	1.1917	0.6160	0.4828	0.3375
320	1.1784	1.7239	1.6403	1.4905	1.0736	0.8758	0.5652
640	1.5611	1.8239	1.7317	1.5360	1.4483	1.2602	0.7828
1280	1.8103	1.9083	1.8356	1.5060	1.6549	1.6054	1.1841

Table 4.1: Relative errors and convergence rate of the distribution function in the whole domain, in L^2 norm.

L_2 relative errors at the boundary

N_x	$\varepsilon = 1$	$\varepsilon = 10^{-1}$	$\varepsilon = 5 \cdot 10^{-2}$	$\varepsilon = 10^{-2}$	$\varepsilon = 10^{-3}$	$\varepsilon = 5 \cdot 10^{-4}$	$\varepsilon = 10^{-4}$
160	3.012e-4	5.294e-4	1.103e-3	5.047e-3	1.520e-2	1.742e-2	1.994e-2
320	7.176e-5	2.013e-4	4.428e-4	2.197e-3	6.871e-3	8.201e-3	1.040e-2
640	1.754e-5	4.876e-5	1.175e-4	7.093e-4	1.931e-3	2.344e-3	2.870e-3
1280	4.405e-6	9.080e-6	2.300e-5	1.920e-4	5.068e-4	7.384e-4	9.022e-4
L_2 orders at the boundary							
320	2.0697	1.3944	1.3172	1.1995	1.1462	1.0872	0.9391
640	2.0323	2.0461	1.9135	1.6314	1.8309	1.8065	1.8579
1280	1.9938	2.4250	2.3533	1.8852	1.9300	1.6667	1.6696

Table 4.2: Relative errors and convergence rate of the distribution function at the boundary, in L^2 norm.

4.3.2 Flow generated by a gradient of temperature.

Now we consider a test case of more interesting physical meaning. We suppose to be in presence of a hot wall, that will generate a flow towards the interior. The initial data is the one used in [19], that is

$$f_0(x,v) = \frac{\rho_0(x)}{2\pi} \exp\left(-\frac{v^2}{2} \right),\ x \in (-0.5, 0.5),\ v \in [-10, 10],$$

with a density $\rho_0(x) = 1$ and $T_0(x) = 1 + 0.44(x + 0.5)$. We consider purely diffusive boundary conditions with a wall temperature $T_L = 1$ and $T_R = 1.44$. We perform numerical simulations on a time interval $[0, t_f]$ with t_f varying from a test to another (varying the Knudsen number the equilibrium is reached at different time), $N_v = 20$, CFL number equal to 4 and a grid space varying with $N_x = 100$. In Fig. 4.5 we can see the temperature and pressure profiles at different Knudsen numbers that are in good agreement with the results presented in [19] and obtained with the inverse Lax-Wendroff method. More precisely, the boundary layer (Knudsen layer) appears in the profiles of the macroscopic quantities. We can observe it without zoom in the pressure profile, because the pressure is almost constant in the bulk of the gas. Moreover, we can observe that the magnitude of the boundary layer is of the order of ε and it tends to disappear in the fluid limit ($\varepsilon \to 0$). Lastly, we perform a similar test, with the only difference that $T_0(x) = 1$. In Fig. 4.6 we can observe the heat wave that propagates in the temperature profile, caused by the difference of temperature between the right wall and the gas.

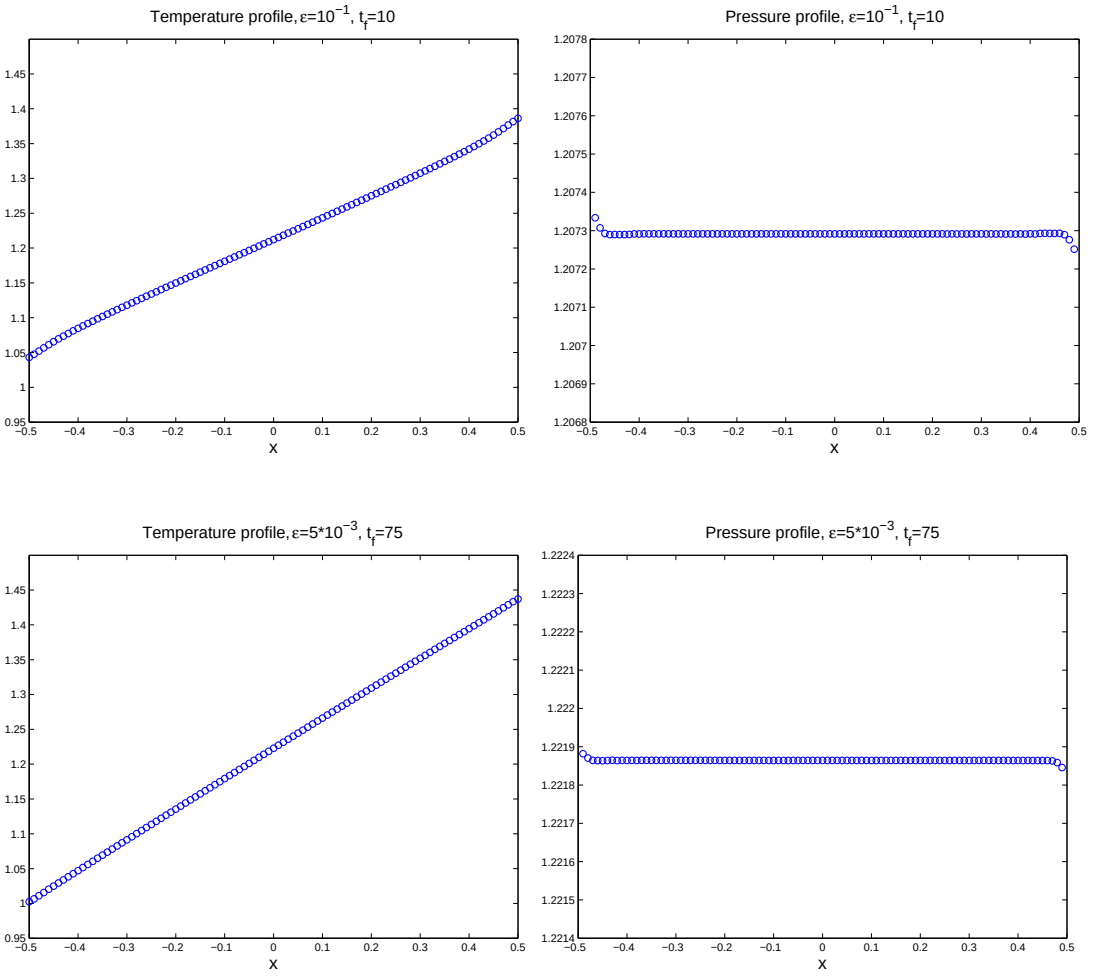

Figure 4.5: Stationary solution of the temperature and pressure profiles generated by a temperature gradient obtained at $t_f = 10$ if $\varepsilon = 10^{-1}$ and at $t_f = 75$ if $\varepsilon = 5 \cdot 10^{-3}$. The magnitude of the Knudsen layer is of the order of ε.

4.4 WENO type extrapolation

The WENO type extrapolation used to the treatment of diffusive boundary is the one developed in [19, 54, 55, 56]. The key point of WENO type extrapolation is to define smoothness indicators, which are designed to choose automatically between the high order accuracy and the low order, but more robust, extrapolation. Here we describe this method in spatially 1D case.

Assume that we have a stencil of three points $S = \{x_1, x_2, x_3\}$ and denote the corresponding distribution function by f_1, f_2, f_3. Instead of extrapolating f at the point x_{ex}

by Lagrange polynomial, we use following Taylor expansion

$$f_{ex} = \sum_{k=0}^{2} \frac{(x_{ex} - x_\ell)^k}{k!} \frac{d^k f}{dx^k}\bigg|_{x=x_\ell}.$$

We aim to obtain a $(3-k)$–th order approximation of $\frac{d^k f}{dx^k}\Big|_{x=x_\ell}$ denoted by $f_\ell^{(k)},\ k = 0, 1, 2.$ Three candidate sub–stencils are given by

$$S_r = \{x_1, ..., x_{r+1}\},\ r = 0, 1, 2.$$

In each sub–stencil S_r, we could construct a Lagrange polynomial $p_r(x) \in \mathbb{P}_r(\mathbb{R})$

$$\begin{cases} p_0(x) = f_1, \\ p_1(x) = f_1 + \frac{f_2 - f_1}{\Delta x}(x - x_1), \\ p_2(x) = f_1 + \frac{f_2 - f_1}{\Delta x}(x - x_1) + \frac{f_3 - 2f_2 + f_1}{2\Delta x^2}(x - x_1)(x - x_2). \end{cases}$$

We now look for the WENO type extrapolation in the form

$$f_\ell^{(k)} = \sum_{r=0}^{2} \omega_r \frac{d^k p_r(x)}{dx^k}(x_\ell),$$

where ω_r are the nonlinear weights depending on f_i. We expect that $f_\ell^{(k)}$ is $(3-k)$–th order accurate in the case $f(x)$ is smooth in S_2. The nonlinear weights are given by

$$\omega_r = \frac{\alpha_r}{\sum_{s=0}^{2} \alpha_s},$$

with

$$\alpha_r = \frac{d_r}{(\varepsilon + \beta_s)^2},$$

where $\varepsilon = 10^{-6}$ and β_r are the new smoothness indicators determined by $\beta_0 = \Delta x^2$,

$$\beta_1 = (f_2 - f_1)^2,$$

$$\beta_2 = \frac{13}{12} f_1^2 + \frac{16}{3} f_2^2 + \frac{25}{12} f_3^2 - \frac{13}{3} f_1 f_2 + \frac{13}{6} f_1 f_3 - \frac{19}{3} f_2 f_3,$$

and $d_0 = \Delta x^2$, $d_1 = \Delta x$, and $d_2 = 1 - d_0 - d_1$. For more details see[54, 55, 56].

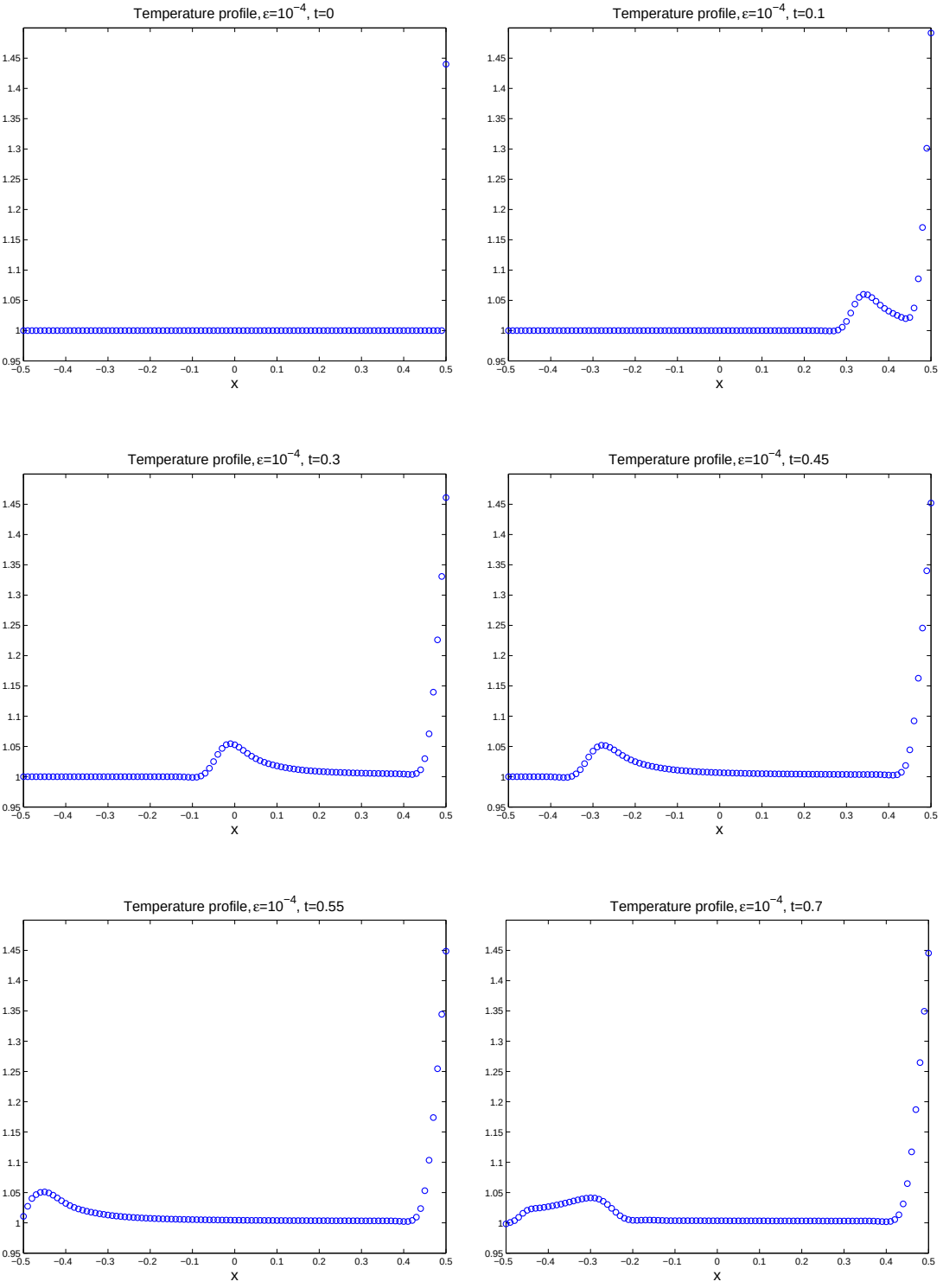

Figure 4.6: Temperature profile. Wave generated by a temperature gradient obtained at different time instants. $\varepsilon = 10^{-4}$, CFL=2, $N_x = 100$, $N_v = 20$.

Chapter 5

BGK models for gas mixtures and semi-Lagrangian approximation

Most of the BGK models have been considered in the case of a single species gas. This seems an important limitation, recalling for example that the atmosphere must be at least considered as a binary mixture of Oxygen and Nitrogen. Although the extension of the Boltzmann equation to a mixture of gases has been well known for a long time, this is not the case for the BGK equation. Considerable troubles are encountered if one tries to extend the BGK philosophy, originally devised for a single species gas, to a gas mixture [52, 21]. Indeed, one faces immediately very basic drawbacks such as loss of positivity of temperature and breakdown of the indifferentiability principle. An accurate and detailed discussion on the subject may be found in [3], where the authors propose a simple and very interesting consistent BGK-type model for gas mixtures which overcomes all previous difficulties. In this Chapter kinetic and BGK equations for both inert and reactive gas mixtures are presented. Moreover, numerical results, obtained by means of the semi-Lagrangian schemes proposed, are shown.

5.1 Boltzmann equation for inert gas mixtures

We consider now a gas mixture of L different species G^s, $s = 1, \cdots, L$. The kinetic description is given by L Boltzmann equations for distribution functions $f^s(t, x, v)$, $(t, x, v) \in \mathbb{R}^+ \times \mathbb{R}^3 \times \mathbb{R}^3$

$$\frac{\partial f^s}{\partial t} + v \cdot \nabla_x f^s = Q^s, \quad s = 1, \cdots, L, \tag{5.1}$$

where

$$Q^s = \sum_{r=0}^{L} Q^{sr}(f^s, f^r), \quad s = 1, \cdots, L,$$

and

$$Q^{sr}(f^s, f^r) = \int_{\mathbb{R}^3} \int_{\mathbb{S}^2} B_{sr}(v, w, \Omega)[f^s(v')f^r(w') - f^s(v)f^r(w)]\, d\Omega\, dw$$

is the usual scattering collision operator for the binary (s, r) interaction.
We introduce notations for macroscopic quantities that will be used later on: m^s is the molecular masses, n^s the number density, ρ^s the density, u^s the average velocity, T^s the temperature of species s. One has:

$$n^s = \int_{\mathbb{R}^3} f^s\, dv, \quad \rho^s = m^s n^s$$

$$u^s = \frac{1}{n^s} \int_{\mathbb{R}^3} v f^s\, dv$$

$$n^s K_B T^s = \frac{1}{3} m^s \int_{\mathbb{R}^3} (v - u^s)^2 f^s\, dv.$$

Then we also have global quantities for the mixture, the number density n, the total density ρ, the mean velocity u, scalar pressure p or temperature T, which are expressed in terms of single component parameters by

$$n = \sum_{s=1}^{L} n^s, \quad \rho = \sum_{s=1}^{L} \rho^s = \sum_{s=1}^{L} m^s n^s,$$

$$u = \frac{1}{\rho} \sum_{s=1}^{L} m^s n^s u^s,$$

$$p = nK_B T = \sum_{s=1}^{L} n^s K_B T^s + \frac{1}{3} \sum_{s=1}^{L} m^s n^s (u^s - u)^2.$$

Of course the Boltzmann equation for mixture has to satisfy the *indifferentiability principle*. It states that, when all the masses m^s and cross-sections B^{sr} are identical, the total distribution function $f = \sum_{s=1}^{L} f^s$ obeys the single species Boltzmann equation. Notice also that the macroscopic quantities associated to f are n, u and T in this case.
For multispecies gases, we have to keep in mind that for each species mass, momentum and energy are not necessarily conserved. If we suppose that there is no chemical reaction between the species, the mass of each species is conserved

$$\int_{\mathbb{R}^3} Q^s\, dv = 0, \quad s = 1, \cdots, L \tag{5.2}$$

Each species may nevertheless exchange momentum and energy with the others, so the species momentum and energy cannot be conserved in general. Such rates can be made explicit for Maxwellian molecules [13]. In detail, the exchange relations can be computed and one obtains [3, 22]:

$$\int_{\mathbb{R}^3} m^s v Q^s \, dv = \sum_{r=1}^{L} \nu_1^{sr} \mu^{sr} n^s n^r (u^r - u^s), \tag{5.3}$$

$$\int_{\mathbb{R}^3} \frac{m^s}{2} v^2 Q^s \, dv = \sum_{r=1}^{L} \nu_1^{sr} \frac{2\mu^{sr}}{m^s + m^r} n^s n^r \left[\frac{3}{2} K_B (T^r - T^s) + \frac{1}{2} (m^r u^r + m^s u^s) \cdot (u^r - u^s) \right], \tag{5.4}$$

where μ^{sr} is the reduced mass

$$\mu^{sr} = \frac{m^s m^r}{m^s + m^r},$$

and $\nu_k^{sr}(g) = \nu_k^{rs}(g)$ are the microscopic collision frequencies

$$\nu_k^{sr}(g) = \nu_k^{rs}(g) = 2\pi g \int_0^{\pi} \sigma^{sr}(g, \chi)(1 - cos\chi)^k \sin\chi \, d\chi, \quad k = 0, 1, \tag{5.5}$$

with $\nu_k^{sr} \leq 2\nu_0^{sr}$ and σ stands for differential cross section and g is the relative speed. Actually, under the hypothesis of Maxwellian molecules ($\sigma^{sr}(g, \chi) \propto 1/g$) the microscopic collision frequencies are constant with respect to the relative speed g. Of course

$$\sum_{s=1}^{L} \int_{\mathbb{R}^3} m^s v \, Q^s \, dv = 0 \quad \text{and} \quad \sum_{s=1}^{L} \int_{\mathbb{R}^3} \frac{1}{2} m^s v^2 Q^s \, dv = 0$$

that is, the momentum and the energy of the global mixture are conserved. Thus, in a mixture without chemical reaction there are $L+4$ collision invariants, relevant to the mass of each species, to the total momentum and total kinetic energy.

The equilibrium in the mixture is obtained when all $Q^s = 0$. Then $Q^{sr} = 0$. It can be proved that if for two species s and r $Q^{sr} = Q^{rs} = 0$ then f^s and f^r are Maxwellians with common velocity and temperature. The conclusion is that at global equilibrium, all distributions are Maxwellians of the form

$$f^s = n^s \left(\frac{m^s}{2\pi K_B T} \right)^{3/2} \exp\left(- \frac{m^s |v - u|^2}{2K_B T} \right), \tag{5.6}$$

with common velocity u and temperature T.
In a spatially uniform state ($\nabla_x f = 0$), the H-theorem can be proved choosing the following H-function [3]

$$H = \sum_{s=1}^{L} \int_{\mathbb{R}^3} f^s \ln(f^s) \, dv, \tag{5.7}$$

and, in the case of mixture, the entropy inequality is

$$\sum_{s=1}^{L} \int_{\mathbb{R}^3} Q^s \ln(f^s)\, dv \leq 0.$$

5.2 BGK models for inert gas mixtures

After the introduction of the BGK model for one-species gas, many attempts have been made to extend the BGK model to gas mixture. The trivial extension

$$\frac{\partial f^s}{\partial t} + v \cdot \nabla_x f^s = \nu^s (M^s - f^s), \quad s = 1, \cdots, L$$

where ν^s is the species collision frequencies and M^s is the local Maxwellian with density, momentum and temperature of the species s is not consistent because it does not reproduce equilibrium conditions $u^s = u$ and $T^s = T\ \forall s$.
Among the pioneering BGK models for mixtures we can cite [26, 52, 21]. The models presented in [26, 52] have an important drawback: when all species are identical one does not recover the BGK equation for a single gas, that is, they do not satisfy the indifferentiability principle. In [21] a different model overcoming this drawback is proposed, but positivity is lost. Here we present two consistent BGK models for inert mixtures which overcome all previous difficulties.

5.2.1 The BGK model of Andries, Aoki and Perthame

The first consistent BGK model for inert mixtures, satisfying the main properties of the Boltzmann equation for mixtures, such as positivity, indifferentiability principle and entropy inequality, was introduced in [3]. The key idea is that instead of approximating each binary collision operator (between specie s and r) by a BGK-type equation, only one global operator is introduced (i.e., taking into account all the species r) for each species s. The model is built as follows. The relaxation occurs toward a Maxwellian distribution M_s, i.e.,

$$\frac{\partial f^s}{\partial t} + v \cdot \nabla_x f^s = Q^s_{BGK} = \nu_s (M_s - f^s), \quad s = 1, \cdots, L, \tag{5.8}$$

where f^s is the distribution function of the species s, M_s is an auxiliary local Maxwellian depending on velocity vector variable v, molecular masses m^s, Boltzmann constant K_B and disposable parameters n_s, u_s, T_s

$$M_s = n_s \left(\frac{m^s}{2\pi K_B T_s} \right)^{3/2} \exp\left(- \frac{m^s}{2K_B T_s} (v - u_s)^2 \right), \quad s = 1, \cdots, L. \tag{5.9}$$

(Note the subscript s, while actual macroscopic fields have a superscript s).
At last, ν_s represents the inverse of the sth relaxation time, possibly depending on macroscopic fields, but independent of v. The authors in [3] emphasize that the choice of ν_s is crucial. In particular the model is well defined with the total collision frequency

$$\nu_s = \sum_{r=1}^{L} \nu_0^{sr} n^r. \tag{5.10}$$

With this choice of ν_s it can be proved [3] that the positivity of the temperature is ensured. The above auxiliary fields n_s, u_s, T_s are determined from the corresponding actual moments of the distribution functions f^s (namely number density n^s, mass velocity u^s and temperature T^s of each component) by requiring that the BGK model prescribes the same exchange rates by collisions of the Boltzmann level given in (5.3)-(5.4). By (5.2) of course $n_s = n^s \, \forall s$, since $\int_{\mathbb{R}^3} Q^s_{BGK} = n_s - n^s$ must be zero. Following [3], we now impose that the Boltzmann equation (5.1) and its approximate model (5.8) prescribe the same exchange rates (5.3) and (5.4), that is:

$$\int_{\mathbb{R}^3} m^s v Q^s_{BGK} \, dv = \int_{\mathbb{R}^3} m^s v Q^s \, dv$$

or equivalently

$$m^s n_s u_s - m^s n^s u^s = \sum_{r=1}^{L} \nu_1^{sr} \mu^{sr} n^s n^r (u^r - u^s)$$

and

$$\int_{\mathbb{R}^3} \frac{1}{2} m^s v^2 Q^s_{BGK} \, dv = \int_{\mathbb{R}^3} \frac{1}{2} m^s v^2 Q^s \, dv$$

or equivalently

$$\nu_s \left[n_s \frac{3}{2} K_B T_s - n^s \frac{3}{2} K_B T^s + n_s \frac{1}{2} m^s u_s^2 - n^s \frac{1}{2} m^s (u^s)^2 \right] =$$

$$= \sum_{r=1}^{L} \nu_1^{sr} \frac{2\mu^{sr}}{m^s + m^r} n^s n^r \left[\frac{3}{2} K_B (T^r - T^s) + \frac{1}{2} (m^r u^r + m^s u^s) \cdot (u^r - u^s) \right].$$

Upon introducing the auxiliary symmetric matrices

$$\xi^{sr} = \xi^{rs} = \nu_1^{sr} \mu_{sr} n^s n^r - \delta^{sr} \sum_{l=1}^{L} \nu_1^{sl} \mu^{sl} n^s n^r,$$

$$\gamma^{sr} = \gamma^{rs} = 3 K_B \nu_1^{sr} \frac{\mu^{sr}}{m^s + m^r} n^s n^r - \delta^{sr} 3 K_B \sum_{l=1}^{L} \nu_1^{sl} \frac{\mu^{sl}}{m^s + m^l} n^s n^l,$$

where δ^{sr} denotes the usual Kronecker symbol, the parameters determining all attracting Maxwellians M_s read explicitly as

$$u_s = \frac{1}{m^s n^s}\left[m^s n^s u^s + \frac{1}{v_s}\sum_{r=1}^{L}\xi^{sr}u^r\right], \tag{5.11}$$

$$T_s = \frac{2}{3n^s K_B}\left[n^s\frac{3}{2}K_B T^s - \frac{1}{2}m^s[n^s(u_s)^2 - n^s(u^s)^2] + \frac{1}{\nu_s}\sum_{r=1}^{L}\gamma^{sr}T^r + \right.$$

$$\left. + \frac{1}{\nu_s}\sum_{r=1}^{4}\nu_1^{sr}\frac{\mu^{sr}}{m^s+m^r}n^s n^r(m^s u^s + m^r u^r)(u^r - u^s)\right]. \tag{5.12}$$

Under the hypothesis (5.10) Andries, Aoki and Perthame proved in [3] that the temperatures (5.12) are positive. The above scheme guarantees that the BGK approximation fulfills the main features of the actual collision operator. Obviously the conservation equations are recovered by construction. Moreover, the main properties, such us indifferentiability principle, H-theorem and entropy inequality are recovered. The H-theorem can be proved using the same H-function (5.7) of the Boltzmann level [3]. Indeed,

$$\frac{\partial}{\partial t}H = \frac{\partial}{\partial t}\sum_{s=1}^{L}\int_{\mathbb{R}^3} f^s \ln(f^s)\,dv \leq 0.$$

As a consequence, in the time evolution the BGK model pushes the distribution function towards the local equilibrium M^s, where M^s is the $L+4$-parameter family of Maxwellians distributions given in (5.6) with global mass velocity u and temperature T.

5.2.2 A new BGK model for inert mixtures

In the previous model for inert mixtures, have been introduced $4L$ auxiliary parameters, namely u^s and T^s, $s = 1, \cdots, L$ in order to recover the same exchange rates of the Boltzmann level and the correct conservation equations. Now we introduce a new BGK model which does not reproduce the species exchange rates of the Boltzmann level, but only the conservation of total momentum and kinetic energy. In this way, one obtains a BGK model of the form

$$\frac{\partial f^s}{\partial t} + v\cdot\nabla_x f^s = \tilde{Q}^s_{BGK} = \nu_s(M_s - f^s), \quad s = 1, \cdots, L, \tag{5.13}$$

where now the attractors $\tilde{M}_s$ are fictitious Maxwellians

$$\tilde{M}_s = \tilde{n}^s\left(\frac{m^s}{2\pi K_B\tilde{T}}\right)^{3/2}\exp\left(-\frac{m^s}{2K_B\tilde{T}}(v-\tilde{u})^2\right), \quad s = 1, \cdots, L, \tag{5.14}$$

defined in terms of $L+4$ (instead of $5L$) auxiliary parameters $\tilde{n}^s$, $s=1,\cdots,L$, $\tilde{u}$, and $\tilde{T}$. The main difference with the previous BGK model is that now the attractor $\tilde{M}_s$ have common fictitious velocities and temperature $\tilde{u}$ and $\tilde{T}$. In other words, the model pushes the gas towards a full, instead of partial, equilibrium. Once again, the auxiliary macroscopic fields depend on the actual macroscopic fields of f^s and are determined in such a way to satisfy the conservation of mass, momentum and energy. Of course $\tilde{n}_s = n^s$ since we are considering inert mixtures. Imposing the total conservation of momentum and energy we obtain

$$\sum_{s=1}^{L} \int_{\mathbb{R}^3} m^s v \tilde{Q}^s_{BGK}\, dv = 0 \tag{5.15}$$

or equivalently

$$\sum_{s=1}^{L} \nu_s m^s n^s (\tilde{u} - u^s) = 0$$

and for the energy

$$\sum_{s=1}^{L} \int_{\mathbb{R}^3} \frac{1}{2} m^s v^2 \tilde{Q}^s_{BGK}\, dv = 0 \tag{5.16}$$

or equivalently

$$\sum_{s=1}^{L} \nu_s \left[\frac{1}{2} m^s n^s \tilde{u}^2 + \frac{3}{2} n^s K_B \tilde{T} - \frac{1}{2} m^s n^s (u^s)^2 - \frac{3}{2} n^s K_B T^s \right] = 0.$$

Therefore, the parameters determining the Maxwellians (5.14) read explicitly as

$$\tilde{u} = \frac{\sum_{s=1}^{L} \nu_s m^s n^s u^s}{\sum_{s=1}^{L} \nu_s m^s n^s}, \tag{5.17}$$

$$\tilde{T} = \frac{\sum_{s=1}^{L} \nu_s n^s \left[\frac{1}{2} m^s ((u^s)^2 - \tilde{u}^2) + \frac{3}{2} K_B T^s \right]}{\frac{3}{2} K_B \sum_{s=1}^{L} \nu_s n^s}. \tag{5.18}$$

As the BGK model of Andries, Aoki and Perthame, the above scheme satisfies the main properties, such us positivity, indifferentiability principle; also the H-theorem and entropy inequality are recovered.

As regards positivity, we have to prove that $\tilde{T}$ in (5.18) is positive.

Theorem 5.2.1. *The global temperature $\tilde{T}$ (5.18) is positive.*

Proof. We observe that $\tilde{T}$ is positive is and only if

$$\left(\sum_{s=1}^{L} \alpha_s u^s \right)^2 \leq \sum_{s=1}^{L} \alpha_s |u^s|^2 \tag{5.19}$$

where $\sum_{s=1}^{L} \alpha_s = 1$. Indeed,

$$\tilde{T} > 0 \Leftrightarrow \sum_{s=1}^{L} \nu_s n^s [m^s((u^s)^2 - \tilde{u}^2) + 3K_B T^s] > 0 \Leftrightarrow$$

$$\Leftrightarrow \sum_{s=1}^{L} \nu_s n^s m^s \tilde{u}^2 < \sum_{s=1}^{L} \nu_s n^s [m^s (u^s)^2 + 3K_B T^s] \Leftrightarrow$$

$$\Leftrightarrow \tilde{u}^2 < \sum_{s=1}^{L} \alpha_s \left[(u^s)^2 + 3K_B \frac{T^s}{m^s} \right],$$

where

$$\alpha_s = \frac{\nu^s n^s m^s}{\sum_{s=1}^{L} \nu^s n^s m^s}.$$

Expression (5.19) follows observing that $\tilde{u} = \sum_{s=1}^{L} \alpha_s u^s$.

Now we prove by induction that $(\sum_{s=1}^{L} \alpha_s u^s)^2 \leq \sum_{s=1}^{L} \alpha_s |u^s|^2$, with $u^s = (u_x^s, u_y^s, u_z^s) \in \mathbb{R}^3$, $\sum_{s=1}^{L} \alpha_s = 1$, $\alpha_s \geq 0 \, \forall s$.

Case $L = 2$.

$$(\alpha_1 u^1 + \alpha_2 u^2)^2 = (\alpha_1 u_x^1 + \alpha_2 u_x^2)^2 + (\alpha_1 u_y^1 + \alpha_2 u_y^2)^2 + (\alpha_1 u_z^1 + \alpha_2 u_z^2)^2 =$$

$$= \alpha_1^2 \left[(u_x^1)^2 + (u_y^1)^2 + (u_z^1)^2 \right] + \alpha_2^2 \left[(u_x^2)^2 + (u_y^2)^2 + (u_z^2)^2 \right] +$$

$$+ 2\alpha_1 \alpha_2 u_x^1 u_x^2 + 2\alpha_1 \alpha_2 u_y^1 u_y^2 + 2\alpha_1 \alpha_2 u_z^1 u_z^2.$$

$$(\alpha_1 u^1 + \alpha_2 u^2)^2 - \alpha_1 |u^1|^2 - \alpha_2 |u^2|^2 =$$

$$= (\alpha_1^2 - \alpha_1) \left[(u_x^1)^2 + (u_y^1)^2 + (u_z^1)^2 \right] + (\alpha_2^2 - \alpha_2) \left[(u_x^2)^2 + (u_y^2)^2 + (u_z^2)^2 \right] +$$

$$+ 2\alpha_1 \alpha_2 u_x^1 u_x^2 + 2\alpha_1 \alpha_2 u_y^1 u_y^2 + 2\alpha_1 \alpha_2 u_z^1 u_z^2 =$$

$$= -\alpha_1 \alpha_2 \Big[(u_x^1)^2 + (u_y^1)^2 + (u_z^1)^2 + (u_x^2)^2 + (u_y^2)^2 + (u_z^2)^2 +$$

$$- 2(u_x^1)^2 (u_x^2)^2 - 2(u_y^1)^2 (u_y^2)^2 - 2(u_z^1)^2 (u_z^2)^2 \Big] =$$

$$= -\alpha_1 \alpha_2 \left[(u_x^1 - u_x^2)^2 + (u_y^1 - u_y^2)^2 + (u_z^1 - u_z^2)^2 \right] = -\alpha_1 \alpha_2 |u^1 - u^2|^2 \leq 0.$$

Finally, supposed that the property holds for $L-1$, now we prove it for L.

$$\sum_{s=1}^{L}\alpha_s u^s = (1-\alpha_L)\sum_{s=1}^{L-1}\beta_s u^s + \alpha_L u^L = \gamma_1\omega_1 + \gamma_2\omega_2,$$

where

$$\beta_s = \frac{\alpha_s}{1-\alpha_L}, \qquad \sum_{s=1}^{L-1}\beta_s = \frac{\sum_{s=1}^{L-1}\alpha_s}{1-\alpha_L} = 1,$$

$$\gamma_1 = 1-\alpha_L, \quad \gamma_2 = \alpha_L, \quad \omega_1 = \sum_{s=1}^{L-1}\beta_s u^s, \quad \omega_2 = u^L.$$

Then, we obtain

$$(\sum_{s=1}^{L}\alpha_s u^s)^2 \le \gamma_1|\omega_1|^2 + \gamma_2|\omega_2|^2 = (1-\alpha_L)(\sum_{s=1}^{L-1}\beta_s u^s)^2 + \alpha_L|u^L|^2 \le$$

$$\le (1-\alpha_L)\sum_{s=1}^{L-1}\beta_s|u^s|^2 + \alpha_L|u^L|^2 = \sum_{s=1}^{L}\alpha_s|u^s|^2.$$

□

The H-theorem can be easily proved.

Theorem 5.2.2. *Let*

$$H = \sum_{s=1}^{L}\int_{\mathbb{R}^3} f^s \ln(f^s)\,dv.$$

Then $\dot{H} \le 0$, *and* $\dot{H} = 0$ *if and only if* $f^s = \tilde{M}_s$

Proof.

$$\dot{H} = \sum_{s=1}^{L}\int_{\mathbb{R}^3} \tilde{Q^s_{BGK}} \ln(f^s)\,dv =$$

$$= \sum_{s=1}^{L}\int_{\mathbb{R}^3} \nu_s(\tilde{M}_s - f^s)\ln(f^s)\,dv.$$

We observe that from conservations (5.15) and (5.16) follows that

$$\sum_{s=1}^{L}\int_{\mathbb{R}^3} \tilde{Q}^s_{BGK}\ln(\tilde{M}^s)\,dv = 0.$$

Then we can write

$$\dot{H} = \sum_{s=1}^{L}\int_{\mathbb{R}^3} \tilde{Q}^s_{BGK}[\ln(f^s) - \ln(\tilde{M}^s)]\,dv = \sum_{s=1}^{L}\int_{\mathbb{R}^3}(\tilde{M}^s - f^s)\ln\left(\frac{f^s}{\tilde{M}^s}\right)dv =$$

$$= \sum_{s=1}^{L} \nu_s \int_{\mathbb{R}^3} \tilde{M}^s \left(1 - \frac{f^s}{\tilde{M}^s}\right) \ln\left(\frac{f^s}{\tilde{M}^s}\right) dv \leq 0.$$

The last inequality holds because the function $(x-1)\ln x$ is always positive except in $x = 1$ where it vanishes. □

As a consequence, the time evolution pushes the distribution function towards the local equilibrium M^s, where M^s is the Maxwellian distribution

$$M^s = n^s \left(\frac{m^s}{2\pi K_B T}\right)^{3/2} \exp\left(-\frac{m^s}{2K_B T}(v-u)^2\right), \quad s = 1, \cdots, L,$$

with global mass velocity u and temperature T.

5.3 BGK model for reactive mixtures

Now we introduce an extension of the previous BGK model (5.8), due to Groppi and Spiga [25], to the much more complicated problems, significant for applications, in which gas components may undergo chemical reactions.
The main difference with the inert BGK model is that now also exchange of mass and of energy of chemical link have to be considered. In particular, the authors in [25] deal with a four species gas mixture and with the reversible chemical reaction

$$A^1 + A^2 \rightleftharpoons A^3 + A^4. \tag{5.20}$$

Molecules A^s are endowed with an energy of chemical bond E^s and may also interact with any, different or equal, species $r = 1, \cdots, 4$ by elastic scattering.
The system of Boltzmann equations describing these processes has been derived and investigate in [47]. Here we just recall that there exist seven independent collision invariants, and they may be chosen as three combinations of number densities $n^s + n^r$, for instance $(s, r) = (1, 3), (1, 4), (2, 4)$, (relevant to the balance between reactants and products), the global mass velocity and the internal (kinetic plus chemical) energy. Consequently, we get seven exact, non-closed, macroscopic conservation equations. Correspondingly, we have now a seven-parameter family of Maxwellians

$$M^s(v) = n^s \left(\frac{m^s}{2\pi K_B T}\right)^{3/2} \exp\left(-\frac{m^s}{2K_B T}(v-u)^2\right),$$

as collision equilibria, with equilibrium densities bound together by the well known mass action law of chemistry

$$\frac{n^1 n^2}{n^3 n^4} = \left(\frac{\mu^{12}}{\mu^{34}}\right)^{3/2} \exp\left(\frac{\Delta E}{K_B T}\right), \tag{5.21}$$

where ΔE is the energy threshold $\Delta E = -\sum_{s=1}^{4} \lambda^s E^s > 0$ (with $\lambda^1 = \lambda^2 = -\lambda^3 = -\lambda^4 = 1$) to be overcome in the endothermic reaction, conventionally assumed to be the one from the left to the right in (5.20). A strict entropy inequality for relaxation to equilibrium has also been established in terms of the H functional [47]

$$H = \sum_{s=1}^{4} \int_{\mathbb{R}^3} f^s \ln(f^s/(m^s)^3).\, dv \tag{5.22}$$

5.3.1 The BGK model of Groppi and Spiga

The main structure of this BGK model for reactive mixture is similar to (5.8), (5.9) and (5.10). The substantial differences consist in expression (5.11) and (5.12), since now also the chemical exchange rates have to be considered. As a consequence, here the single number densities n^s are not conserved quantities, and therefore also number density of the attracting sth Maxwellian is different from that of the actual distribution function. In detail, under the assumption of tempered reaction regime, the parameters determining all Maxwellian M_s read explicitly as [25]

$$n_s = n^s + \frac{\lambda^s}{\nu_s} \mathcal{S}, \tag{5.23}$$

$$m^s n_s u_s = m^s n^s u^s + \frac{1}{\nu_s} \sum_{r=1}^{4} \xi^{sr} u^r + \frac{\lambda^s}{\nu_s} m^s u \mathcal{S}, \tag{5.24}$$

$$\begin{aligned} n_s \frac{3}{2} K_B T_s = n^s \frac{3}{2} K_B T^s - \frac{1}{2} m^s [n_s u_s^2 - n^s (u^s)^2] + \frac{1}{\nu_s} \sum_{r=1}^{4} \gamma^{sr} T^r + \\ \frac{1}{\nu_s} \sum_{r=1}^{4} \nu_1^{sr} \frac{\mu^{sr}}{m^s + m^r} n^s n^r (m^s u^s + m^r u^r) \cdot (u^r - u^s) + \\ + \frac{\lambda^s}{\nu_s} \mathcal{S} \left[\frac{M - m^s}{M} K_B T \left(\frac{\Delta E}{K_B T} \right)^{3/2} \frac{e^{-\Delta E / K_B T}}{\Gamma(\frac{3}{2}, \frac{\Delta E}{K_B T})} \right. \\ \left. + \frac{1}{2} m^s n^s + \frac{3}{2} K_B T - \frac{1 - \lambda^s}{2} \frac{M - m^s}{M} \Delta E \right], \end{aligned} \tag{5.25}$$

where

$$\mathcal{S} = \nu_{12}^{34} \frac{2}{\sqrt{2}} \Gamma\left(\frac{3}{2}, \frac{\Delta E}{K_B T} \right) \left[n^3 n^4 \left(\frac{m^1 m^2}{m^3 m^4} \right)^{3/2} e^{\Delta E / K_B T} - n^1 n^2 \right], \tag{5.26}$$

$$\nu_{12}^{34}(g) = 2\pi g \int_0^{\pi} \sigma_{12}^{34}(g, \chi) \sin\chi \, d\chi,$$

Γ denotes an incomplete Gamma function, $M = m^1 + m^2 = m^3 + m^4$.
This BGK model is a robust approximation of the Boltzmann-type kinetic equation describing the reaction mixtures, since it correctly reproduces equilibria (including mass action low) and conservation equations. As regards the H-theorem, an analytical proof using the H function (5.22) is still lacking in [25], due to the considerable difficulties introduced by the chemical reaction. However, numerical results show the expected trend of the H-functional.

5.4 Numerical treatment

The numerical methods presented in Chapter 3 have been successfully extended to the case of inert and reactive mixtures. We have considered problems 3D in velocity (here we denote the full velocity vector $\mathrm{v} = (v_1, v_2, v_3)$), 1D in space, in slab geometry. The starting point is the Chu reduction [15] introduced in Section 1.4, which, under suitable symmetry assumption, allows to transform a 3D equation (in velocity) in a system of two equations 1D (in velocity).
For the sake of simplicity, we fix $L = 4$, and discretize the BGK model of Andries, Aoki and Perthame; the discretizazion of the other BGK models described in Section 5.2.2 is similar.

5.4.1 First order SL scheme for the AAP BGK model

Let us introduce the new unknowns

$$g_1^s(t,x,v) = \int_{\mathbb{R}^2} f^s(t,x,\mathrm{v})\, dv_2 dv_3, \quad g_2^s(t,x,v) = \int_{\mathbb{R}^2} (v_2^2 + v_3^2) f^s(t,x,\mathrm{v})\, dv_2 dv_3, \tag{5.27}$$

each depending only on one space and one velocity variable $v = v_1$. Multiplication of (5.8) by 1 and $(v_2^2 + v_3^2)$ and integration with respect to $(v_2, v_3) \in \mathbb{R}^2$ yields then the following system of BGK equations for the unknown vector $g^s = (g_1^s, g_2^s)$, coupled with initial conditions

$$\begin{cases} \dfrac{\partial g_i^s}{\partial t} + v \dfrac{\partial g_i^s}{\partial x} = \nu_s (M_{s,i} - g_i^s), & (t,x,v) \in \mathbb{R}_+ \times \mathbb{R} \times \mathbb{R}, \\ \\ g_i^s(0,x,v) = g_{i,0}^s(x,v), & s = 1, ..., 4,\ i = 1, 2. \end{cases} \tag{5.28}$$

The BGK system (5.28) describes a relaxation process towards the vector Maxwellians

$(M_{s,1}, M_{s,2})$, which is obtained by Chu transform of (5.9) and has the form

$$(M_{s,1}, M_{s,2}) = \Big(M_s, \frac{2K_B T_s}{m^s} M_s \Big),$$

where

$$M_s = n^s \Big(\frac{m^s}{2\pi K_B T_s} \Big)^{1/2} \exp\Big(- \frac{m^s}{2K_B T_s} (v - u_s)^2 \Big), \quad s = 1, \cdots, 4.$$

To determine the auxiliary parameters u_s and T_s we have to solve (5.11) and (5.12). Relations (5.11) and (5.12) involve fundamental macroscopic moments of distribution functions f^s, n^s, u^s and T^s, which are given in terms of g_1^s and g_2^s as

$$n^s = \int_{\mathbb{R}} g_1^s \, dv, \qquad u^s = \frac{1}{n^s} \int_{\mathbb{R}} v g_1^s \, dv,$$

$$\frac{3K_B T^s}{m^s} = \frac{1}{n^s} \Big[\int_{\mathbb{R}} (v - u^s)^2 g_1^s \, dv + \int_{\mathbb{R}} g_2^s \, dv \Big].$$

Now we apply the first order SL scheme to the system (5.28). In this case it reads as

$$\begin{cases} g_{1,ij}^{s,n+1} = \tilde{g}_{1,ij}^{s,n} + \Delta t \nu_{s,ij}^{n+1} (M_{s,1,ij}^{n+1} - g_{1,ij}^{s,n+1}), \quad s = 1, ..., 4, \\ \\ g_{2,ij}^{s,n+1} = \tilde{g}_{2,ij}^{s,n} + \Delta t \nu_{s,ij}^{n+1} (M_{s,2,ij}^{n+1} - g_{2,ij}^{s,n+1}), \quad s = 1, ..., 4, \end{cases} \tag{5.29}$$

where $\tilde{g}_{1,ij}^{s,n} = g_1^s(t^n, x_i - v_j \Delta t, v_j)$ and $\tilde{g}_{2,ij}^{s,n} = g_2^s(t^n, x_i - v_j \Delta t, v_j)$. The main drawback is how to solve the implicit equations in (5.29), where the Maxwellians now depend on the auxiliary fields.

By integrating over v the first equation of (5.29) for $s = 1, \cdots, 4$ we obtain $n^{s,n+1} = \tilde{n}^{s,n}$, and then the collision frequencies ν_s, at time t^{n+1} can be evaluated.

The first task is to compute the fictitious mean velocities u_s^{n+1}. To this end we recall that

$$u^s = \frac{1}{n^s} \int_{\mathbb{R}} v g_1^s \, dv,$$

$$u_s = \frac{1}{m^s n^s} \Big[m^s n^s u^s + \frac{1}{\nu_s} \sum_{r=1}^{L} \xi^{sr} u^r \Big].$$

Thus, if we multiply by v and then integrate on v the first equation of (5.29) for $s = 1, ..., 4$ we obtain (omitting the indexes relevant to the discretization)

$$n^s u^s = \tilde{n}^s \tilde{u}^s + \Delta t\, \nu_s (n_s u_s - n^s u^s), \quad s = 1, \cdots, 4, \tag{5.30}$$

but, since $n^{s,n+1} = \tilde{n}^{s,n}$, one obtains

$$u^s = \tilde{u}^s + \Delta t\, \nu_s (u_s - u^s), \quad s = 1, \cdots, 4, \tag{5.31}$$

then using (5.11) one has

$$u^s = \tilde{u}^s + \Delta t\, \nu_s \left(\frac{1}{m^s n^s \nu_s} \sum_{r=1}^{4} \xi^{sr} u^r \right), \quad s = 1, \cdots, 4, \tag{5.32}$$

from which

$$\begin{cases} \left(\xi^{11} - \dfrac{m^1 n^1}{\Delta t} \right) u^1 + \xi^{12} u^2 + \xi^{13} u^3 + \xi^{14} u^4 = -\dfrac{m^1 n^1}{\Delta t} \tilde{u}^1 \\ \xi^{21} u^1 + \left(\xi^{22} - \dfrac{m^2 n^2}{\Delta t} \right) u^2 + \xi^{23} u^3 + \xi^{24} u^4 = -\dfrac{m^2 n^2}{\Delta t} \tilde{u}^2 \\ \xi^{31} u^1 + \xi^{32} u^2 + \left(\xi^{33} - \dfrac{m^3 n^3}{\Delta t} \right) u^3 + \xi^{34} u^4 = -\dfrac{m^3 n^3}{\Delta t} \tilde{u}^3 \\ \xi^{41} u^1 + \xi^{42} u^2 + \xi^{43} u^3 + \left(\xi^{44} - \dfrac{m^4 n^4}{\Delta t} \right) u^4 = -\dfrac{m^4 n^4}{\Delta t} \tilde{u}^4 \end{cases} \tag{5.33}$$

Thus we have to solve the system $A\underline{u} = \underline{b}$, where

$$A = \xi - \frac{1}{\Delta t} diag(\underline{m}. * \underline{n})$$

$$\underline{b} = -\frac{1}{\Delta t} (\underline{m}. * \underline{n}. * \underline{\tilde{u}})$$

where, in general, the notation $\underline{a}$ stands for $(a^1, a^2, a^3, a^4)^{\mathrm{T}}$, and $a.*b = (a^1 b^1, a^2 b^2, a^3 b^3, a^4 b^4)^{\mathrm{T}}$.

Known the actual mean velocities, by (5.11) we are able to update the fictitious mean velocities at time t^{n+1}.

Now we have to compute the fictitious temperatures T_s^{n+1}. To this end we recall that

$$\frac{3K_BT^s}{m^s} = \frac{1}{n^s}\left[\int_{\mathbb{R}}(v-u^s)^2 g_1^s\,dv + \int_{\mathbb{R}} g_2^s\,dv\right], \tag{5.34}$$

$$T_s = \frac{2}{3n^sK_B}\left[n^s\frac{3}{2}K_BT^s - \frac{1}{2}m^sn^s[(u_s)^2-(u^s)^2] + \frac{1}{\nu_s}\sum_{r=1}^{L}\gamma^{sr}T^r + \right.$$

$$\left. + \frac{1}{\nu_s}\sum_{r=1}^{4}\nu_1^{sr}\frac{\mu^{sr}}{m^s+m^r}n^sn^r(m^su^s+m^ru^r)(u^r-u^s)\right].$$

Thus, computing the species temperatures at time t^{n+1} by using (5.34) and replacing the marginal distribution function g_1 and g_2 by their expression in (5.29) one obtains:

$$\frac{3n^sK_BT^s}{m^s} = \frac{3\tilde{n}^sK_B\tilde{T}^s}{m^s} + \Delta t\nu_s\left(n^s(u_s-u^s)^2 + \frac{3n^sK_BT_s}{m^s} - \frac{3n^sK_BT^s}{m^s}\right) \quad s=1,...4 \tag{5.35}$$

$$T^s - \Delta t\nu_s(T_s-T^s) = \tilde{T}^s + \Delta t\nu_s\frac{m^s}{3K_B}(u_s-u^s)^2 \quad s=1,...4 \tag{5.36}$$

We denote

$$\alpha_s = \frac{m^s}{3K_B}(u_s-u^s)^2$$

$$\beta_s = \frac{m^s}{3K_B}[(u_s)^2-(u^s)^2]$$

$$\gamma_s = \frac{2}{3K_B}\frac{1}{\nu_s}\sum_{r=1}^{4}\nu_1^{sr}\frac{\mu^{sr}}{m^s+m^r}n^r(m^su^s+m^ru^r)(u^r-u^s)$$

thus (5.36) becomes

$$T^s - \frac{2\Delta t}{3n^sK_B}\sum_{r=1}^{4}\gamma^{sr}T^r = \tilde{T}^s + \Delta t\nu_s(\alpha_s-\beta_s+\gamma_s) \quad s=1,...4 \tag{5.37}$$

Thus we have to solve the system $A\underline{u} = \underline{b}$, where

$$A = \gamma - \frac{3K_B}{2\Delta t} diag(\underline{n})$$

$$b_r = -\frac{3K_B n^r}{2\Delta t}\left(\tilde{T}^r + \Delta t \nu_r(\alpha_r - \beta_r + \gamma_r)\right) \quad r = 1, ...4.$$

Once the actual temperatures are known, by (5.12) we are able to update the fictitious temperatures at time t^{n+1}.
In such a way we solve the implicit step. In analogous way it is possible to treat the other BGK model (5.13) for inert mixtures with relations (5.17) and (5.18).
The extension to higher order schemes, once how to solve the implicit step is clear, is an easy application of the schemes presented in Chapter 3. Numerical results in Section 5.5 are performed using the BDF2 scheme.

5.4.2 Sketch of the first order SL scheme for the reactive BGK model

The structure of the scheme is the same of the inert case. The solution of the BGK models for reacting mixtures described in Section 5.3.1 leads to additional drawbacks, since we have also auxiliary number densities n_s, given in terms of the actual macroscopic fields in equation (5.23), and the computation of the auxiliary fields now requires the solution of a transcendental system of equations at each time step and at each spatial node, due to the exponential term relevant to the mass action law (5.21), appearing in the term $\mathcal{S}$ in the equations (5.23)-(5.26). Moreover, we do not get three uncoupled linear 4×4 systems, one for densities, one for the velocities and one for the temperatures, as in the inert case. Indeed, each equation depends on all the twelve actual fields, since all of them involve the term (5.26). As a consequence, the equations do not decouple, and we have a 12×12 non linear system. Solve this non linear system by Newton method is prohibitive, owing to the very complex expressions of the auxiliary fields (5.23), (5.24) and (5.25). To overcome these difficulties we adopted an iterative procedure, similar to the one used for the treatment of the diffusive boundary conditions in Chapter 4. At the step $k = 0$, we suppose to have

$$\begin{cases} g_{1,ij}^{s,n+1,0} = \tilde{g}_{1,ij}^{s,n} \\ g_{2,ij}^{s,n+1,0} = \tilde{g}_{2,ij}^{s,n}. \end{cases} \tag{5.38}$$

With this first approximation of $g_{1,ij}^{s,n+1}$ and $g_{2,ij}^{s,n+1}$ we compute a first approximation of the actual fields and therefore of the auxiliary fields at time t^{n+1}. Then we iterate the procedure

$$\begin{cases} g_{1,ij}^{s,n+1,k} = \tilde{g}_{1,ij}^{s,n} + \Delta t \nu_{ij}^{s,n+1,k-1}(M_{1,ij}^{s,n+1,k-1} - g_{1,ij}^{s,n+1,k-1}) \\ g_{2,ij}^{s,n+1,k} = \tilde{g}_{2,ij}^{s,n} + \Delta t \nu_{ij}^{s,n+1,k-1}(M_{2,ij}^{s,n+1,k-1} - g_{2,ij}^{s,n+1,k-1}), \end{cases} \tag{5.39}$$

until convergence. Fixed a tolerance *tol*, we stop the iterations when the 2-norm of the difference of two consecutive iterates is smaller than *tol* for each marginal distribution function g_1^s, g_2^s, $s = 1, ..., 4$. The number of iterates depends on $\varepsilon/\Delta t$. It increases as $\varepsilon \to 0$, and decreases as $\Delta t \to 0$. Thus, if we do not use very large CFL number we can simulate fluid regime with a reasonable number of iterations without affecting the computational cost.

In a straightforward way we can extend these numerical scheme to high order schemes. Numerical results are performed using the BDF2 scheme.

5.5 Numerical results

We have used the numerical test proposed in [1]. We consider a mixture of four monoatomic gases with the following values of the molecular masses:

$$m_1 = 58.5, \quad m_2 = 18, \quad m_3 = 40, \quad m_4 = 36.5.$$

We present some results for the following Riemann problem for both reactive and non-reactive cases. The collision frequencies for elastic scattering are the same used in [1]:

$$\begin{aligned} \nu_0^{11} = 500, \quad \nu_0^{12} = 600, \quad \nu_0^{13} = 200, \quad \nu_0^{14} = 700, \\ \nu_0^{22} = 400, \quad \nu_0^{23} = 500, \quad \nu_0^{24} = 800, \\ \nu_0^{33} = 400, \quad \nu_0^{34} = 300, \\ \nu_0^{44} = 600, \end{aligned}$$

with $\nu_0^{sr} = \nu_0^{rs}$ and $\nu_1^{sr} = \nu_0^{sr}$ for $s, r = 1, ..., 4$. The above frequencies will be multiplied by a factor $1/\varepsilon$ in the numerical experiments, where ε is the Knudsen number, to simulate by varying ε both rarefied and fluid regimes. The chemical collision frequency is $\nu_{12}^{34} = 0$ in the non-reactive case, whereas we set $\nu_{12}^{34} = 100$ in the reactive case. The initial data

are chosen as Maxwellians reproducing the following macroscopic fields:

$$(\rho_0, u_0, p_0) = \begin{cases} (1, 0, 5/3), & x < 0.5, \\ (1/8, 0, 1/6), & x > 0.5, \end{cases}$$

$$(\rho_{01}, \rho_{02}, \rho_{03}, \rho_{04}) = \begin{cases} (1/10, 2/10, 3/10, 4/10), & x < 0.5, \\ (1/80, 2/80, 3/80, 4/80), & x > 0.5, \end{cases} \tag{5.40}$$

$$u_{0i} = 0,\ i = 1, ..., 4.$$

The presented results are obtained using BDF2 scheme, the best performing due to the low number of interpolation required. In Figure 5.1 we present the result obtained in the inert case. In this case, we set $N_v = 30$, $N_x = 200$, $CFL = 2$. In Figure 5.1 we compare the result obtained with the two BGK models for inert case presented in subsections 5.2.1 and 5.2.2, respectively. The results are in good agreement with the ones present in [1]. We can observe that at the final time $t_f = 0.2$, for $\varepsilon = 10^{-1}$ that implies in our case $\nu_s \approx 10^{-2}$, left column in Fig. 5.1, the equilibrium is not yet reached and species velocities and temperatures are not yet relaxed to common values. Instead, we can observe that for $\varepsilon = 10^{-2}$ ($\nu_s \approx 10^{-3}$, right column in Fig. 5.1) at the same final time we are closer to the equilibrium, namely species velocities and temperatures almost overlap and give the mean velocity and temperature of the mixture. In Fig. 5.2 the differences between the mean velocity and temperature of the mixture and the species velocities and temperatures are plotted. We can observe that the differences are smaller for the BGK model (5.13), with respect to the ones obtained by the BGK model of Andries, Aoki and Perthame. This is due to the fact that the BGK model (5.13) relaxes towards the attractors (5.14), characterized by the presence of a common velocity and temperature. Instead the BGK model of Andries, Aoki and Perthame relaxes towards attractors with different velocities and temperatures, then species velocities and temperature equalize later.

Fig. 5.3, 5.4, 5.5 and 5.6 are relevant to the case of reactive mixture. We use a energy threshold $\Delta E = 500$. The results are relevant to the BGK model described in subsection 5.3.1. We can observe the variation of the number densities (Fig. 5.5) for different values of ε. The density of the mixture is conserved, whereas the species densities are not, according to conservations. The variations of the profiles for different values ΔE are shown in Fig. 5.7 and 5.8. In Figure 5.7 we report the global density ρ and densities ρ^1 and ρ^3 at time $t = 0.2$ for non reactive e reactive case with $\Delta E = 0$, 500, 1000. The global moments of the inert mixture overlap the profiles obtained for $\Delta E = 0$, whereas this is not the case for the single components of the gas. The higher ΔE, the greater the variations with respect to the inert case. The results obtained are in good agreement with those obtained in [1]

with a different numerical technique (splitting, lower order).
Finally, in Tables 5.1 and 5.2 we present the accuracy order obtained using BDF2 scheme for the BGK model presented in subsection 5.3.1. The test is performed in order to show the efficiency of the iterative procedure used in presence of the reaction to solve the implicit step arising from the discretization.

L_1 relative errors

N_x	global n	global u	global T	η
40	6.5535e-03	3.9862e-01	4.2436e-03	54
80	2.5973e-03	1.7275e-01	1.8118e-03	33
160	6.6116e-04	4.0854e-02	4.3127e-04	21
320	1.3625e-04	8.1096e-03	8.9780e-05	14
640	2.6564e-05	1.4325e-03	1.8282e-05	11

L_1 orders

80	1.3353	1.2063	1.2278	
160	1.9739	2.0801	2.0708	
320	2.2788	2.3328	2.2641	
640	2.3587	2.5011	2.2960	

Table 5.1: Relative errors and accuracy order approximating the reactive BGK model of Groppi and Spiga, using BDF2. $CFL = 2$, $\varepsilon = 10^{-1}$, ($\nu_s \approx 10^{-2}$). η denotes the average number of iterations.

In this case, as smooth initial data we use the Maxwellians reproducing the following initial macroscopic fields.

$$n_0^s(x) = \frac{1}{m^s}, \qquad T_0^s(x) = \frac{4}{\sum_{s=1}^{4} n_0^s(x)},$$

$$u_0^s(x) = \frac{s}{\sigma_s}\left[\exp\left(-\left(\sigma_s x - 1 + \frac{s}{3}\right)^2\right) - 2\exp\left(-\left(\sigma_s x + 3 - \frac{s}{10}\right)^2\right)\right],$$

$s = 1, ..., 4$, where $\sigma_s = (10, 13, 16, 19)$. We use $CFL = 2$, $N_v = 30$, $tol = 10^{-8}$ as tolerance to stop the iterations. In Tables 5.1 and 5.2 η denotes the average number of iterations performed during each time step.

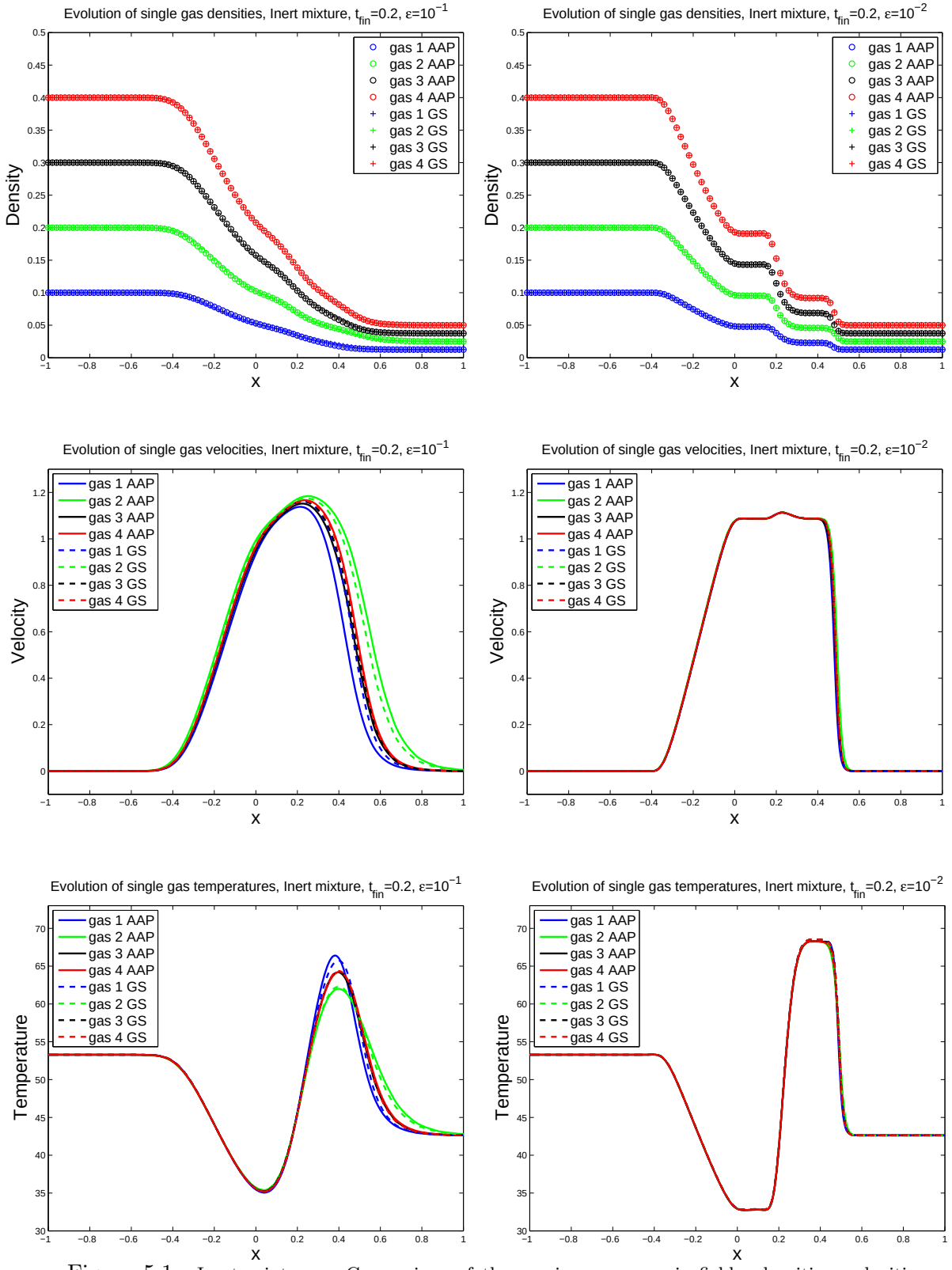

Figure 5.1: Inert mixtures. Comparison of the species macroscopic fields, densities, velocities and temperatures, using (5.40) as initial data, obtained from the numerical approximations of the BGK model of Andries, Aoki and Perthame and the one presented in Section 5.2.2. Left column $\varepsilon = 10^{-1}$; right column $\varepsilon = 10^{-2}$.

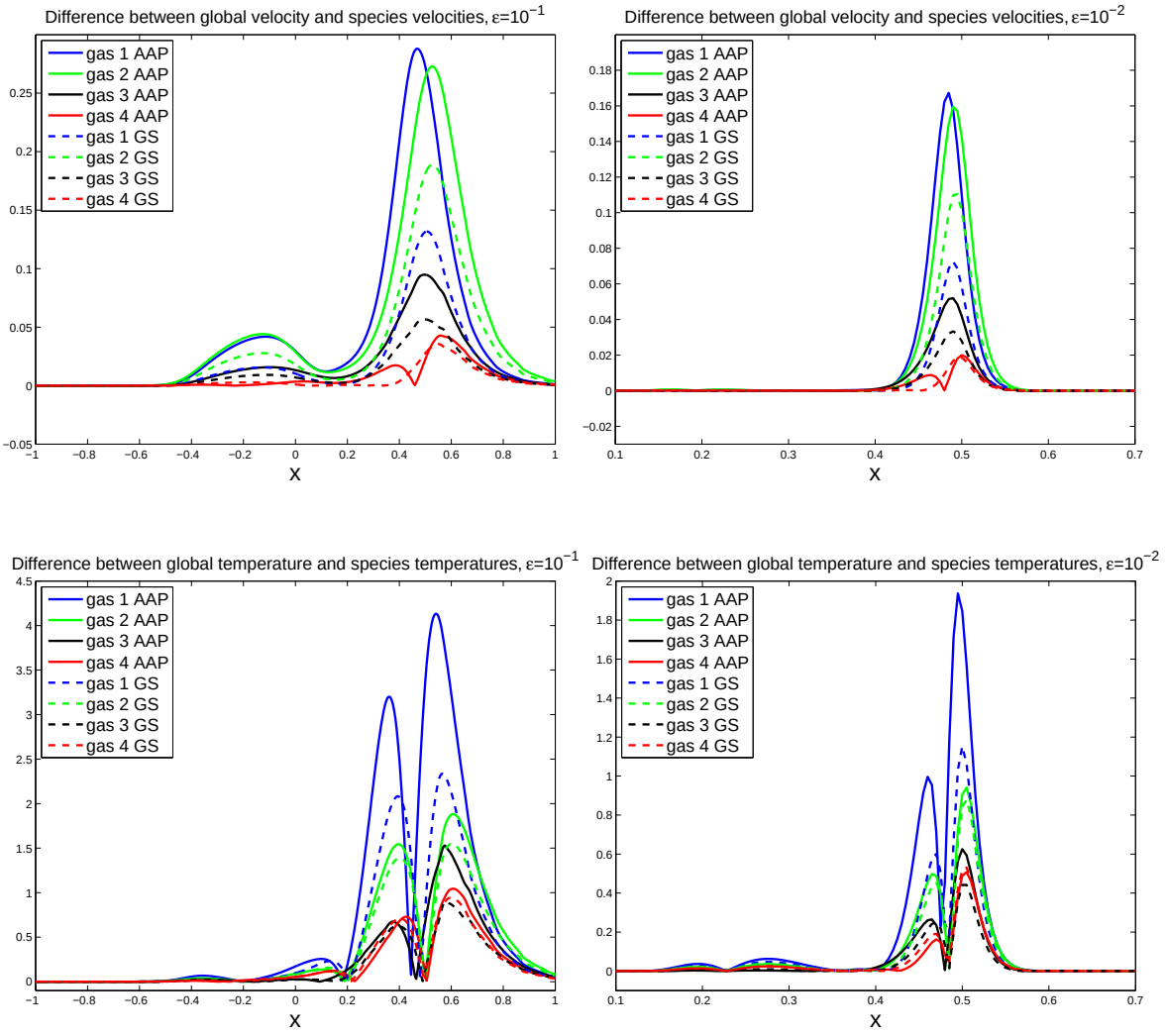

Figure 5.2: Inert mixtures. Differences between mixture velocity and species velocities in the top. Differences between mixture temperature and species temperatures below. Left $\varepsilon = 10^{-1}$, right $\varepsilon = 10^{-2}$. We can observe that the differences are smaller for the BGK model presented in Section 5.2.2, respect the ones obtained by the BGK model of Andries, Aoki and Perthame.

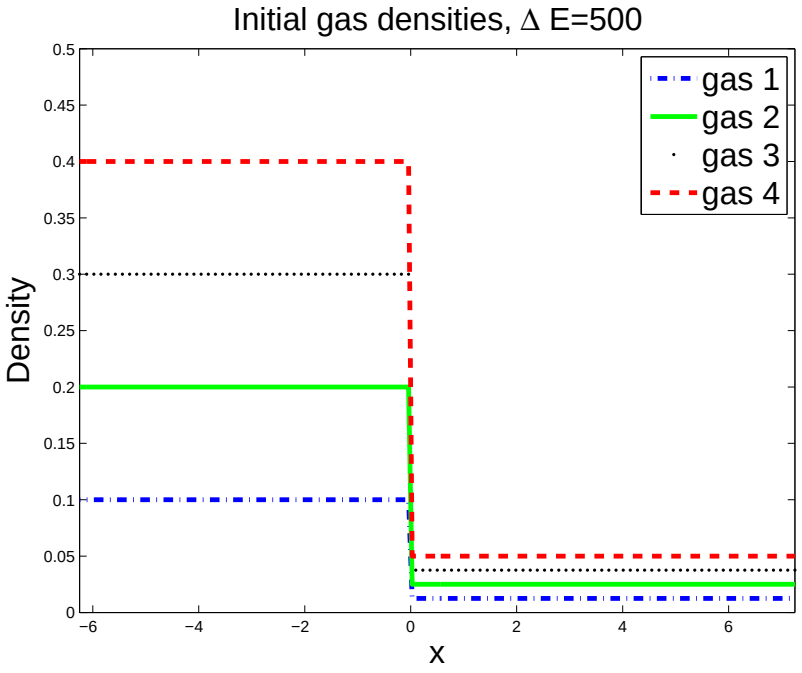

Figure 5.3: Representation of the initial species densities profiles using (5.40) as initial data.

L_1 relative errors

N_x	global n	global u	global T	η
40	7.3747e-03	4.3970e-01	4.8548e-03	395
80	3.1298e-03	1.9845e-01	2.1617e-03	218
160	1.2041e-03	7.0644e-02	7.5636e-04	120
320	3.3898e-04	1.8127e-02	2.2317e-04	68
640	7.1701e-05	3.0637e-03	5.3147e-05	40

L_1 orders

80	1.2365	1.1477	1.1673	
160	1.3782	1.4901	1.5150	
320	1.8286	1.9624	1.7610	
640	2.2411	2.5648	2.0701	

Table 5.2: Relative errors and accuracy order approximating the reactive BGK model of Groppi and Spiga, using BDF2. $CFL = 2$, $\varepsilon = 10^{-2}$, ($\nu_s \approx 10^{-3}$). η denotes the average number of iterations.

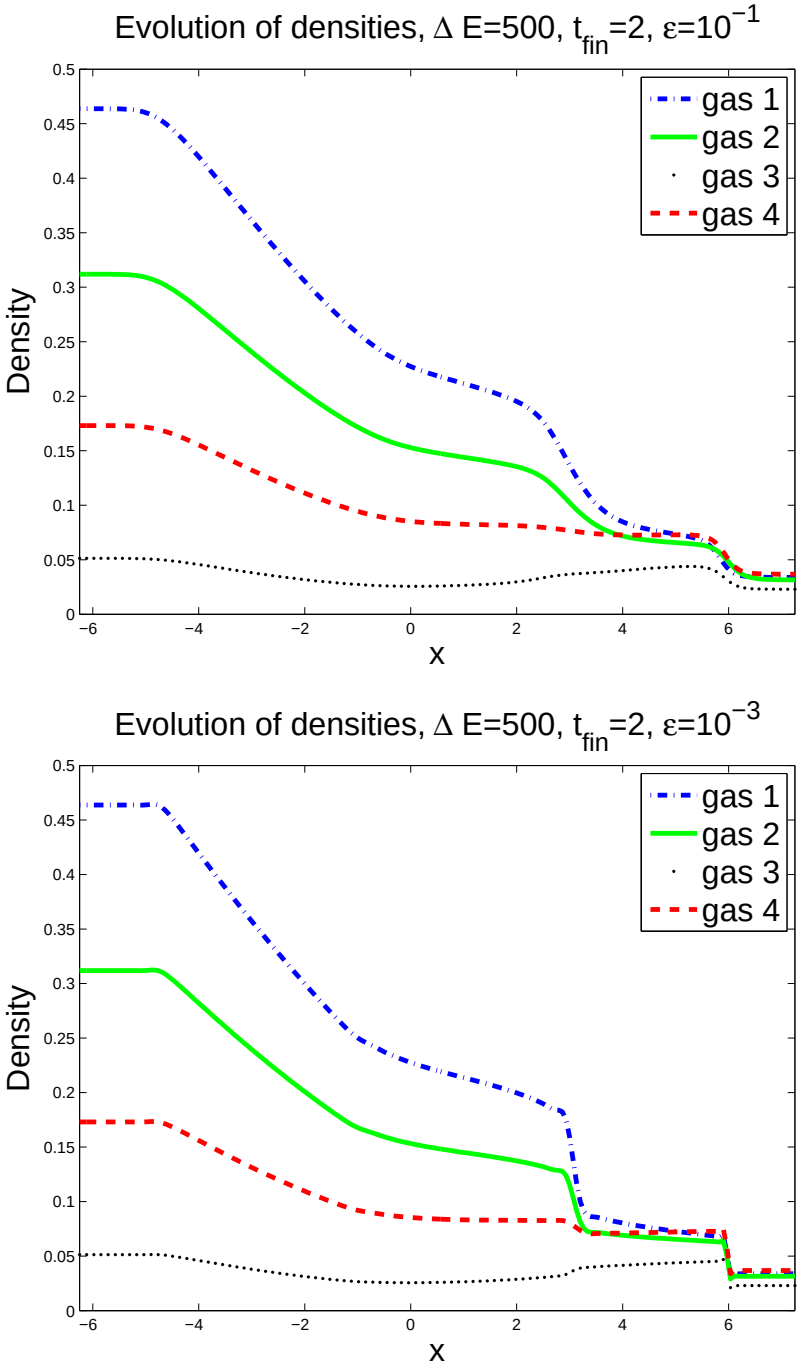

Figure 5.4: Reactive mixtures. Numerical approximation of the BGK model of Groppi and Spiga. $CFL = 2$, $N_x = 400$, $N_v = 60$, $t_f = 2$. Species densities profiles: top $\varepsilon = 10^{-1}$, low $\varepsilon = 10^{-3}$. With respect to Fig. 5.3 we can observe the variation of the species densities due to the reaction (5.20).

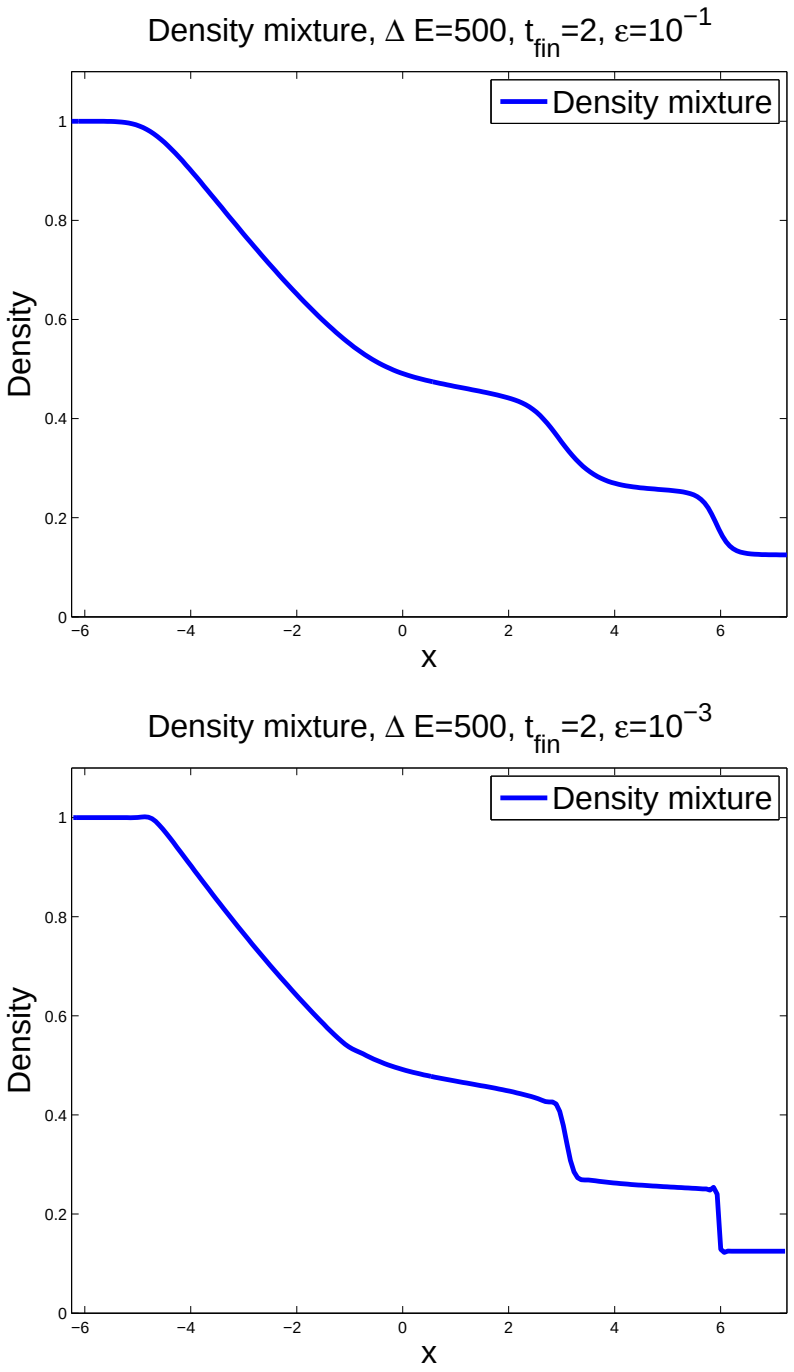

Figure 5.5: Reactive mixtures. Numerical approximation of the BGK model of Groppi and Spiga. $CFL = 2$, $N_x = 400$, $N_v = 60$, $t_f = 2$. Global mass density profiles: top $\varepsilon = 10^{-1}$, low $\varepsilon = 10^{-3}$.

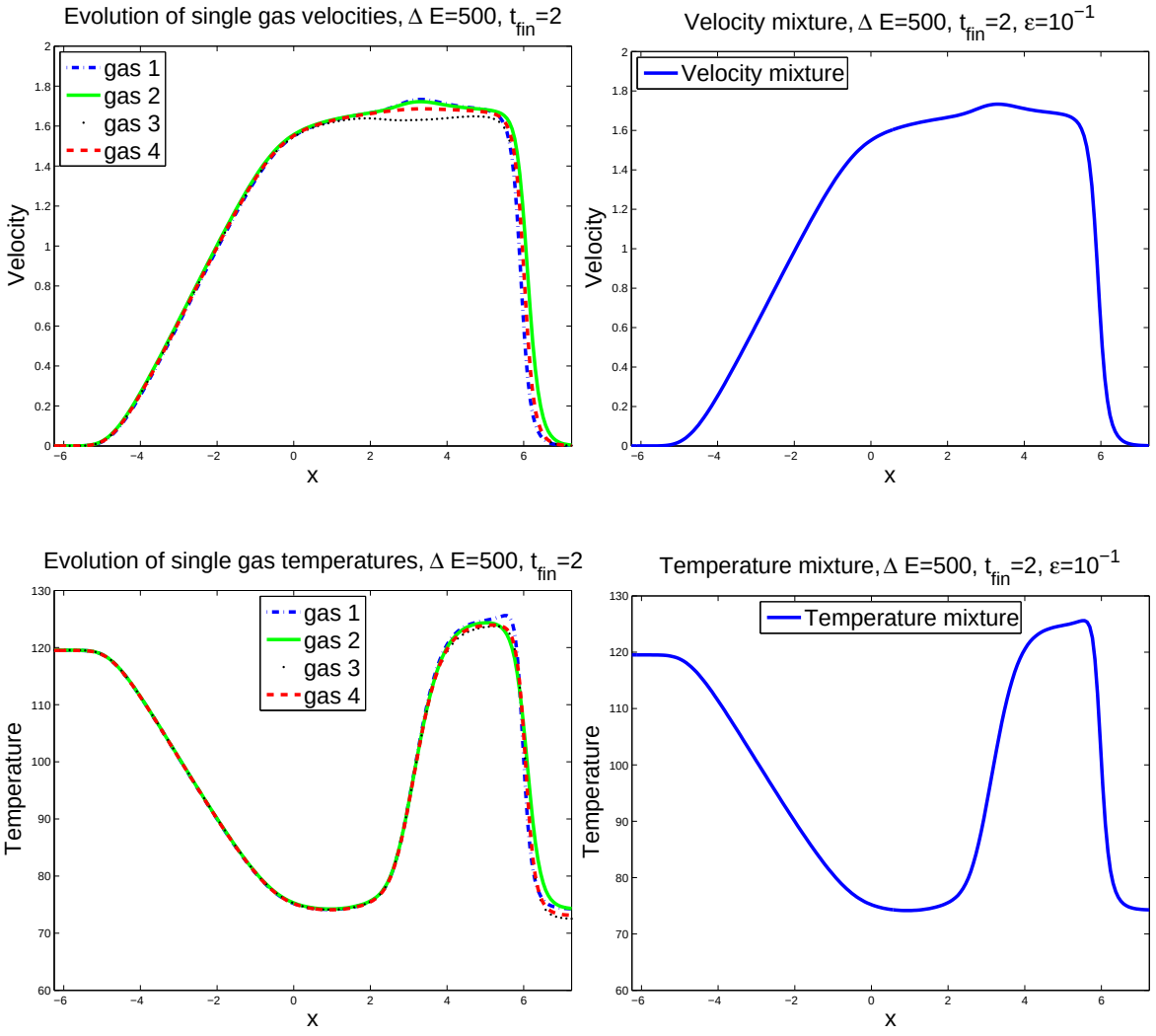

Figure 5.6: Reactive mixtures. Numerical approximation of the BGK model of Groppi and Spiga. $CFL = 2$, $N_x = 400$, $N_v = 60$, $\varepsilon = 10^{-1}$, $t_f = 2$. Left: species macroscopic fields; right: global macroscopic fields. Top: velocity; below: temperature.

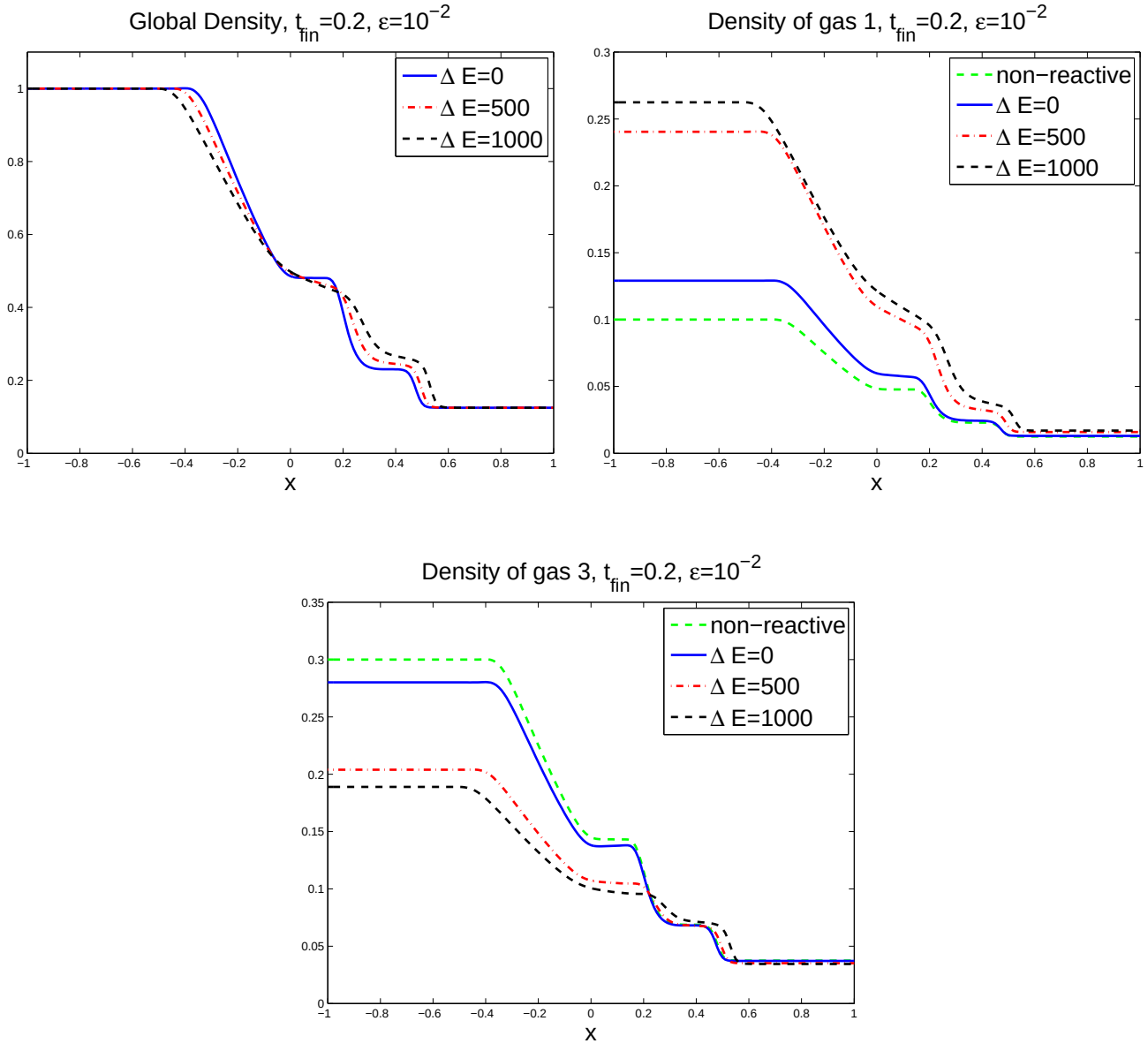

Figure 5.7: Reactive mixtures. Numerical approximation of the BGK model of Groppi and Spiga. $CFL = 2$, $N_x = 200$, $N_v = 60$, $\varepsilon = 10^{-2}$, $t_f = 0.2$. Global mass density ρ and density ρ^s, $s = 1, 3$ (gases 1 and 3) for different values of ΔE. The global density when $\Delta E = 0$ overlaps that of non-reactive case.

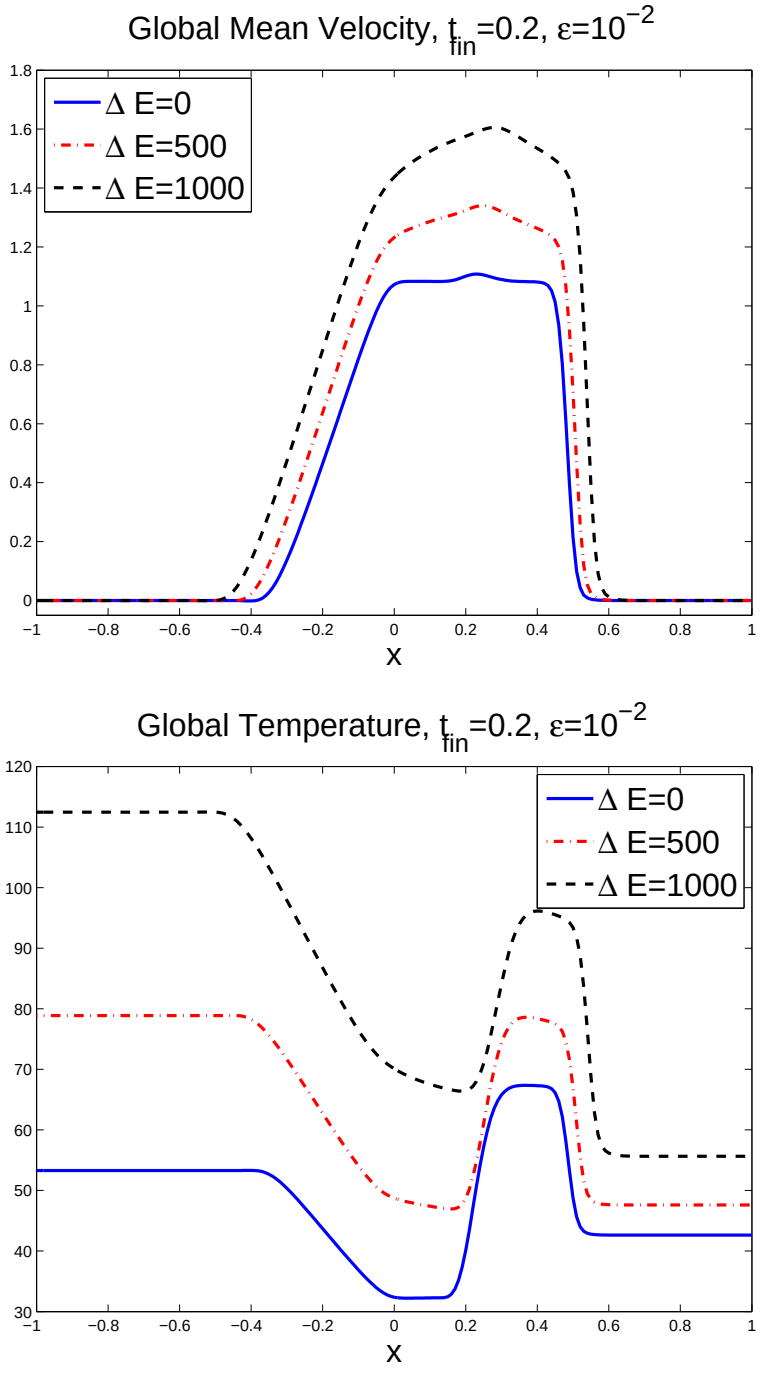

Figure 5.8: Reactive mixtures. Numerical approximation of the BGK model of Groppi and Spiga. $CFL = 2$, $N_x = 200$, $N_v = 60$, $\varepsilon = 10^{-2}$, $t_f = 0.2$. Global mean velocity u and temperature T for different values of ΔE.

Conclusions and Perspectives

This thesis focuses on high order shock capturing semi-Lagrangian methods for the numerical solutions of BGK-type equations.
The methods are based on L-stable schemes for the solution of the BGK equations along the characteristics, and are asymptotic preserving, in the sense that they are able to capture the fluid dynamic limit.
Two families of schemes are presented, which differ for the choice of the time integrator, Runge-Kutta or BDF, respectively. A further distinction concerns space discretization: some schemes are based on high order reconstruction, while others are constructed on the lattice in phase space, thus requiring no space interpolation.
Numerical experiments show that schemes without interpolation can be cost-effective, especially for problems that do not require a fine mesh in velocity. In particular, BDF3 without interpolation appears to have the best performance in most tests.
We investigated some applications and extensions to more physical interesting problems of the numerical schemes proposed for the one dimensional BGK equation. By means of the Chu reduction [15], we extended the schemes to more realistic physical domains, 3D in velocity. Moreover, we considered boundary-value problems and we studied the treatment of reflective and diffusive boundary conditions. Two numerical techniques to deal with diffusive boundary conditions are presented. The numerical results obtained are in good agreement with the ones present in literature [19].
Finally, the methods have been extended to different BGK models for inert [3] and reactive [25] gas mixtures in three dimensional velocity space.

Future plans includes extension of such schemes to problems in several space dimensions and treatment of more general boundary conditions, the case of moving boundaries. Moreover, applications of these schemes to the numerical approximation of other BGK equations for mixtures of rarefied gases are in progress. In particular, we will investigate the dis-

cretization of the BGK model [23], that is the extension to the reactive case of the inert BGK model (5.13).
Furthermore, on the modelling side, other BGK approximation could be developed and then numerically solved by means of the schemes investigated in this thesis, like for instance multitemperature models. Typically, relaxation to thermodynamical equilibrium in a gas mixture might occur on different scales: for instance, when masses are disparate, a first Maxwellization step within each species is followed by a slower equilibration of velocities and temperatures [22]. Indeed, when vibrational and chemical relaxations proceed at the slower gas-dynamic time scale, a one-temperature gas flow description is not valid any more [32]. On the other hand, a multi-temperature approach is needed in several problems of aerothermodynamics [9] or in plasmas at high temperatures [45]. A BGK model for mixture, characterized by attractors with auxiliary species temperatures and only one auxiliary global velocity, thus at an intermediate stage between the two BGK for inert mixtures considered in this thesis, could be suitable to describe such problems.

Bibliography

[1] A. Aimi, M. Diligenti, M. Groppi, C. Guardasoni, *On the numerical solution of a BGK-type model for chemical reactions,* European J. Mech. B/Fluids 26, 455-472, 2007.

[2] A. Alaia, G. Puppo, *A hybrid method for hydrodynamic-kinetic flow - Part II - Coupling of hydrodynamic and kinetic models*, J. Comp. Phys. 231 (16), 5217–5242, 2012.

[3] P. Andries, K. Aoki and B. Perthame, *A consistent BGK-type model for gas mixtures*, J. Stat. Phys. 106, 993–1018, 2002.

[4] K. Aoki, Y. Sone, and T. Yamada, *Numerical analysis of gas flows condensing on its plane condensed phase on the basis of kinetic theory*, Phys. Fluids A 2, 10, 1867–1878, 1990.

[5] U. M. Ascher, S. J. Ruuth, R. J. Spiteri, *Implicit-Explicit Runge-Kutta methods for time-dependent partial differential equations*, Appl. Numer. Math. 25, 151–167, 1997.

[6] G. A. Bird, *Molecular Gas Dynamics and the Direct Simulation of Gas Flows*, Oxford Engineering Science Series. Clarendon Press, 1994.

[7] M. Bisi, M. Groppi, G. Spiga, *Kinetic Bhatnagar-Gross-Krook model for fast reactive mixtures and its hydrodynamic limit*, Phys. Rev. E 81 036327, 1–9, 2010.

[8] P.L. Bhatnagar, E.P. Gross and K. Krook, *A model for collision processes in gases*, Phys. Rev. 94, 511–525, 1954.

[9] T.K. Bose, *High Temperature Gas Dynamics*, Springer, Berlin, 2003.

[10] C. Buet, *A discrete velocity scheme for the Boltzmann operator of rarefied gas dynamics*, Transport Theor. Stat., 25, 33–60, 1996.

[11] E. Carlini, R. Ferretti and G. Russo, *A weighted essentially nonoscillatory, large time-step scheme for Hamilton-Jacobi equations*, SIAM J. Sci. Comput. 27, 1071–1091, 2005.

[12] R. Caflisch, *The fluid dynamical limit of the nonlinear Boltzmann equation*, Commun. Pure Appl. Math., 666, 33–651,1980.

[13] C. Cercignani, *The Boltzmann Equation and its Applications*, Springer, New York, 1988.

[14] C. Cercignani, *Slow Rarefied Flows: Theory and Application to Micro-Electro-Mechanical Systems*, Birkhäuser, Base, 2006.

[15] C.K. Chu, *Kinetic-theoretic description of the formation of a shock wave*, Phys. Fluids 8, 12–21, 1965.

[16] G. Dimarco, R. Loubere, *Towards an ultra efficient kinetic scheme. Part I: Basics on the BGK equation*, J. Comput. Phys. 255, 680–698, 2013.

[17] G. Dimarco, R. Loubere, *Towards an ultra efficient kinetic scheme. Part II: The high order case*, J. Comput. Phys. 255, 699–719, 2013.

[18] M. Falcone , R. Ferretti, *Semi-Lagrangian Approximation Schemes For Linear And Hamilton-Jacobi Equations*, SIAM, Philadelphia, 2014.

[19] F. Filbet, C. Yang, *Inverse Lax-Wendroff method for boundary conditions of Boltzmann type models*, arXiv:1209.3103 [math.NA], 12 September 2012.

[20] F. Filbet, G. Russo, *Semilagrangian schemes applied to moving boundary problems for the BGK model of rarefied gas dynamics*, Kinet. Relat. Models 2, 231–250, 2009.

[21] V.Garzó, A. Santos, J. J. Brey, *A kinetic model for a multicomponent gas,* Phys. Fluids A, 1(2), 380–383, 1989.

[22] E. Goldman, L.Sirovich, *Equations for gas mixtures,* Phys. Fluids, 10(9), 1928–1940, 1967.

[23] M. Groppi, S. Rjasanow, G. Spiga, *A kinetic relaxation approach to fast reactive mixtures: shock wave structure,* J. Stat. Mech., 1–15, 2009.

[24] M. Groppi, G. Russo, G. Stracquadanio., *High order semi-Lagrangian methods for BGK models.* Preprint n.519, Department of Mathematics and Computer Science, University of Parma, 2014, submitted.

[25] M. Groppi, G. Spiga, *A Bhatnagar-Gross-Krook type approach for chemically reacting gas mixtures*, Phys. Fluids 16, 4273–4284, 2004.

[26] E. P. Gross, M. Krook, *Model for collision processes in gases: Small-amplitude oscillations of charged two-component systems*, Phys. Rev, 102, 593, 1956.

[27] E. Hairer, S.P. Nørsett, G. Warner, *Solving Ordinary Differential Equations I: Non-Stiff Problems*, Springer Series in Computational Mathematics 8. Springer, Berlin, 1987.

[28] E. Hairer, G. Warner, *Solving Ordinary Differential Equations II: Stiff and Differential-Algebraic Problems*, Springer Series in Computational Mathematics 14. Springer, Berlin, 1991.

[29] L.H. Holway, *New statistical models for kinetic theory: methods of construction*, Phys. Fluids 9, 1658–1673, 1966.

[30] L. Huang, C.-W. Shu and M. Zhang, *Numerical boundary conditions for the fast sweeping high order WENO methods for solving the Eikonal equation*, J. Comput. Math., 26, 336–46, 2008.

[31] S. Jin, *Efficient asymptotic-preserving (AP) schemes for some multiscale kinetic equations*, SIAM J. Sci. Comput., 21, 441–452, 1999.

[32] E. Kustova, E. Nagnibeda, *On a correct description of a multi-temperature dissociating CO2 flow*, Chem. Phys., 321, 293–310, 2006.

[33] R.J. LeVeque, *Numerical methods for conservation laws*, Lectures in Mathematics, ETH-Zurich Birkhäuser-Verlag, Basel, 1990.

[34] R.J. LeVeque, *Finite volume methods for hyperbolic problems*, Cambridge University Press, 2002.

[35] J. C. Maxwell, *Phil. Trans. Royal Soc.* I, Appendix, 1879; reprinted in *The Scientific Parers of J. C. Maxwell*, Dover Publications, 1965.

[36] L. Mieussens, *Discrete-velocity models and numerical schemes for the Boltzmann-BGK equation in plane and axisymmetric geometries*, J. Comp. Phys. 162 (2), 429–466, 2000.

[37] L. Mieussens, *Discrete velocity model and implicit scheme for the BGK equation of rarefied gas dynamics*, Math. Models Meth. Appl. Sci. 10, 1121–1149, 2000.

[38] T. Nishida, *Fluid dynamical limit of the nonlinear Boltzmann equation at the level of the compressible euler equations*, Commun. Math. Phys., 148, 61–119, 1978.

[39] L. Pareschi, G. Russo, *Efficient asymptotic preserving deterministic methods for the Boltzmann equation*, AVT-194 RTO AVT/VKI, Models and Computational Methods for Rarefied Flows, Lecture Series held at the von Karman Institute, Rhode St. Genèse, Belgium, 24 -28 January 2011.

[40] L. Pareschi and G. Russo, *Implicit-explicit Runge-Kutta methods and applications to hyperbolic systems with relaxation*, J. Sci. Comp. 25, 129–155, 2005.

[41] B. Perthame, *Global existence to the BGK model of Boltzmann equation*, J. Differ. Equations 82, 191–205, 1989.

[42] S. Pieraccini, G. Puppo, *Implicit-explicit schemes for BGK kinetic equations*, J. Sci. Comput. 32, 1–28, 2007.

[43] S. Pieraccini, G. Puppo, *Microscopically implicit-macroscopically explicit schemes for the BGK equation*, J. Comput. Phys. 231, 299–327, 2012.

[44] G. Puppo, personal communications, 2013.

[45] J.D. Ramshaw, *Hydrodynamic theory of multicomponent diffusion and thermal- diffusion in multitemperature gas mixtures*, J. Non–Equilib. Thermodyn., 18, 121–134, 1993.

[46] F. Rogier, J. Schneider, *A direct method for solving the Boltzmann Equation*, Transport Theor. Stat., 23, 313–338, 1994.

[47] A. Rossani, G. Spiga, *A note on the kinetic theory of chemically reacting gases,* Physica A, 272, 563–573, 1999.

[48] G. Russo, *High Order Shock-Capturing Schemes for Balance Laws*, in: S.Bertoluzza, S. Falletta, G. Russo, C-W. Shu, *Numerical Solution of Partial Differential Equations*, Advanced Courses in Mathematics CRM Barcelona, Birkhäuser, Basel, 2009.

[49] G. Russo, P. Santagati, S.-B. Yun, *Convergence of a semi-lagrangian scheme for the BGK model of the Boltzmann equation*, SIAM J. Numer. Anal. 50, 1111–1135, 2012.

[50] G. Russo and P. Santagati, *A new class of large time step methods for the BGK models of the Boltzmann equation*, arXiv:1103.5247v1, 2011.

[51] P. Santagati, *High order semi-Lagrangian schemes for the BGK model of the Boltzmann equation*, Department of Mathematics and Computer Science, University of Catania, PhD. thesis, 2007.

[52] L. Sivorich, *Kinetic modeling of gas mixtures,* Phys. Fluids, 5, 908–918, 1962.

[53] C.W. Shu, *Essentially non-oscillatory and weighted essentially non-oscillatory schemes for hyperbolic conservation laws, in Advanced Numerical Approximation of Nonlinear Hyperbolic Equations*, Lecture Notes in Math. 1697, Papers from the C.I.M.E. Summer School held in Certraro, June 23-28, 1997, A. Quarteroni, Ed. Springer-Verlag, Berlin, 1998.

[54] S. Tan, C.W. Shu, *Inverse Lax-Wendroff procedure for numerical boundary conditions of conservation laws*, J. Comput. Phys., 229, 8144–8166, 2010.

[55] S. Tan and C.W. Shu, *A high order moving boundary treatment for compressible inviscid flows*, J. Comput. Phys., 230, 6023–6036, 2011.

[56] S. Tan, C. Wang, C.W. Shu, J. Ning, *Efficient implementation of high order inverse Lax-Wendroff boundary treatment for conservation laws*, J. Comput. Phys., 231, 2510–2527, 2012.

[57] L. Saint-Raymond, *From the BGK model to the Navier-Stokes equations*, Ann. Scient. Ec. Norm. Sup. 36, 271–317, 2003.

[58] P. Welander, *On the temperature jump in a rarefied gas*, Ark. Fys. 7, 507–553, 1954.

[59] T. Xiong, M. Zhang, Y.-T. Zhang and C.-W. Shu, *Fast sweeping fifth order WENO scheme for static Hamilton-Jacobi equations with accurate boundary treatment*, J. Sci. Comput., 45, 514–536, 2010.

[60] S. Yun, *Cauchy problem for the Boltzmann-BGK model near a global Maxwellian*, J. Math. Phys. 51, 123514, 2010.